COMPUTATIONAL MODELING OF THE EXPLOSION AND DETONATION OF HIGH EXPLOSIVES

by

Jacqueline Beckvermit

A dissertation submitted to the faculty of
The University of Utah
in partial fulfillment of the requirements for the degree of

Doctor of Philosophy

Department of Chemistry

The University of Utah

May 2016

The University of Utah Graduate School

STATEMENT OF DISSERTATION APPROVAL

The dissertation of **Jacqueline Beckvermit**

has been approved by the following supervisory committee members:

Charles Wight	, Chair	**12/17/2015** Date Approved
Martin Berzins	, Member	**12/17/2015** Date Approved
Valeria Molinero	, Member	**12/17/2015** Date Approved
Michael D. Morse	, Member	**12/17/2015** Date Approved
Ryan P. Steele	, Member	**12/17/2015** Date Approved

and by **Cynthia J. Burrows**, Chair/Dean of

the Department/College/School of **Chemistry**

and by David B. Kieda, Dean of The Graduate School.

ABSTRACT

The detonation of hundreds of explosive devices from either a transportation or storage accident is an extremely dangerous event. Motivation for this work came from a transportation accident where a truck carrying 16,000 kg of seismic boosters overturned, caught fire and detonated. The damage was catastrophic, creating a crater 24 m wide by 10 m deep in the middle of the highway. Our particular interest is understanding the fundamental physical mechanisms by which convective deflagration of cylindrical PBX 9501 devices can transition to a fully-developed detonation in transportation and storage accidents. Predictive computer simulations of large-scale deflagrations and detonations are dependent on the availability of robust reaction models embedded in a computational framework capable of running on massively parallel computer architectures. Our research group has been developing such models in the Uintah Computational Framework, which is capable of scaling up to 512 K cores. The current Deflagration to Detonation Transition (DDT) model merges a combustion model from Ward, Son, and Brewster that captures the effects of pressure and initial temperature on the burn rate, with a criteria model for burning in cracks of damaged explosives from Berghout et al., and a detonation model from Souers describing fully developed detonation. The prior extensive validation against experimental tests was extended to a wide range of temporal and spatial scales. We made changes to the reactant equation of state-enabling predictions of combustions, explosions, and detonations over a range of pressures spanning five orders of magnitude. A resolution dependence was eliminated from the reaction model facilitating large scale simulations to be run at a resolution of 2 mm without loss of fidelity. Adjustments were also made to slow down the flame propagation of conductive and convective deflagration. Large two- and three-dimensional simulations revealed two dominant mechanisms for the initiation of a DDT, inertial confinement and Impact to Detonation Transition. Understanding these mechanisms led to identifying ways to package and store explosive devices that reduced the probability of a detonation. We determined that the arrangement of the explosive cylinders and the number of devices packed in a box greatly affected the propensity to transition to a detonation.

For inspiring my love of science.
For encouraging me to pursue my dreams.
For their never ending love and support.
This dissertation is dedicated to my parents,
Jeff and Trish Beckvermit.
I love you. Thank you.

CONTENTS

LIST OF FIGURES

LIST OF TABLES

NOTATION AND SYMBOLS

A	Constant in JWL equation of state
A_c	Condensed phase frequency factor
A_{id}	Induction time constant
$adjCell$	Adjacent cell
B	Constant in JWL equation of state
B_g	Gas phase frequency factor
BFA	Burn Front Area
BFA_{new}	New Burn Front Area
BFA_{ref}	Reference Burn Front Area
c	Speed of sound
CFD	Computational Fluid Dynamics
C_p	Specific heat of the condensed phase
C_v	Heat capacity
CPU	Central Processing Unit
D_a	Damkohler number
DDT	Deflagration to Detonation Transition
$delF$	Burn fraction
E_c	Condensed phase activation energy
EOS	Equation of State
$FLIP$	Fluid-Implicit-Particle

FSI	Fluid-Structure Interactions
G	Rate constant in detonation model
PVF	Packing Volume Fraction
g_x	x component of the normalized density gradient
g_y	y component of the normalized density gradient
g_z	z component of the normalized density gradient
IC	Induction time constant
ICE	Implicit Continuous-fluid Eulerian algorithm
K_0	Bulk modulus
m_b	Mass flux
$max(g)$	Maximum of the three components in the normalized density vector
MB	Mass burned per timestep
MPM	Material Point Method
$MPMICE$	Combination of MPM and ICE algorithm
MW	Molecular Weight
$numPPC$	Number of particles in cell
P	Pressure
P_c	Critical pressure
P_d	Dimensionless pressure $P_d = P/0.1MPa$
P_{ref}	Reference pressure
$press\_CC$	Cell centered pressure
Q_c	Chemical heat release from condensed phase reaction
Q_g	Chemical heat release from gas phase reaction
R	Ideal gas constant

R_1	Constant in JWL equation of state
R_2	Constant in JWL equation of state
SDT	Shock to Detonation Transition
S_f	Flame propagation
T	Temperature
T_s	Surface temperature of the condensed phase
T_0	Initial temperature of condensed phase
$temp\_CC$	Cell centered temperature
V	Volume
V_r	Relative Volume
V_0	Initial Volume
vol_frac	Cell centered volume fraction
w	Crack radius
WSB	Ward, Son and Brewster burn model
x_{cd}	Convective-diffusive length
x_g	Gas phase flame thickness
κ_c	Condensed phase thermal conductivity
κ_0	Bulk modulus
κ_g	Gas phase thermal conductivity
γ	Phase shift 90 degrees
ρ	Density
ρ_0	Initial Density
ρ_c	Density of condensed phase
ρ_{prod}	Product density

ρ_{rct}	Reactant density
τ	Induction time
ω	Gruneisen coefficient
Δt	Change in time
Δx	Length of cell in the x direction
Δy	Length of cell in the y direction
Δz	Length of cell in the z direction
θ_{hotgas}	Induction angle

ACKNOWLEDGMENTS

I could have never completed this dissertation without the help, support, guidance, and efforts of a lot of people. I am grateful to my advisor, Dr. Charles Wight, whose expertise, understanding, guidance and support made it possible for me to work on a topic that was of great interest to me. I am highly indebted and thoroughly grateful to Dr. Todd Harman, whose never-ending support and valuable discussions pushed my academic understanding and interest. I would like to express my gratitude to Dr. Martin Berzins for supporting my research and giving thoughtful feedback, always aimed at moving me forward. Furthermore, I am sincerely grateful to my peer Nathan Miller for his editorial help and all of his encouragement. In addition, five other scholars have done work which was pivotal in my dissertation's development: Dr. John Schmidt, Dr. Qingyu Meng, Joseph Peterson, Andrew Bezdjian, and Alan Humphrey, thank you. This work was supported by the National Science Foundation under subcontract No. OCI0721659. Uintah was written by the University of Utah's Center for the Simulation of Accidental Fires and Explosions (C-SAFE) and funded by the Department of Energy, subcontract No. B524196. The University of Utah Women's Resource Center is especially thanked for funding. An award of computer time was provided by the Innovative and Novel Computational Impact on Theory and Experiment (INCITE) program. This research used resources of the Argonne Leadership Computing Facility at Argonne National Laboratory, which is supported by the Office of Science of the U.S. Department of Energy under contract DE-AC02-06CH11357 (sub-award Uintah_Safety). This research used resources from the Oak Ridge Leadership Computing Facility at the Oak Ridge National Laboratory, which is supported by the Office of Science of the US DOE under contract DE-AC05-00OR22725 (sub-award ENP009). This work also used the Extreme Discovery Environment (XSEDE), which is supported by NSF grant OCI1053575 (sub-awards TG-MCA08X004 and TG-ASC150004). The support and resources from the Center for High Performance Computing at the University of Utah are gratefully acknowledged.

CHAPTER 1

INTRODUCTION

On August 10th, 2005 a semi-tractor-trailer carrying 16,000 kg of seismic boosters traveling on Highway 6 through Spanish Fork Canyon, Utah overturned and caught fire. The deflagration quickly transitioned into a fully developed detonation, made apparent by the 24 m wide by 10 m deep crater formed in the middle of the road, with burning debris found up to 400 m away. Though these accidents are rare, the damage caused by the detonation of thousands of explosive devices can be extremely dangerous. This thesis is focused on the development of the science-based computational tools needed to accurately model all aspects of a Deflagration to Detonation Transition (DDT) in a large array of explosive cylinders. These tools were embedded in the Uintah Computational Framework, allowing for large-scale DDT simulations. The goal of this research was to understand the initiation mechanisms for the DDT in an array of explosive cylinders and to determine how packing configurations for the devices could help to prevent a detonation. Presented in this chapter is an evaluation of the combustion of the explosive of interest, Section 1.1. The governing equations used in the Uintah Computational Framework and an explanation of the simplified reaction model are examined in Section 1.2. Chapter 2 is an overview of the Uintah Computational Framework, describing its wide range of modeling capabilities. Chapter 3 discusses changes made to the reactant Jones-Wilkins-Lee (JWL) equation of state-enabling material response predictions for a wide range of pressures. Chapter 4 presents the resolution dependence on the conductive deflagration and detonation models, permitting simulations to be run at a 2 mm grid resolution. Chapter 5 discusses the adjustments made to Uintah's DDT model to eliminate a resolution dependence in convective deflagration and accurately model the flame propagation velocity in all stages of combustion. Chapter 6 analyzes the DDT initiation mechanisms for an array of explosive cylinders. They were determined to be inertial confinement and Impact to Detonation Transition (IDT). Chapter 7 examines possible packaging configuration variations that may reduce the probability of detonation in transportation and storage.

1.1 Combustion of PBX 9501

This research focused on the combustion of PBX 9501 (95% 1,3,5,7-octahydro-1,3,5,7-tetranitro- 1,3,5,7-tetrazocine (HMX, Figure 1.1) and 5% of a plastic binder). PBX 9501 is extensively used by the military, and thus, comprehensive research has gone into understanding all aspects of its decomposition, deflagration, and detonation. There are three important regions in the combustion of HMX and PBX 9501, depicted in Figure 1.2. The first is the condensed phase. On the edge of the condensed phase exists a melt layer, where HMX evaporates and decomposes. This results in a large temperature increase and intermediates being formed. According to Charkaborty et al.[1] there are three hypothesized mechanisms for the unimolecular decomposition of HMX. First is a successive methylenenitramine elimination, forming four methylenenitramines that further decompose into formaldehyde and nitrous oxide. The second mechanism is the homolytic cleavage of the $N - NO_2$ bond forming four nitrogen dioxide molecules and a ring that further eliminates into the final byproducts. The last path proposed is the successive HONO elimination leading to four HONO and four HCN molecules. The intermediates then further decompose. Using the DFT(B3LYP) method Charkaborty et al.[1] concluded the consecutive HONO elimination was the initiation step in the decomposition of HMX. Multiple scientists agree with the dominant mechanisms but disagree on the initiation step. Lewis et al.[2] and Sharia et al.[3] determined the $N - NO_2$ dissociation was the initiation mechanism based on its energies. Even though the exact mechanism for decomposition is undecided, it is understood that the final products include but are not limited to NO_2, N_2O, H_2O, N_2, CO, NO, HCN, H_2, NH_3, CH_3OH, CH_2O, and CO_2.[1,4,5]

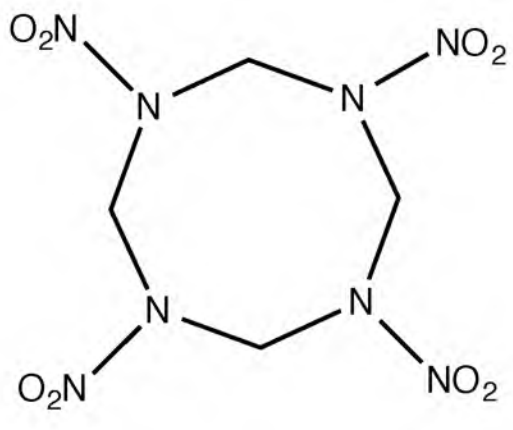

Figure 1.1: Molecular structure of HMX.

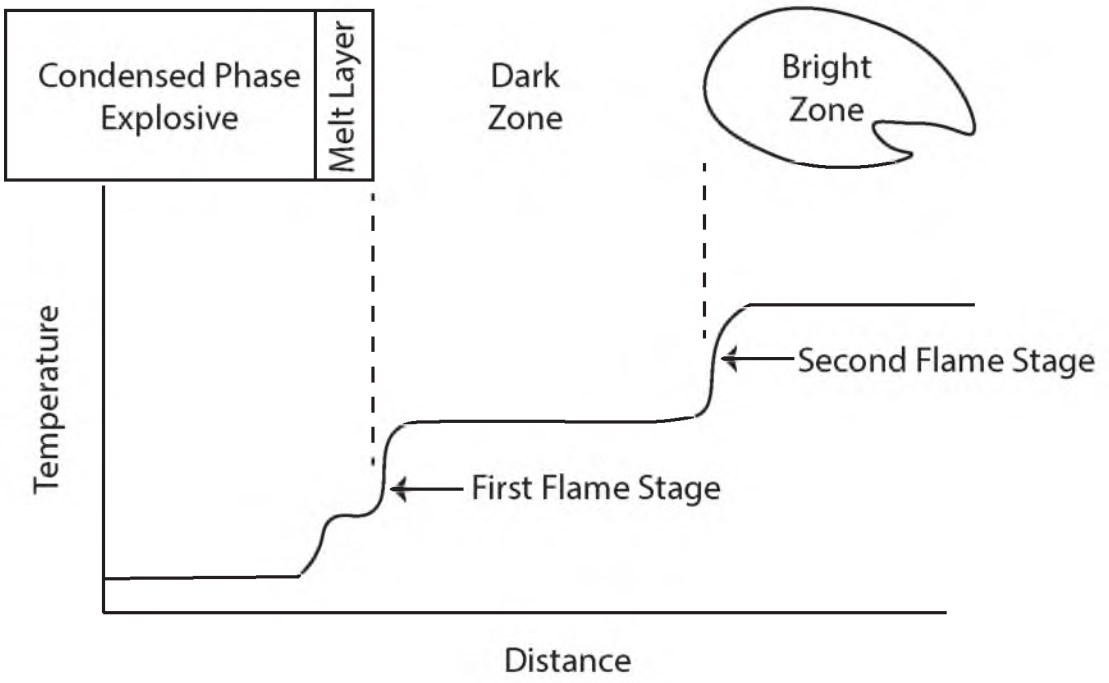

Figure 1.2: Schematic of idealized steady deflagration of a solid explosive.

The second region in the combustion of HMX-based explosives is the dark zone (Figure 1.2). Between the propellant surface and the dark zone the first flame stage occurs. In this region the rapid exothermic reactions consume most of the CH_2O, NO_2, HONO, and N_2O produced from the decomposition of the solid. This results in a relatively small temperature increase.[6] Examples of such reactions include:

$$N_2O + H \rightarrow N_2 + OH \tag{1.1}$$

$$CH_2O + NO_2 \rightarrow HCO + HONO \tag{1.2}$$

$$HONO(+M) \rightarrow NO + OH(+M). \tag{1.3}$$

Within the dark zone, the intermediate products are comparatively unreactive, causing a time delay for the radicals to build up in concentration before ignition in the luminous flame.[6] The dark zone primarily contains HCN, N_2, CO, CO_2, H_2O, NO, and small leftover traces of N_2O, CH_2O, and NO_2. This zone is also known as the flame standoff distance and is very important in determining the flame structure at low pressures and the burn rate at high pressures. The species concentrations and temperature profile have been

measured experimentally by planar laser-induced fluorescence, UV/VIS absorption, Raman spectroscopy, and thermocoupling techniques.[6,7]

The third region in the combustion of condensed phase explosives is the bright zone, known for its luminous flame. Within this region, a large temperature increase occurs and is primarily caused by the heat released as HCN and NO go to final products.[6] Some of the reactions which occur in this region include the following:

$$HCN + M \rightarrow HNC + M \tag{1.4}$$

$$HCN + O \rightarrow NCO + H \tag{1.5}$$

$$HCN + OH \rightarrow HNCO + H \tag{1.6}$$

$$HNCO + H \rightarrow NH_2 + CO \tag{1.7}$$

$$NCO + H \rightarrow NH + CO \tag{1.8}$$

$$N + NO \rightarrow N_2 + O \tag{1.9}$$

$$NH + NO \rightarrow N_2 + OH \tag{1.10}$$

$$NH + NO \rightarrow N_2O + H \tag{1.11}$$

$$NH_2 + NO \rightarrow N_2 + H_2O. \tag{1.12}$$

Due to the extreme conditions of combustion it is very difficult to determine all species and reactions occurring. It has been concluded that over 230 reactions, including more than 45 species, are involved in the combustion of HMX and PBX 9501.[5]

Breaking the combustion of condensed-phase explosives into three regions is a simplified view of the deflagration occurring. With condensed-phase combustion there are two types of deflagration which can occur, conductive deflagration and convective deflagration. Conductive deflagration, or on-surface burning, was described previously as the process where the flame is on the surface of the solid explosive. This deflagration occurs at low pressures and propagates along the surface at velocities of a few m/s. As intermediate product concentrations and relative pressures increase, the luminous flame extends closer to the condensed phase, decreasing the flame standoff distance and increasing the reaction rate and propagation velocity of the flame. When the flame standoff distance is small enough, convective deflagration can occur. Convective deflagration occurs within the solid material when the pressure is great enough for the hot gases to penetrate the damaged solid. The pressure at which this occurs is defined as the critical pressure and is dependent on the porosity of the material.[8] The more porous or damaged the explosive, the lower

the critical pressure. Convective deflagration is sustained by the convective feedback of the hot product gases rapidly penetrating the damaged explosive. This deflagration occurs at much faster propagation velocities of 100's to 1000's of m/s and rapidly increases the rate of reaction. Convective deflagration is considered to have a very important role in the transition to detonation in solid explosives and will be discussed in more detail in Chapters 5 and 6.

1.2 Uintah Computational Framework

The Uintah Computational Framework is a collaboration of work from computer scientists, engineers, and chemists, developed at the University of Utah. This framework was first developed to model the response of energetic devices to hydrocarbon pool fires and has since been expanded to modeling solid explosives, coal burning plants, and flow through urban environments. Uintah is a component-based software that accurately resolves the fluid-structure interactions (FSI) of the combustion of high explosives. The framework is comprised of numerous physics-based components, three of which were used in the work described here. These are the Material Point Method (MPM),[9–12] a compressible flow computational fluid dynamics (CFD) algorithm (ICE),[13,14] and a FSI algorithm (MPMICE).[9,15,16] The FSI algorithm was developed at Los Alamos National Laboratory and was specifically designed to simulate high deformation rate FSI. ICE is a finite volume method and uses an adaptive hexahedral mesh. MPM is used to evaluate the distortion and evolution of the solid material using Lagrangian points (particles) on a Eulerian grid. The particle's state vector is then extrapolated to the cell centers to be used in the multimaterial CFD model. This allows multiphase materials to use the same Eulerian mesh. The MPMICE algorithm is unique in the way in which solid and gas phase materials interact, and this approach facilitates treatment of solid $\rightarrow$ gas phase reactions. The Uintah Computational Framework has exhibited linear strong and weak scaling up to 512 K cores on DOE's Mira.[17] This enabled the execution of macroscale simulations with a relatively small grid cell resolution (2 mm). Substantial changes in the Uintah infrastructure were required in order to run these numerical experiments at the scales required. The MPMICE component was updated to dynamically execute the task graph[18] by way of message passing to communicate between nodes.[19,20] This method has been shown to be portable across a number of different supercomputers. A full description of the changes made was presented in.[17] Adaptive Mesh Refinement (AMR)[21] was also utilized for large-scale simulations to decrease the computational costs.

1.2.1 Multimaterial Governing Equations

This section is a reprint of a portion of the accepted article " M. Berzins, J. Beckvermit, T. Harman, A. Bezdjian, A. Humphrey, Q. Meng, J. Schmidt, C. Wight. Accepted to SIAM Journal on Scientific Computation 2015".[17]

"The governing multi material model equations are stated and described, but not developed, here. Their development and the methods for solving them can be found in.[9,15,16,22] Here, we identify the 8 quantities of interest and the equations (or closure models) which govern their behavior. Consider a collection of N materials, and let the subscript r signify one of the materials, such that r $= 1, 2, 3, \ldots, N$. In most simulations discussed in this thesis two materials are used, a solid (PBX 9501) and a gas (products of reaction). In an arbitrary volume $V(\mathbf{x}, t)$, the averaged thermodynamic state of a material is given by the vector $[M_{\rm r}, \mathbf{u}_{\rm r}, e_{\rm r}, T_{\rm r}, v_{\rm r}, \theta_{\rm r}, \boldsymbol{\sigma}_{\rm r}, p]$, where the elements are the r-material mass,velocity, internal energy, temperature, specific volume, volume fraction, stress, and the "equilibration" pressure. The r-material averaged density is $\rho_{\rm r} = M_{\rm r}/V$. The rate of change of the state in a volume moving with the velocity of r-material is

$$\frac{1}{V}\frac{D_{\rm r}M_{\rm r}}{Dt} = \sum_{s=1,n\neq r}^{N} S_{\rho}^{s\rightarrow r} \tag{1.13}$$

$$\frac{1}{V}\frac{D_{\rm r}(M_{\rm r}\mathbf{u}_{\rm r})}{Dt} = \theta_{\rm r}\boldsymbol{\nabla}\cdot\boldsymbol{\sigma} + \boldsymbol{\nabla}\cdot\theta_{\rm r}(\boldsymbol{\sigma}_{\rm r}-\boldsymbol{\sigma}) + \rho_{\rm r}\mathbf{g} + \Sigma_{s=1}^{N}\mathbf{F}_{\rm rs} + \sum_{s=1,n\neq r}^{N} S_{\rho\mathbf{u}}^{s\rightarrow r} \tag{1.14}$$

$$\frac{1}{V}\frac{D_{\rm r}(M_{\rm r}e_{\rm r})}{Dt} = -\rho_{\rm r}p\frac{D_{\rm r}v_{\rm r}}{Dt} + \theta_{\rm r}\boldsymbol{\tau}_{\rm r} : \nabla\mathbf{u}_{\rm r} - \boldsymbol{\nabla}\cdot\mathbf{j}_{\rm r} + \Sigma_{s=1}^{N}Q_{\rm rs} + \sum_{s=1,n\neq r}^{N} S_{\rho e}^{s\rightarrow r} \tag{1.15}$$

Equations (1.13-1.15) are the averaged model equations for mass, momentum, and internal energy of r-material, in which $\boldsymbol{\sigma}$ is the mean mixture stress, taken here to be isotropic, so that $\boldsymbol{\sigma} = -p\mathbf{I}$ in terms of the hydrodynamic pressure p. The effects of turbulence have been omitted from these equations.

In Eq. (1.14) the term $\sum_{s=1}^{N}\mathbf{F}_{\rm rs}$ signifies a model for the momentum exchange among materials and is a function of the relative velocity between materials at a point. For a two-material problem we use $\mathbf{F}_{12} = K_{12}\theta_1\theta_2(\mathbf{u}_1 - \mathbf{u}_2)$, where the coefficient K_{12} determines the rate at which momentum is transferred between materials. Likewise, in Eq. (1.15), $\sum_{\rm s=1}^{N} Q_{\rm rs}$ represents an exchange of heat energy among materials. For a two-material problem $Q_{12} = H_{12}\theta_1\theta_2(T_2 - T_1)$, where $T_{\rm r}$ is the r-material temperature and the coefficient $H_{\rm rs}$ is analogous to a convective heat transfer rate coefficient. The heat flux is $\mathbf{j}_{\rm r} = -\rho_{\rm r}b_{\rm r}\boldsymbol{\nabla}T_{\rm r}$ where the thermal diffusion coefficient $b_{\rm r}$ includes both molecular and turbulent effects (when the turbulence is included).

The temperature, T_r, specific volume, v_r, volume fraction, θ_r, and hydrodynamic pressure p are related to the r-material mass density, ρ_r, and specific internal energy, e_r, by way of equations of state. The four relations for the four quantities $(T_\mathrm{r}, v_\mathrm{r}, \theta_\mathrm{r}, p)$ are:

$$e_\mathrm{r} = e_\mathrm{r}(v_\mathrm{r}, T_\mathrm{r}) \tag{1.16}$$

$$v_\mathrm{r} = v_\mathrm{r}(p, T_\mathrm{r}) \tag{1.17}$$

$$\theta_\mathrm{r} = \rho_\mathrm{r} v_\mathrm{r} \tag{1.18}$$

$$0 = 1 - \textstyle\sum_{s=1}^{N} \rho_\mathrm{s} v_\mathrm{s} \tag{1.19}$$

Equations (1.16) and (1.17) are, respectively, the caloric and thermal equations of state. Equation (1.18) defines the volume fraction, θ, as the volume of r-material per total material volume, and with that definition, Equation (1.19), is referred to as the multi material equation of state. It defines the unique value of the hydrodynamic pressure, p, that allows arbitrary masses of the multiple materials to identically fill the volume, V. This pressure is called the "equilibration" pressure.[23]

A closure relation is still needed for the material stress, $\boldsymbol{\sigma}_\mathrm{r}$. For a fluid $\boldsymbol{\sigma}_\mathrm{r} = -p\mathbf{I} + \boldsymbol{\tau}_\mathrm{r}$ where the deviatoric stress is well known for Newtonian fluids. For a solid, the material stress is the Cauchy stress. The Cauchy stress is computed using a solid constitutive model and may depend on the rate of deformation, the current state of deformation ($\mathbf{E}$), the temperature, and possibly a number of history variables:

$$\boldsymbol{\sigma}_\mathrm{r} \equiv \boldsymbol{\sigma}_\mathrm{r}(\boldsymbol{\nabla}\mathbf{u}_\mathrm{r}, \mathbf{E}_\mathrm{r}, T_\mathrm{r}, \ \ldots) \tag{1.20}$$

Equations (1.13-1.20) form a set of eight equations for the eight-state vector with components $[M_\mathrm{r}, \mathbf{u}_\mathrm{r}, e_\mathrm{r}, T_\mathrm{r}, v_\mathrm{r}, \theta_\mathrm{r}, \boldsymbol{\sigma}_\mathrm{r}, p]$, for any arbitrary volume of space, V, moving with the r-material velocity. This approach uses the reference frame most suitable for a particular material type. The Eulerian frame of reference for the fluid and the Lagrangian for the solid. There is no guarantee that the arbitrary volumes will remain coincident for the two materials. This problem is addressed by treating the specific volume as a material state which is integrated forward in time from the initial conditions. The total volume associated with all of the materials is given by

$$V_t = \textstyle\sum_{r=1}^{N} M_\mathrm{r} v_\mathrm{r} \tag{1.21}$$

where the volume fraction is $\theta_\mathrm{r} = M_\mathrm{r} v_\mathrm{r} / V_t$ (which sums to one by definition). An evolution equation for the r-material specific volume has been developed in[22] and is stated here as:

$$\frac{1}{V}\frac{D_{\mathrm{r}}(M_{\mathrm{r}}v_{\mathrm{r}})}{Dt} = f_{\mathrm{r}}^{\theta}\boldsymbol{\nabla}\cdot\mathbf{u} \quad + \quad \left[v_{\mathrm{r}}S_{\rho_{\mathrm{r}}}^{s\to r} - f_{\mathrm{r}}^{\theta}\textstyle\sum_{s=1}^{N} v_{\mathrm{s}}S_{\rho_{\mathrm{s}}}^{s\to r}\right] + \left[\theta_{\mathrm{r}}\beta_{\mathrm{r}}\frac{D_{\mathrm{r}}T_{\mathrm{r}}}{Dt} - f_{\mathrm{r}}^{\theta}\textstyle\sum_{s=1}^{N}\theta_{\mathrm{s}}\beta_{\mathrm{s}}\frac{D_{\mathrm{s}}T_{\mathrm{s}}}{Dt}\right]. \tag{1.22}$$

where $f_{\mathrm{r}}^{\theta} = \frac{\theta_{\mathrm{r}}\hat{\kappa}_{\mathrm{r}}}{\sum_{s=1}^{N}\theta_{\mathrm{s}}\hat{\kappa}_{\mathrm{s}}}$, and $\hat{\kappa}_{\mathrm{r}}$ is the r-material bulk compressibility, β is the constant pressure thermal expansivity.

The evaluation of the multi-material equation of state (Eq. (1.19)) is required to determine an equilibrium pressure that results in a common value for the pressure, as well as specific volumes that fill the total volume identically."

1.2.2 Reaction Model

As discussed in Section 1.1, the combustion of HMX-based explosives is very complex. Many research groups have looked into modeling the combustion on all scales, from detailed kinetics models to simple combustion models. The detailed kinetics models are very in-depth, using thermal decomposition reactions for the condensed phase and elementary kinetics mechanisms to describe the gas phase. Simple kinetics models, on the other hand, do not account for the chemical kinetics of combustion. Instead they examine the reaction rate by conserving energy, mass, and momentum.

Detailed kinetics models are useful in fully simulating the different aspects of combustion on the microscale. One challenge of detailed kinetic modeling is determining how to treat the condensed phase decomposition, because the exact mechanism is still unknown for HMX-based explosives. The approximations presented here for the condensed-phase are considered acceptable approaches because most of the energy release in the combustion of HMX comes from the gas-phase reactions. To account for this uncertainty, some modelers have allowed two global pathways for the condensed-phase decomposition.[24] Allowing the condensed phase to decompose by the exothermic path of HMX$\rightarrow 4CH_2O + 4N_2O$ or the endothermic path of HMX$\rightarrow 4HCN + 2NO_2 + 2NO + 2H_2O$.[5] Other groups have opted to use a simplified modeling approach where they employ known surface temperatures and species concentrations as a boundary condition without solving any laws of conservation between the solid and gas.[25,26] Another approach is to avoid modeling the condensed-phase structure by solving the mass burn rate iteratively as a function of the heat flux at the surface.[27,28] A more in-depth model was developed by Washburn and Beckstead,[29] and is able to closely represent the temperature sensitivities of the burn rate at low pressures. This was done by including the surface tension of the bubbles to more accurately represent the melt layer at the surface of the propellent.

At higher pressures the flame stand off distance is much smaller than at lower pressures, resulting in the gas phase reactions dominating the burn rate. Detailed kinetics models excel in this region. Since the combustion of many high explosives results in similar final reactions with varying species concentrations, the kinetics are fairly well known for this region. Modeling packages such as CHEMKIN[30] and CHEETAH[31] can be used for such calculations. Other detailed kinetics models have shown good agreement with the species' concentration and temperature profiles in the gas phase combustion of HMX.[32–36] The advantages of using detailed kinetics models is their ability to examine the temperature and species' concentration profiles. This gives insight into the flame structure and heat release mechanisms. The burn rate temperature sensitivities over a wide range of pressures can also be calculated.

In order to model the detailed kinetics of the reactions involved in the combustion of HMX-based explosives, the grid cell sizes must be on the micron scale to fully resolve the flame standoff distance and melt layer. This is unfeasible for the scales this research was focused on. Therefore Uintah was set to utilize a simple combustion model which assumed global kinetics to describe the deflagration of HMX. The Ward, Son, and Brewster (WSB) steady deflagration model, developed at Los Alamos National Laboratory,[37] describes the deflagration mass conversion rates in a simplified algebraic solution. This model was developed to describe the flame structure, along with the temperature and pressure sensitivities of the mass burn rate in a simplified form. The reaction model is a two-phase chemistry model, in which the solid explosive (A) is converted to gas-phase intermediates (B) which react to form the final products (C), that is, A(Solid)$\rightarrow$ B(gas) $\rightarrow$ C(gas). Therefore only two phases of the combustion are modeled; the condensed and gas phases. The melt layer is assumed to have little impact on the overall combustion and is therefore ignored.

Previous simple combustion models[38–41] assumed a high activation energy associated with the condensed and gas-phase reactions. In doing so the models produced a concave-up temperature profile that increased much more sharply than the empirical data did when moving away from the material surface. Zenin et al.[42] discovered through thermocouple experiments that the unconfined deflagration of HMX exhibited a concave-down flame temperature profile adjacent to the surface of the solid. This suggested that there is not a large convective diffusion zone on the surface of the solid as was observed with previous models. To account for this the WSB model assumes a negligible activation energy for the gas-phase reactions. The temperature profile from the improved model matched the empirical data very well and exhibited the correct concave-down shape with a positive

slope at the surface. The negligible gas-phase activation energy assumption was justified by the gas-phase reactions being radical chain reactions. This chemistry is easily explained with the Zeldovich mechanism[43] for a hydrogen/oxygen combustion system. This breaks the combustion into two steps, initiation/branching and recombination/termination. In these systems there is a high activation energy associated with the initiation/branching step,

$$H + O_2 + 3H_2 \rightarrow 3H + 2H_2O \tag{1.23}$$

needed for the dissociation of H_2. This step is analogous to the decomposition of the condensed phase and is very temperature sensitive. The recombination/termination step,

$$H + H + M \rightarrow H_2 + M \tag{1.24}$$

on the other hand, is temperature insensitive, resulting in a negligible activation energy. This step exhibits most of the energy release of the system, similar to the chemistry seen with radical gas-phase reactions in the steady combustion of HMX.

The WSB model therefore assumes the condensed phase thermal decomposition is a unimolecular, irreversible, zeroth-order reaction, such that A→B. The gas-phase then undergoes an irreversible, first-order with respect to B, second-order with respect to C, chain reaction (B+M→C+M). This model has a large pressure dependence associated with the conductive heat transfer, which greatly affects the rate of the gas-phase reactions. The main assumptions in the WSB model[37] are:

1. The specific heat of the gas-phase and the condensed-phase are equal.
2. There is no mass diffusion assumed in the condensed-phase.
3. Mass diffusion of the gas-phase is described by Fick's Law.
4. The gas-phase follows the ideal gas law.
5. The condensed-phase is considered incompressible.
6. There is no pressure dependence associated with the heat release of the condensed-phase, only the gas-phase.
7. The thermal conductivities and specific heat are constant.
8. The thermal diffusivity and mass diffusivity are assumed to be equal in the gas-phase.

With these assumptions the WSB model closely represents the experimentally determined flame temperature profile, and similar surface temperature and heat release profiles.[37] The model also exhibited good agreement with the pressure and temperature sensitivities of the mass burn rate and the flame standoff distance.[37]

The mass burn rate, $S_{\rho}^{s \to r}$, is computed using

$$S_{\rho_r}^{s \to r} = \left[\frac{\kappa_s \rho_s A_s R (T_{surf})^2 exp(-E_s / R T_{surf})}{C_p E_s [T_{surf} - T_0 - Q_s / 2C_p]} \right]^{1/2} \tag{1.25}$$

$$T_{surf} = T_0 + \frac{Q_s}{C_p} + \frac{Q_r}{C_p (1 + \frac{x_s (S_{\rho_r}^{s \to r}, P)}{x_{cd} (S_{\rho_r}^{s \to r})})} \tag{1.26}$$

where T_0 is the initial bulk solid temperature, κ is the thermal conductivity, E_s is the condensed phase activation energy, R is the ideal gas constant, C_P is specific heat, Q is the heat released, ρ_s is the condensed phase density, A_s is the condensed phase frequency factor, x_{cd} is the convective diffusion length, and x_s is the flame thickness.[44] T_{surf} is a subscale surface temperature. Equations 1.25 and 1.26 are solved iteratively until a convergence criteria is met. A further, more detailed description, including the equations used in the WSB reaction model, is discussed in Chapter 5.

It is understood that the WSB model is a simplified view of the complex reactions occurring in the combustion of HMX and PBX 9501. Due to the need for deterministic modeling on a macroscale and the good agreement with experimental results, the WSB steady deflagration model was implemented in the Uintah DDT reaction model. The one-dimensional WSB model was modified from its original form to include three-dimensional effects.[47] Extensive validation on Uintah's DDT model was previously done by Peterson and Wight.[45] The simulated DDT model was validated at multiple pressures and initial temperatures (273, 298, and 423 K) for the conductive burn rate of HMX. The burn rates closely matched experimental results, as seen in Figure 1.3. The burn rate was measured by a strand burner experiment described in.[46] This experiment allows for the regression rate, the rate the material is consumed, to be measured as a function of temperature and pressure. Experimentally a wide range of pressures can be analyzed using the photocinemicrographic method.[46] This method allows for control over the pressure and initial temperature of the condensed phase combustion. In these experiments the explosive was ignited by a flash wire and high-speed cameras were used to determine the regression rate of the combustion. Experiments were carried out in a window bomb apparatus. Computationally, measurements were taken from a one-dimensional simulation consisting of a stick of HMX surrounded by symmetric wall boundary conditions on nonprinciple faces and Neumann pressure boundary

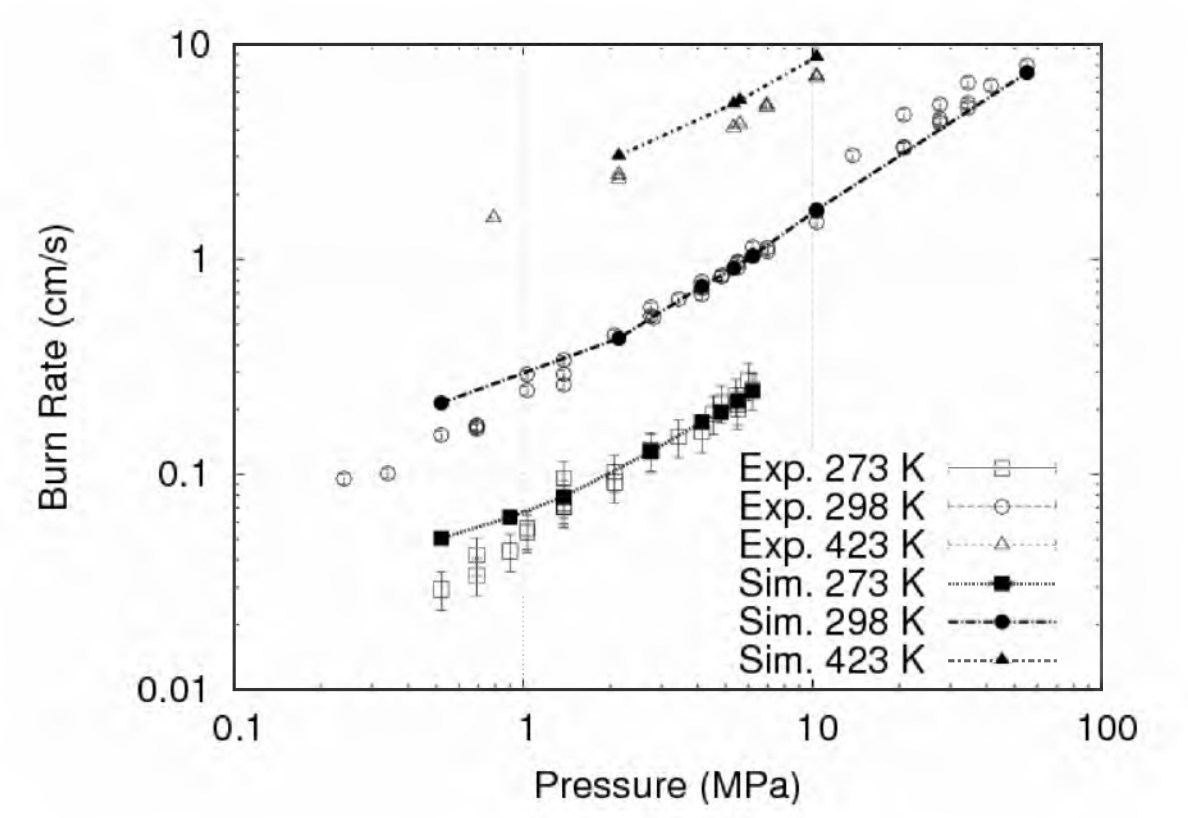

Figure 1.3: Simulated surface burn rates compared with experimental values. The simulated data is from Peterson et al.,[45] while the experimental data is from Atwood et al.[46] Plot used with permission from J. Peterson and C. Wight.[45]

conditions on the open end. The HMX was ignited by 600 K gas on the open end which was pressurized to the desired pressure. Measurements were taken as an average of the mass converted from solid → gas in the amount of time it took to burn a few cells (≈1 mm) after the initial deflagration instabilities subsided.[45]

The simulated burn rate agreed well with experimental values for pressures from 1-70 MPa, the pressure range within which DDT occurs (Figure 1.3). The large deviations seen at low pressures would occur in simulations of unconfined deflagration, where convective deflagration does not occur. Thus the simulations presented in this thesis should not occur in this region. When the model was previously adapted to three dimensions, a resolution dependence for convective deflagration was introduced. Chapter 5 discusses the changes made to account for this.

The DDT model is embedded within the MPMICE component and is used to describe deflagration, detonation, Shock to Detonation Transitions (SDT), and DDT in condensed phase explosives. The WSB model was combined with the the ViscoSCRAM constitutive

model[48] to evaluate the crack propagation in the solid material to model the transition to convective deflagration as defined by Berghout.[49] This model has been designed to match experimental relaxation times as determined by the visco-elastic response for PBX 9501.[48] At a pressure of 5.3 GPa or higher Uintah's DDT model switches from deflagration to detonation. The JWL++ simple reactive flow model[50,51] is used to describe the detonation. The pressure threshold of 5.3 GPa for HMX and PBX 9501 was chosen by Peterson and Wight[45] for three main reasons. First, this threshold gave reasonable results for the run distance to detonation for aluminum impact experiments.[45] Second, it is well known that the reaction rate increases with increasing pressure. It was discovered there is a discontinuity in this increase at 5 GPa, and the reaction rate exhibits a large increase at this pressure. At pressures above 5 GPa the reaction rate continues to increase with pressure, but more dramatically than it did at pressures below the discontinuity.[45,52] Third, the internal energy produced by the reversible adiabatic compression of solid HMX to 5.3 GPa was calculated to be 138.9 kJ/mol.[45] This amount of energy is relatively close to the activation energy found for HMX, which lies between 140 and 165 kJ/mol.[45] More details of Uintah's DDT reaction model are presented in[45,47] and Chapters 2-5.

This thesis examines the DDT in a large array of explosive cylinders. In doing so the reaction models needed to be further validated from what Peterson et al.[45] had previously reported. Chapter 2 is an overview of the Uintah Computational Framework. This chapter examined work done by many collaborators in an effort to describe the full capabilities of Uintah. Research on the mesoscale of explosions was examined by Joseph Peterson and Scott Bardenhagen, and macroscale simulations were examined by Jacqueline Beckvermit, Joseph Peterson, and Monica Hall. A brief discussion also looks at the Uintah infrastructure, including strong and weak scaling studies, the fluid structure interactions, and the task graph used. Todd Harman, John Schmidt, Martin Berzins, and Qingyu Meng were the main contributors to the computational infrastructure and fluid-structure interactions. Chapter 3 examines the equation of state used for the reactant and products. Due to the fit parameters for the reactant equation of state, negative pressure was observed when the material was in tension. This is not allowed within the MPMICE component, which was thus modified from the original to eliminate the possibility of negative pressures. Chapter 4 evaluates the resolution dependence on the DDT reaction model and a comparison between mesoscale and bulkscale modeling of explosions. This chapter was a collaboration with Joseph Peterson, who focused on the mesoscale simulations. The results showed the conductive deflagration rate was not effected by the grid cell size. The detonation model on the other hand

exhibited an 8% error associated with the detonation velocity when increasing the cell size from 1 to 12 mm. Chapter 5 describes a resolution dependence in the convective deflagration model and changes made to eliminate it. The propagation velocity of conductive and convective deflagration was also modified to match experimentally determined values. Andrew Bezdjian contributed a grid convergence study, examining the time to detonation dependence on grid cell size. With the completion of validating the known quantities of the DDT reaction model, the initiation mechanism for a DDT in an array of explosive cylinders is examined in Chapter 6. Two mechanisms were observed: inertial confinement and impact to detonation transition. Inertial confinement occurred as the explosive cylinders compacted into one another, forming a high-density barrier. This barrier trapped the product gases, building the pressures to that needed for the reaction model to transition to detonation. Impact to detonation transition occurs when the deflagrating cylinders are at an elevated pressure and are impacted by a pressure wave or explosive fragment. The impact causes the stress waves to reach pressures above the detonation pressure threshold. The DDT initiation mechanisms were used in order to propose safer ways to package cylinders. The results of that work are reported in Chapter 7. It was determined that the packing configuration can inhibit DDT in an array of explosive cylinders.

1.3 References

[1] D. Chakraborty, R. P. Muller, S. Dasgupta, W. Goddard. Mechanism for Unimolecular Decomposition of HMX (1,3,5,7-Tetranitro-1,3,5,7-tetrazocine), an ab Initio Study. *J. Phys. Chem.* **2001**, *195*, 1302–1314.

[2] J. Lewis, T. Sewell, R. Evans, G. Voth. Electronic Structure Calulation of the Structures and Energies of the Three Pure Polymorphic Forms of Crystalline HMX. *J. Phys. Chem. B* **2000**, *104*, 1009–1013.

[3] O. Sharia, M. M. Kuklja. Ab Initio Kinetics of Gas Phase Decomposition Reactions. *J. Phys. Chem. A* **2010**, *114*, 12656–12661.

[4] L. Fried, R. Manaa, J. Lewis, *Modeling the Rections of Energetic Materials in the Condensed Phase*, United States Department of Energy, Washington, DC, **2003**.

[5] M. W. Beckstead, K. Puduppakkam, P. Thakre, V. Yang. Modeling of Combuston and Ignition of Solid-Propellant Ingredients. *Prog. Energy Combust. Sci.* **2007**, *33*, 497–551.

[6] W. R. Anderson, N. E. Meagher, J. A. Vanderhoff. Dark Zones of Solid Propellant Flames: Critically Assessed Datasets, Quantitative Model Comparision, and Detailed Chemical Analysis. *Combust. Flame* **2011**, *158*, 1228–1244.

[7] T. Parr, D. Hanson-Parr. Cyclotetramethylene tetranitramine/glycidyl azide polymer/butanetriol trinitrate propellant flame structure. *Combust. Flame* **2004**, *137*, 38–49.

[8] H. L. Berghout, S. F. Son, B. W. Asay, *Convective Burning in Gaps of PBX 9501* in *Proc. Comb. Inst.*, pp. 911–917.

[9] J. E. Guilkey, T. B. Harman, B. Banerjee. An Eulerian-Lagrangian Approach for Simulating Explosions of Energetic Devices. *Comput. Struct.* **2007**, *85*, 660–674.

[10] D. Sulsky, Z. Chen, H. L. Schreyer. A Particle Method for History Dependent Materials:Dynamic Prioritation of Material Ineterfaces. *Comput. Methods Appl. Mech. Eng.* **1998**, *151*, 343–360.

[11] D. Sulsky, S. Zhou, H. L. Schreyer. Application of Particle-in-Cell Method to Solid Mechanics. *Comput. Phys. Commun.* **1995**, *87*.

[12] S. G. Bardenhagen, E. M. Kober. The Generalized Interpolation Material Point Method. *Comp. Mod. Eng. Sci.* **2004**, *5*.

[13] B. A. Kashiwa, E. S. Gaffney, *Design Basis for CFDLIB*, Tech. Report LA-UR-03-1295, Los Alamos Natl. Lab., **2003**.

[14] F. H. Harlow, A. A. Amsden. Nemerical Calculations of almost incompressible flow. *J. Comp. Phys.* **1968**, *3*, 80–93.

[15] J. E. Guilkey, T. B. Harman, B. A. Kashiwa, J. Schmidt, P. A. McMurtry, *An Eulerian-Lagrangian Approach for Large Deformation Fluid-Structure Interaction Problems, part 1: Algorithm Development* in *Fluid Struct. Interact. II*, WIT Press, Cadiz, Spain, 2003.

[16] T. Harman, J. Guilkey, B. A. Kashiwa, J. Schmidt, P. A. McMurtry, *An Eulerian-Lagrangian Approach for Large Deformation Fluid-Structure Interaction Problems, Part 2: Multi-Physics Simulations within a Modern Computational Framework* in *Fluid Struct. Interact. II, 2003*, pp. 157–166.

[17] M. Berzins, J. Beckvermit, T. Harman, A. Bezdjian, A. Humphrey, Q. Meng, J. Schmidt, C. Wight. Extending the Uintah Framework to Enable Petascale Modeling of Detonation in Arrays of High Explosive Devices. *Accepted SIAM J. Sci. Comput.* **2015**.

[18] Q. Meng, J. Luitjens, M. Berzins, *Dynamic Task Scheduling for the Uintah Framework* in *in Proc. of the 3rd IEEE Workshop on Many-Task Computing on Grids and Supercomputers (MTAS10), 2010*, pp. 1–10.

[19] Q. Meng, M. Berzins, J. Schmidt, *Using Hybrid Parallelism to Improve Memeory use in Uintah* in *TeraGrid 2011 Conference, 2011*, Salt Lake City, UT, 2011, p. 24.

[20] Q. Meng, M. Berzins. Scalable Large-Scale Fluid-Structure Interaction Solvers in the Uintah Framework via Hybrid Task-Based Parallelism Algorithms. *Concurr. Comput.* **2014**, *26*, 1388–1407.

[21] J. Luitjens, M. Berzins. Scalable parallel regridding algorithms for block-stuctured adaptive mesh refinement. *Concurr. Comput.* **2011**, *23*, 1522–1537.

[22] B. A. Kashiwa, *A Multifield Model and Method for Fluid-Stucture Interaction Dynamics*, Tech. Report LA-UR-01-1136, Los Alamos Natl. Lab., **2001**.

[23] B. A. Kashiwa, R. M. Rauenzahn, *A Multimaterial Formalism*, Tech. Report LA-UR-94-771, Los Alamos Natl. Lab., **1994**.

[24] E. S. Kim, V. Yang, Y.-C. Liau. Modeling of HMX/GAP Pseudo-Propellant Combustion. *Combust. Flame* **2002**, *131*, 227–245.

[25] N. E. Ermolin, O. Korobeinichev, A. G. Tereshchenko, V. M. Fomin. Kinetic calculations and Mechanism Definition for Reactions in an Ammonium Perchlorate Flame. *Combust. Explosion Shock Waves* **1982**, *18*, 180–189.

[26] N. E. Ermolin, O. Korobeinichev, L. V. Kuibida, V. M. Fomin. Study of the Kinetics and Mechanism of Chemical Reactions in Hexogen Flames. *Combust. Explosion Shock Waves* **1986**, *22*, 544–553.

[27] M. S. Miller, W. R. Anderson, *Solid Propellant Chemistry Combustion and Motor Interior Ballistics*, *Vol. 185*, V. Yang, T. B. Brill, W. Z. Ren (Eds.), **2000; p.501-531**.

[28] B. E. Homan, M. S. Miller, J. A. Vanderhoff. Absorption Diagnostics and Modeling Investigations of RDX Flame Structure. *Combust. Flame* **2000**, *120*, 301–317.

[29] E. B. Washburn, M. W. Beckstead. Moedeling Multi-Phase Effects in the Combustion HMX and RDX. *J. Propul. Power* **2006**, *22*, 938–946.

[30] R. J. Kee, F. M. Rupley, J. A. Miller, *CHEMKIN II: A FORTRAN Chemical Kinetics Package for the Analyisi of Gas-Phase Chemical Kinetics*, report SAND89-8009, Sandia Natl. Lab., **1985**.

[31] L. Fried, P. Souers, *CHEETAH: A Next Generation Thermochemical Code*, Tech. Report UCRL-ID-117240, Lawrence Livermore Natl. Lab., **1994**.

[32] J. E. Davidson, M. W. Beckstead, *A Three-Phase Model of HMX Combustion* in *26th Sym. (int.) on Combust., The Combust. Inst., 1996*, pp. 1989–1996.

[33] K. Prasad, R. A. Yetter, M. D. Smooke. An Eigenvalue Method for Computing the Burning Rates of HMX Propellants. *Combust. Flame* **1998**, *115*, 406–416.

[34] C. Melius. Thermochemical modeling, I: application to decomposition of energetic materials. *Chem. Phys. Energetic Mater.* **1990**, 21–49.

[35] C. Melius. Thermochemical modeling, II: application to ignition and combustion of energetic materials. *Chem. Phys. Energetic Mater.* **1990**, 51–78.

[36] R. A. Yetter, F. L. Dryer, M. T. Allen, J. L. Gatto. Development of gas-phase reaction mechanism for nitramine combustion. *J. Propul. Power* **1995**, *11*, 683–697.

[37] M. Ward, S. F. Son, M. Brewster. Steady Deflagration of HMX with Simple Kinetics: A Gas Phase Chain Reaction Model. *Combust. Flame* **1998**, *114*, 556–568.

[38] W. B. Bush, F. E. Fendell. Asymptotic Analysis of Laminar Flame Propagation for General Lewis Numbers. *Compos. Sci. Technol.* **1970**, *1*.

[39] F. A. Williams. Quasi-steady gas-phase flame theory in unsteady burning of a homogeneous solid propellant. *AIAA J.* **1973**, *11*, 1328–1330.

[40] G. Lengelle. Thermal degradation kinetics and surface pyrolysis of vinyl polymers. *AIAA J.* **1970**, *8*, 1989–1998.

[41] M. Q. Brewster, S. F. Son. Quasi-steady combustion modeling of homogeneous solid propellants. *Combust. Flame* **1995**, *103*, 11–26.

[42] A. Zenin. HMX and RDX - Combustion Mechanism and Influence on Modern Double-Base Propellant Combustion. *J. Propul. Power* **1995**, *11*, 752–758.

[43] Y. B. Zeldovich, G. I. Barenblatt, V. B. Librovich, G. M. Makhviladze, *The Mathematical Theory of Combustion and Explosions*, Plenum, New York, NY, **1985; p. 393-414**.

[44] J. Beckvermit, T. Harman, A. Bezdjian, C. Wight. Modeling Deflagration in Energetic Materials using the Uintah Computational Framework. *Procedia Comput. Sci.* **2015**, *51*, 552–561.

[45] J. R. Peterson, C. A. Wight. An Eulerian-Lagrangian Computational Model for Deflagration and Detonation of High Explosives. *Combust. Flame* **2012**, *159*, 2491–2499.

[46] A. I. Atwood, T. L. Boggs, P. O. Curran, T. P. Parr, D. M. Hanson-Parr. Burning Rate of Solid Propellant Ingredients, Part 1: Pressure and Initial Temperature Effects. *J. Propul. Power* **1999**, *15*, 740–747.

[47] C. A. Wight, E. Eddings. Science-Based Simulation Tools for Hazard Assessment and Mitigation. *Int. J. Energetic Mater. Chem. Propul.* **2009**, *8*, 373–389.

[48] J. G. Bennett, K. S. Haberman, J. N. Johnson, B. W. Asay, B. F. Henson. A Constitutive Model for the Non-Shock Ignition and Mechanical Response of High Explosives. *J. Mech. Phy. Solids* **1998**, *46*, 2303–2322.

[49] H. L. Berghout, S. F. Son, C. B. Skidmore, D. J. Idar, B. W. Asay. Combustion of Damaged PBX 9501 Explosive. *Thermochim. Acta* **2002**, *384*.

[50] P. C. Souers, S. Anderson, J. Mercer, E. McGuire, P. Vitello. JWL++: A Simple Reactive Flow Code Package for Detonation. *Propellants Explos. Pyrotech.* **2000**, *25*, 54–58.

[51] P. Souers, R. Garza, P. Vitello. Ignition and Growth and JWL++ Detonation Models in Coarse Zones. *Propellants Explos. Pyrotech.* **2002**, *27*.

[52] A. P. Esposito, D. L. Farber, J. E. Reaugh, J. M. Zaug. Reaction Propagation Rates in HMX at HIgh Pressure. *Propellants Explos. Pyrotech.* **2003**, *28*, 83–88.

CHAPTER 2

MULTISCALE MODELING OF ACCIDENTAL EXPLOSIONS AND DETONATIONS

Editors: Muhammad Sahimi, moe@iran.usc.edu
Barry I. Schneider, nsfphyman@gmail.com
and Gabriel Wainer, Gabriel.Wainer@sce.carleton.ca

MULTISCALE MODELING OF ACCIDENTAL EXPLOSIONS AND DETONATIONS

By Jacqueline Beckvermit, Joseph Peterson, Todd Harman, Scott Bardenhagen, Charles Wight, Qingyu Meng, and Martin Berzins

The Uintah Computational Framework is the first software to enable effectively simulating the development of detonation in semi-truck-scale transportation accidents.

Accidental explosions are exceptionally dangerous and costly, both in lives and money. Regarding worldwide conflict with small arms and light weapons, the Small Arms Survey has recorded more than 297 accidental explosions in munitions depots across the world that have resulted in thousands of deaths and billions of dollars in damage in the past decade alone.[1] As the recent fertilizer plant explosion that killed 15 people in the town of West, Texas demonstrates, accidental explosions aren't limited to military operations. Transportation accidents also pose risks, as illustrated by the occasional train derailment/explosion in the nightly news, or the semi-truck explosion detailed in the following section. Unlike other industrial accident scenarios, explosions can easily affect the general public, a dramatic example being the Pacific Engineering and Production Company of Nevada (PEPCON) plant disaster in 1988, where windows were shattered, doors were blown off their hinges, and flying glass and debris caused injuries up to 10 miles away.

While the relative rarity of accidental explosions speaks well of our understanding of the safety hazards to date, their violence rightly gives us pause. A better understanding of these materials is clearly still needed, but a significant barrier is the complexity of these materials and the various length-scales involved. In typical military applications, explosives are known to be ignited by the coalescence of hot spots that occur on micrometer scales. Whether this reaction remains a deflagration (burning) or builds to a detonation depends both on the stimulus and boundary conditions or level of confinement. Boundary conditions are typically on the scale of engineered parts, approximately meters. Additional dangers are present at the scale of trucks and factories. The interaction of various entities, such as barrels of fertilizer or crates of detonators, admits the possibility of a sympathetic detonation—that is, the unintended detonation of one entity by the explosion of another, generally caused by an explosive shock wave or blast fragments.

Although experimental work has been and will continue to be critical to developing our fundamental understanding of explosive initiation, deflagration, and detonation, there's no practical way to comprehensively assess safety on the scale of trucks and factories experimentally. The scenarios are too diverse and the costs too great. Numerical simulation provides a complementary tool that, with the steadily increasing computational power of the past decades, makes simulations at this scale begin to look plausible. Simulations at both the micrometer scale (the *mesoscale*) and at the scale of engineered parts (the *macroscale*), have contributed increasingly to our understanding of these materials. Still, simulations on this scale require both a massively parallel computational infrastructure and selective sampling of mesoscale response, such as advanced computational tools and modeling. With this in mind, we developed the computational framework Uintah (see www.uintah.utah.edu) for exactly this purpose.

Motivation

In 2005, a truck carrying 16,000 kilograms of seismic boosters, driving through Spanish Fork Canyon, Utah took a corner too quickly and overturned. The semi-truck caught fire and within three minutes detonated, creating a crater in the road approximately 24 meters wide and 10 meters deep (see Figure 1). The detonation hurled hot metal shards as far as one-quarter mile away, which started grass fires in the surrounding hills. Fortunately, the driver was coherent enough to relay to nearby drivers that the truck was carrying mining explosives, and to evacuate the area immediately. Only minor injuries were sustained, but if this had occurred in a densely populated region, the death toll could have been substantial. What has scientists and engineers puzzled is the extent of the damage. The crater's

Copublished by the IEEE CS and the AIP 1521-9615/13/$31.00 © 2013 IEEE

size and the lack of any unexploded boosters suggest that a mode of combustion called *detonation* occurred. The safety characteristics of a single device suggest detonation should never occur in transportation accidents; instead, a mild, relatively slow mode of combustion, called *deflagration*, should have occurred. In confined deflagrations, only a small percentage of the explosive is consumed before it's ejected away from the ignition site. We hypothesize that it was inertial confinement or the way the explosives were loaded inside the trailer that caused the deflagration reaction to transition into a detonation. This accident, along with several other petascale simulation efforts, has driven the development of the Uintah Computational Framework. The complex physics of this accident requires modeling at multiple spatial and temporal scales to provide predictive simulations.

Because the reaction rates and subsequent energy release rates of deflagration and detonation differ by roughly five orders of magnitude, a Deflagration-to-Detonation Transition (DDT) leads to extremely violent events. The mechanism of a DDT in solids is still unknown, but various mechanisms have been proposed. One such mechanism involves the advection of hot combustion gases through cracks in the explosive, a process called *convective deflagration*. Convective deflagration occurs when the pressure outside a damaged combustible forces hot gases into the explosive, increasing the burning surface area, damaging the material in several different directions simultaneously, and accelerating the reaction. In this particular accident, 8,400 explosive boosters were arranged in a way that's reminiscent of a porous material rather than a monolithic solid. We suspect that the convective burning mechanism was partially responsible for DDT. Using large-scale simulations, we intend to investigate why DDT occurred and determine if inertial confinement contributed to the detonation. If inertial confinement was the cause, we'll use our simulation capabilities to suggest alternative, safe packing configurations.

Figure 1. A 24-meter-wide crater produced from an unexpected Deflagration-to-Detonation Transition (DDT) of 16,000 kilograms of high explosives, carried by a truck through Spanish Fork Canyon, Utah.

Challenges in Modeling Explosives

The deflagration-to-detonation transition of high explosive materials is a multistep process with fluid-structure interactions (FSIs) during the slow deflagration and rapid detonation regimes. As deflagration is occurring, a cold solid reactant is heated to the point of ignition to form hot gas, which can flow through pores or cracks in the damaged material. The greatest difficulty of a DDT simulation is accurately modeling stress-induced material damage so that it statistically captures cracking and the formation of pores in the explosive, which allows convective burning in the cracks.

Cracking, porosity, and convective burning are difficult to capture at the macroscale, due to averaging, necessitating the use of statistically based, subgrid scale models. Mesoscale modeling has the potential to provide the statistics needed for subgrid models that live on the discrete elements of the simulation domain. Mesoscale simulations are computationally expensive, requiring sophisticated material models capable of capturing the material fracture, elastic yield, plastic flow, melting, and heating due to the energy conversion from these forms of mechanical work. Finally, detailed reaction modeling of explosives at the mesoscale involves many reaction species and the complex interplay of the reacting species further complicates the problem. The development of simple reaction models that capture the complex behaviors at this scale are needed, which we'll discuss later.

Uintah Computational Framework

The open source (MIT license) Uintah software originated in the University of Utah Department of

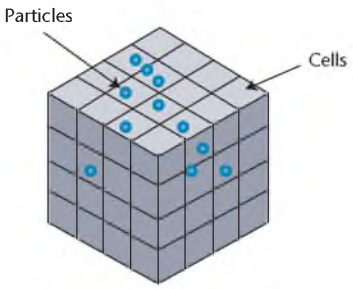

Figure 2. The Uintah patch—a Uintah mesh with particles. The Implicit, Continuous-fluid Eulerian (ICE) algorithm uses a hexahedral block of cells and the Material Point Method (MPM) particles reside within that block.

Energy (DOE) Center for the Simulation of Accidental Fires and Explosions (C-SAFE),[2] and has been in use for a number of years. The present status of Uintah, including applications, documentation, and releases, is described in a recent report.[3] Uintah is a computational framework that integrates multiple simulation components, analyzes the data dependencies and communication patterns between them, and efficiently executes the resulting multiphysics simulation. Uintah presently contains four main simulation components or algorithms:

- the finite volume mulitmaterial computational flow dynamics (CFD) formulation (the Implicit, Continuous-fluid Eulerian algorithm, or ICE),[4,5]
- the Material Point Method (MPM)[6] for structural mechanics,
- the combined FSI algorithm MPMICE,[7] and
- the ARCHES turbulent-reacting Large Eddy CFD component.[8]

Uintah exhibits good scalability characteristics,[9] runs on both National Science Foundation (NSF) and DOE parallel computers (Stampede, Kraken, Titan, Lonestar, and Vesta), and is used by many National Nuclear Security Association (NNSA), Department of Defense (DOD), DOE, and NSF projects.

The main Uintah component used in this research is the MPMICE, in which the multimaterial CFD formulation (ICE) is used to model fluids, and the MPM code is used to model the solid explosive. The ICE algorithm uses a hexahedral block of cells and the MPM particles reside within that block as shown in Figure 2.

A unique feature of Uintah is that the application developer is only asked to write code to solve equations on a hexahedral patch of the computational domain, and doesn't have to worry about parallelism and communications between patches, because this is all automatically resolved by the framework. The Uintah computation framework has a wide range of material models, reaction models, and equations of state that allow simulations of exothermic FSIs at different length- and time-scales. These embedded models live inside a framework that hides the method's parallelization, allowing simple science or engineering models to scale to hundreds of thousands of processors.

Fluid-Structure Interactions

Our methodology for solving FSIs uses a strong coupling between the fluid and solid phases, with a full Navier-Stokes representation of the fluids and transient, nonlinear response of the solids, including exothermic solid-to-gas reactions. The Eulerian-based ICE method[4,5] is used to represent materials on a hexahedral grid. It allows simulation of complex gas flows with heat and momentum coupling inside a compressible flow paradigm. For solid mechanics, a Lagrangian-based MPM[6] is used that's capable of simulating complex behaviors, including material damage, stress and strain, and elastic and plastic responses.

The algorithm has its foundation in a "multimaterial" CFD approach in which each material (either fluid or solid) is defined at the continuum level over the entire computational domain, including regions where a material doesn't exist. In addition to the physical state (that is, mass, momentum, and energy) at each discrete point, the volume fraction of each material is tracked with the constraint that the volume fractions of all materials must sum to unity in any grid cell.[4]

To solve the discretized multimaterial equations, we use a cell-centered formulation of the ICE method of Harlow, further developed by Kashiwa and others at the Los Alamos National Laboratory.[4,5] The use of a cell-centered, finite volume solution technique is convenient in that a single control volume is used for all materials, simplifying the conservation of mass, momentum, and energy, and the exchange of these quantities between the materials. The method is fully compressible, an important consideration in simulations involving explosions of any type, particularly detonations. In addition to the source terms present in any CFD formulation, the multimaterial equations also include exchange terms for mass, momentum, and heat. Intermaterial mass exchange is based on the reaction models, such as those described in the next section. Momentum and heat exchange is typically modeled as a drag law based on relative material velocities or temperatures, respectively, computed in a point-wise implicit manner to ensure conservation.

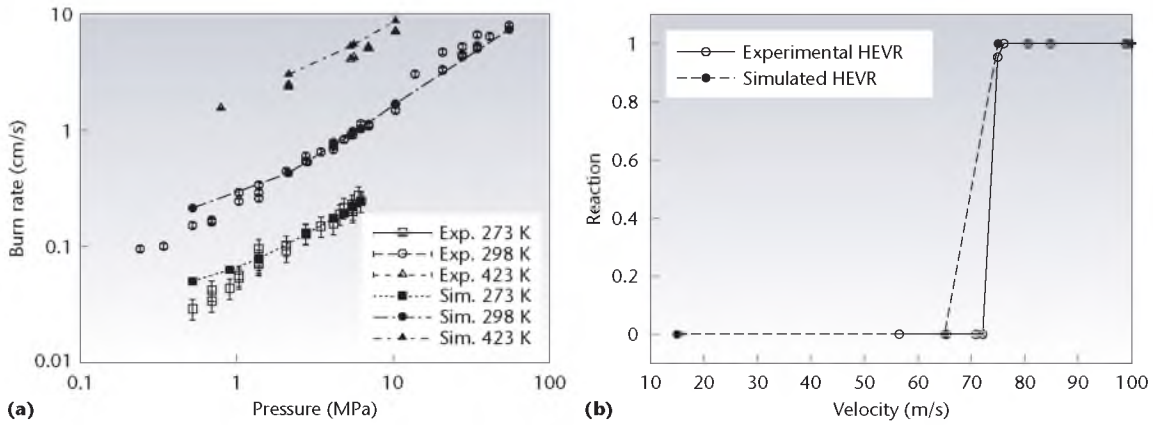

Figure 3. DDT reaction model results compared with experimental results. (a) The burn rate at three initial solid temperatures versus pressure where simulated data is compared against data from A.I. Atwood and her colleagues for the plastic-bonded explosive PBX9501.[18] (b) Comparison of the threshold for reaction against velocity for weak impacts.[20] Plots used with permission from Joseph Peterson and Charles Wight.[16] (HEVR = high explosive violent reaction.)

This formulation makes no explicit distinction between the fluid and solid materials in the model equations. FSIs aren't tracked, nor are boundary conditions passed through them. To maintain the integrity of the fluid-solid interface and provide a mechanism to track the deformation history of the solid(s), we employ the Lagrangian particle technique MPM. The MPM is used to evolve the equations of motion for solid materials, in part on account of advantages in interfacing with the ICE method. The MPM[6] is an extension to solid mechanics of the Fluid-Implicit-Particle (FLIP) method,[10] which is a particle-in-cell method for fluid-flow simulations. Development of the MPM has continued, both studying and improving the MPM algorithm,[11,12] as well as extending the technique by generalizing particle shapes.[13] The MPM has become a powerful technique for computational solid mechanics in its own right, and has found favor in applications involving complex geometries,[14] contact mechanics,[13] large deformations, and fracture,[15] to name a few.

Lagrangian particles or material points are used to discretize a material's volume, and each particle carries state information (such as mass, volume, velocity, and stress) about the portion of the material that it represents. Our implementation uses a Cartesian grid as a computational scratchpad for computing spatial gradients—the same grid used by the ICE component. In MPM, particles with properties (such as velocity or mass) are defined on a mesh, and particle properties are then mapped onto the mesh points. Forces, accelerations, and velocities are then calculated on the mesh points. The mesh-point motion is calculated, but only particles are moved by mapping velocities back to particles.

The combination of MPM and the multimaterial CFD algorithm to form our FSIs algorithm (MPMICE) involves a complex 14-step algorithm described elsewhere.[7] What makes this methodology unique is that the exchange of mass, momentum, and energy between the solid reactant and product gases occurs in the governing equations, and also that boundary conditions aren't applied to tracked surfaces. Clearly, surface tracking in these types of simulations would be difficult.

Deflagration and Detonation Models

Our reaction models convert mass from the energetic materials (for example, the plastic-bonded explosive PBX9501) to product gases, with the appropriate release of heat and exchange of momentum. Uintah now includes models validated against various detonation, deflagration, DDT, and shock-to-detonation transition (SDT) experiments. These models give us the capability to simulate steady and unsteady thermally activated deflagration and pressure-induced detonation of high explosives, including the DDT.[16]

The numerical model for deflagration is based on a two-step global kinetics model described by M.J. Ward, S.F. Son, and M.Q. Brewster (called WSB).[17] As originally formulated, this model predicts the steady combustion rate of the energetics as a function of the product gas's pressure and the solid material's temperature. We extended the 1D WSB model to 3D, and validated the parameters against the experimental strand burner measurements of A.I. Atwood and her colleagues for the correct temperature and pressure dependence of the burn rate.[18,19] Figure 3 shows a validation of our burn model over a range of temperatures and pressures.

A simple shock-to-detonation model known as JWL++[21] is used to simulate detonation formed when a

shock wave, initiated by a mechanical insult, passes through the explosive. The model captures the SDT as a function of pressure in the solid-gas mixture, allowing for the advantageous use of simple equations of state. These equations of state model pressure at high-compression levels, while neglecting the calculation of complicated material processes. Shock-based ignition can occur when an explosive is dropped or perhaps impacted by a forklift or other moving objects, and has the potential to lead to an accidental explosion. We validated our SDT model with a standard test developed at Los Alamos National Laboratory, in which an approximate 0.15-meter radius, hockey puck-shaped explosive is impacted at increasing speeds. A sharp speed threshold was observed in impact under about 75 meters per second (m/s), which caused cracking and other material damage but no reaction, while anything higher caused an explosion. Figure 3 compares experimental and simulated results for the test, where "0" indicates cracking and material damage, while "1" indicates a highly explosive, violent reaction.

The general approach for simulating the DDT process relies on the idea that high pressure forces hot gases through the voids (pores, cracks, and so on) in an explosive, which increases the reaction rate. Relating this to the normal factors cited for causing DDT, such as hot-spot nucleation and growth, shear and heating of a solid near hot-cavity gases, and frictional heating, leads to the startling conclusion that all of these phenomena can be related to the simple process of hot products of reaction flowing through the solid explosive. By merging the WSB deflagration model with the JWL++ detonation model inside a fluid-structure algorithm with a few experimentally derived thresholds, we're able to model the DDT in solid materials.

Our DDT model agreed well with experimental data for the pressure and temperature dependence of the burn rate and detonation velocities (see Figure 3), including *convective deflagration* propagation. Convective deflagration is the process of burning within the cracks of the energetic solid, rapidly increasing the reaction rates and pressure. Without convective deflagration, DDT wouldn't occur in an unconfined explosive, because deflagration would only occur on the solid's surface. We're able to model convective deflagration by using a crack model that describes the crack development as a function of pressure.[22] With this model, we're able to represent a material's damage, dependent on the surface pressure and the propagation of the reaction through a damaged explosive.

Scaling

Modeling explosions from mesoscale up to a full semi-truck requires a linearly scalable framework—in other words, the time to solution decreases with the number of processing units. Though mesoscale simulations are small in physical size, they can be computationally expensive, when the explosive grains and binders are fully resolved. At the other end of the scale, simulating an entire semi-truck with high spatial resolution is also expensive, and requires the largest computing platforms. The Uintah Computational Framework has been shown to linearly scale from 16 cores to 256,000 cores, running the MPMICE component. This scalability has relied heavily upon the asynchronous task-graph approach that allows components to be written as a series of tasks, where each task is a major step in the MPMICE algorithm. Each task has required inputs from the data warehouse and writes outputs to the data warehouse. The actual execution of the tasks is managed by a runtime system that maps the tasks onto processors after an analysis of the task's data dependencies. Figure 4 shows an example of a high-level Uintah task graph for the MPM.

The scalability of Uintah has proceeded in three distinct phases. In Phase 1 (1998–2005), Uintah overlapped communications with computation and executed the task graph in a static manner using standard data structures and one message-passing process per core (see www.uintah.utah.edu).[23] In the second phase, the data structures were greatly improved and fast mesh-refinement algorithms were developed to scale to 100,000 cores.[9,24,25] In this phase, tasks were executed in a dynamic or even out-of-order way. Finally, in the third and current phase, we're moving to a hybrid MPI-Pthread model, in which there's only one MPI process per node and individual task threads are bound to available CPU cores. Individual tasks are sent to available CPU cores and GPUs when available. This approach reduces the total global memory usage per node by up to 90 percent on the Jaguar XT5 system.[26] Using a recently designed decentralized multithreaded scheduler and lock-free data warehouse, the overhead of using this hybrid approach has been significantly reduced, and both

single-node performance and overall scalability of Uintah are further improved.[27]

The scalability of the MPMICE component used for modeling explosives with adaptive mesh refinement has been tested in both the weak and strong sense on the Jaguar XK6 system.[27] The performance was tested with four problem sizes, with each problem containing approximately eight times as many cells as the previous problem. The numbers of particles representing the solid material created in the four runs were 7.1 million, 56.6 million, 452.9 million, and 3.62 billion respectively. The grid contained three levels of mesh refinement, with each level being a factor of four more refined than the coarser level. Figure 5 shows good weak and strong scaling, for macroscale simulations up to 256,000 cores on the then Jaguar XK6 (now Titan) architecture at DOEs Oak Ridge Laboratory.[27]

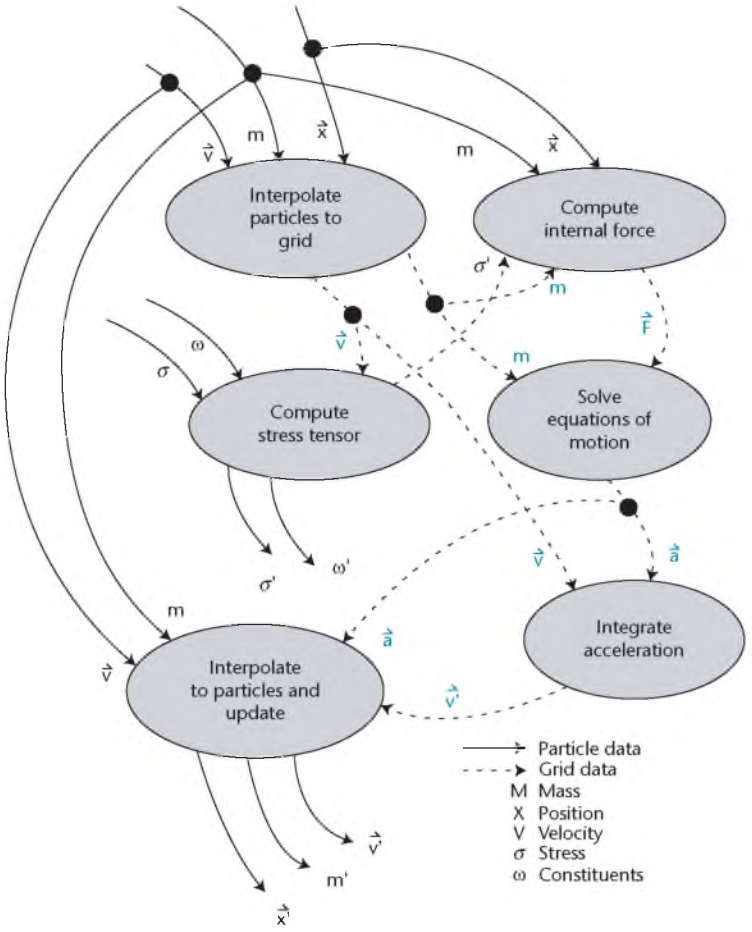

Figure 4. An example of a Uintah task graph for the MPM.

Mesoscale Explosions

When the relevant physics occurs on scales smaller than the computational resolution, additional information is needed. For accidental explosions, the vast majority of the simulation scenario needs only to resolve the macroscale. However, ignition occurs on the mesoscale, by the coalescence of hot spots. Hot spots are energy-localizing mechanisms that occur on the scale of explosive heterogeneity—that is, the explosive grains. There are many possible hot-spot mechanisms,[28] and it's clear that the dominant mechanisms vary with the scenario considered. Here, we use mesoscale simulations to gain insight into the ignition process. Our long-term goal is to judiciously place mesoscale simulations directly in macroscale simulations, to resolve hot-spot distributions and predict ignition in areas of interest. These simulations bridge the gap between molecular and macroscale modeling.

At the micrometer-length scale, interactions between explosive grains and the plastic binder that hold them together, or other explosive grains, are explicitly resolved (see Figure 6). When the binder and grains are fully resolved, we can investigate the different mechanisms. When a sufficient force is applied to the explosive and binder, there will be plastic deformation or work that generates hot spots, as Figure 6c shows. These hot spots could either dissipate their energy to colder surrounding material, or coalesce and cause a sustained reaction, depending on their size, intensity, and number density.

Initially, our studies utilized idealized geometries of the explosive grains that were impacted by a piston at varying speeds and compared against experimental results.[29] These studies were designed to validate our material model, which includes the elastic and plastic response as well as temperature-varying thermal parameters. We compared the velocity and stress traces at the impact surface, for all of the impact speeds, and found good comparison within 10 percent.[29] With this agreement, we sought to study hot-spot distributions to find what

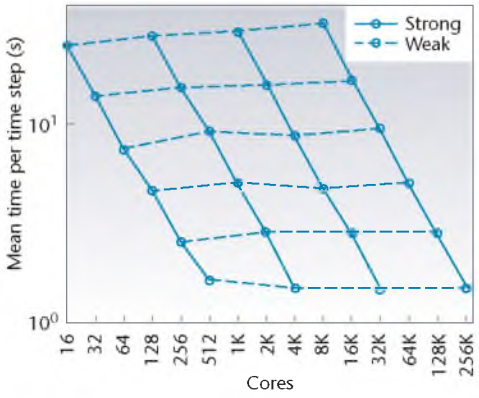

Figure 5. Strong and weak scaling of an MPMICE problem with a steel container traveling at Mach-2 through ideal gas.[27] We used adaptive mesh refinement.

critical densities could cause a sustained reaction.

The WSB reaction model was used to determine if the hot spots could sustain a reaction.[17] The simple temperature threshold used in the original formulation[19] was incorrect at the time- and length-scales of the mesoscale simulation, necessitating the use of an Arrhenius-based adiabatic induction time model. The model is able to capture the time to rapid reaction based on the local temperature in the material. We applied this model to impacts of approximately 100 and 700 m/s. An insufficient number of hot spots were formed in the low-velocity impact, and the reaction was ultimately quenched. At the high-velocity impact, the material temperature rises immediately, and a sustained reaction is formed as one pore is collapsed (see Figure 6d). The reaction then propagated through the bed. These results are qualitatively in agreement with experiments. Further investigation is needed to see if the model is able to capture hot-spot criticality for the initiation of rapid reaction that was seen to be somewhere in the range of 400–500 m/s for the scenario studied.

It's unlikely that idealized mesoscale geometries will result in the same hot-spot distributions and the same ignition behavior as real explosives. X-ray microtomography has been used to determine mesoscale morphology for a mock explosive, as seen in Figure 6a. Analysis of this mesostructure gave grain-sized distributions in good agreement with formulation measurements. Fractured bits, as well as conglomerates (see Figure 6b) created during formulation, were also identified. Using these same morphological tools, hot-spot size and shape distributions were quantified. An example calculation, with hot spots depicted in magenta, may be seen in Figure 6b. It was found that different mock materials had substantially different grain and simulated hot-spot morphologies.

We're in the process of studying the critical-impact velocity that our model predicts, and the associated hot-spot distributions from our idealized simulations. Looking further, we plan to use full 3D simulations of the real microstructures to either validate or refute the utility of the ideal simulations. The knowledge learned from these simulations will then be used to develop subgrid scale models that are applicable on the millimeter-length scale to validate our current work on truck-sized explosions (see Figure 6e).

Macroscale Explosions

The exact mechanism of DDT is still being investigated, but numerical analysis has shown that this transition takes place when the local pressure exceeds a threshold of 5.3 gigapascals (GPa) for the explosive PBX9501. What's interesting about this pressure is that under adiabatic conditions, the deflagration of PBX9501 will produce pressures around 2 GPa—far below what's required for detonation. To investigate the possible mechanism, we ran small-scale (a few millimeters) simulations of confined PBX9501. In these simulations the explosive was enclosed in a steel shell and heated externally. We discovered that the collision of two pressure waves yielded the pressures needed for detonation (see Figure 7).[30] By analyzing the interference of the waves over a range of device sizes and applied heat fluxes, a trend was discovered. Depending upon the applied heat flux, the convective deflagration traversed the explosives at different rates, producing pressure waves. Depending upon the heating rate, the origins of the pressure waves and the resulting interference pattern varied.

In a separate series of simulations, we looked at the crack propagation and the resultant flame-propagation velocities, and qualitatively compared them with experiments.[31] In these tests, a hot wire ignited a disk of explosives in the center and high-speed photography captured the crack and flame-propagation velocities and patterns (see Figure 8). These results are an important step towards simulating explosions at the semi-truck scale, and show the utility of subgrid-scale statistical models for material damage and crack propagation in macroscale simulations.

The ultimate goal of our research is to assess the safety of transporting arrays of explosives. Specifically, we're interested in the 2005 transportation accident described in the motivation section, since a detonation should not have occurred. Our macroscale simulations involve homogeneous solid materials to

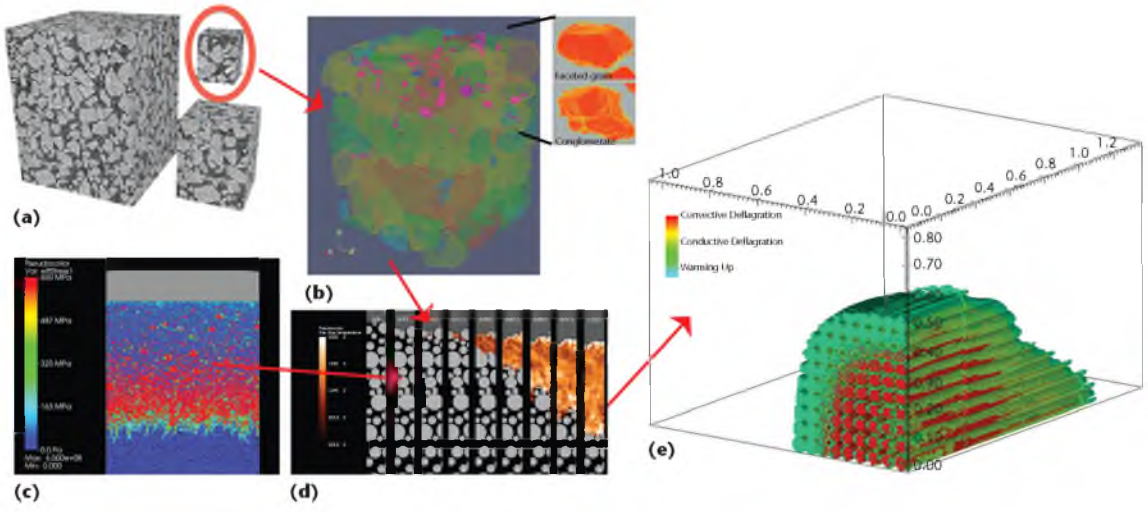

Figure 6. A schematic of how mesoscale simulations can be used to inform macroscale simulations. (a, b) Real microstructures can be included in shock studies and hot-spot distributions can be quantified. At the same time, idealized microstructures can be used to study many different initial setups and (c, d) the resulting reactions. Real microstructure simulations can be used to validate the idealized microstructures when possible, which will provide some certainty of the validity of the idealized simulations. From the many-varied simulation setups for the idealized simulations, statistics can be extracted regarding hot-spot distributions, average reaction rates, and time to reaction as a function of some metric such as the average stress rate. These can then be formulated as subgrid scale models that are used in macroscale simulations, such as those damage and cracking materials we already use. (e) The deflagration on the macroscale of explosive cylinders using the reaction models validated on the mesoscale. In this simulation, deflagration and convective burning can propagate as far as 0.5 m or more prior to detonation. (MPa = megapascal.)

represent the PBX9501 grains and binder. With validation from mesoscale simulations and experimental data, we developed reaction models for deflagration and detonation that are helping us understand the underlying mechanism of DDT. To keep the computational costs reasonable, the reaction models rely on a global kinetics model, with the understanding that reactants go to products at a known energy release.

In the 2005 accident, explosive cylinders were packaged in boxes containing approximately 20 cylindrical boosters, 5.7 cm in diameter, ranging from 33–74 cm in length. Our simulations are being used to investigate if inertial confinement was a significant contributor to the DDT, considering how the explosives were packed in the semi-truck. Determining the level of confinement needed for DDT is computationally expensive, requiring machines like Titan. Through our simulation, we hope to understand how pressures can reach the necessary threshold and produce an extremely violent detonation reaction. We hypothesize that the individual boosters reacted and the pressure forces deformed the nearby unreacted boosters, creating "pores" or regions where the product gases were trapped. Pressure or stress waves propagated outward from the "pores" and collided, forming regions of high pressure, sufficient for a DDT.

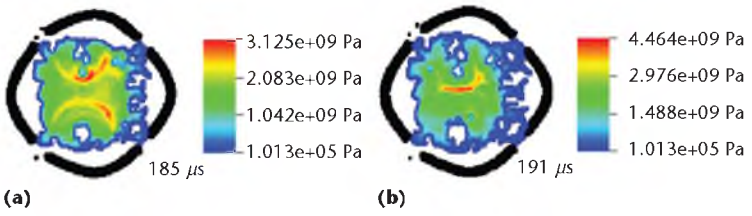

Figure 7. A simulation of a square explosive device heated on one side. As the material decomposes, the pressure increases, deforming the steel case (shown in black) until it ruptures. Pockets of hot combustion gas cause stress waves to propagate out from those points. These waves can collide, forming a high-pressure region that initiates a detonation. (Pa = pascal; μs = microseconds.)

Figure 9 shows results from our initial effort. In the simulation, we used realistic booster geometries ignited by hot gas (in the lower left corner of each graph), with burning propagating outward. These preliminary results suggest that inertial confinement can lead to a DDT. These results are preliminary, and we used artificial wall boundaries in the x, y, and z directions. This research is ongoing, and we're looking

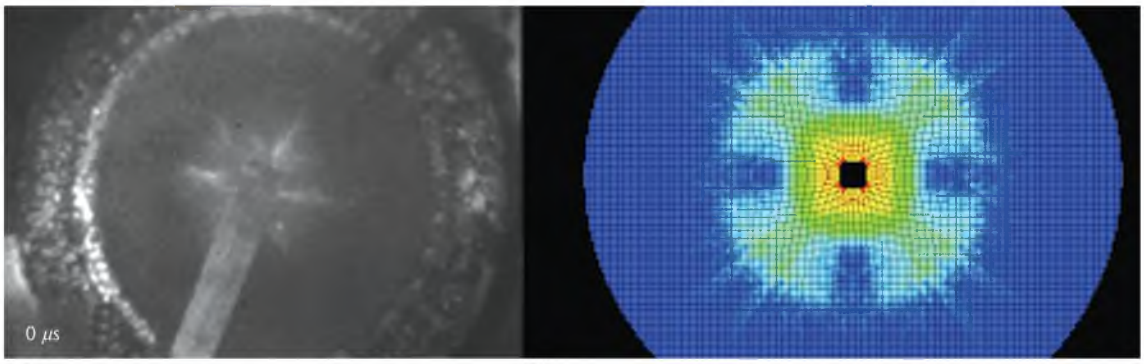

Figure 8. Comparison of an experiment with a simulation. A one-inch hockey puck-shaped disk is heated to just under the ignition point of the material, approximately 200° C, and then ignited via a wire in the center. In the experiment shown on the left, cracks can be seen to form as the reaction stresses the material, and convective burning spreads through the cracks, which is seen as regions of high illumination.[31] The simulation at the same physical time shows considerably more cracking, but the general structures appear to be similar. The subgrid scale cracking/damage model we use, as well as the convective burning model, result in similar reaction characteristics. The plots shown are used with permission.[31]

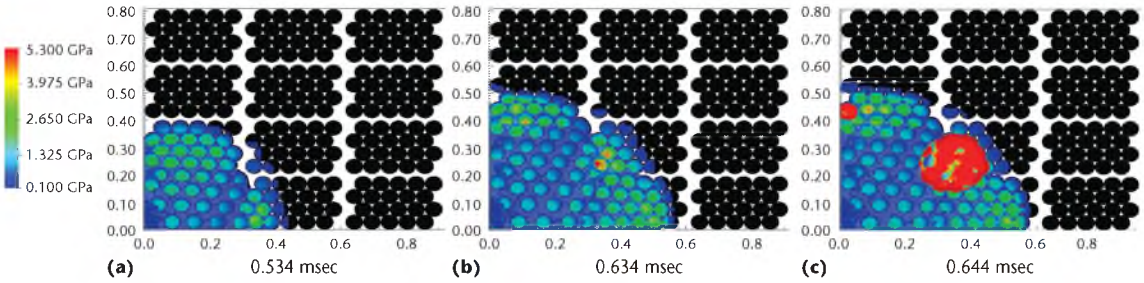

Figure 9. Pressure profile of a DDT in an array of tightly packed explosive cylinders confined by symmetric boundaries on all sides: (a) at 0.534 milliseconds (msec), (b) at 0.634 msec, and (c) at 0.644 msec. Realistic booster geometries were used. Thermally activated deflagration occurred in the lower left corner. This simulation suggests inertial confinement can be reached with six cases of tightly packaged explosives, as seen by detonation (in red) occurring before the pressure wave hits a symmetric boundary.

at how the explosive boosters interact without wall boundaries. These simulations are being run on Oak Ridge's Titan machine.

With a strong understanding of the inertial confinement needed for DDT to occur in an array of explosives, considerations will be made on the proper packing configuration needed to prevent large transportation accidents. The main goal is to reduce the possibility of the pressure building to the detonation threshold, diminishing the risk of a detonation transition.

Our approach to preventing a DDT in truck-size shipments of explosives is to simulate the effect of packing arrangements that can avoid inertial confinement and rapid pressurization that causes the DDT. Considerations will be made for a variety of "what-if" local packing geometries (for example, a 3D checkerboard with alternating empty containers) as well as more global arrangements (large open areas in the center of the load) to maximize the mitigation effect on explosion violence without compromising the load's structural integrity.

The capability of modeling explosive devices on a wide range of temporal and spatial scales will give great insight into the many chemical and physical processes involved with explosives. Although a great deal of our focus is on the DDT, the Uintah Computational Framework has the capability of one day modeling all aspects of explosives and similar substances.

Acknowledgments

We especially thank Monica Hall, John Schmidt, and James Guilkey. This work was supported by US National Science Foundation (NSF) PetaApps award 0905068. Uintah was developed by the University of Utah's Center for

the Simulation of Accidental Fires and Explosions (C-SAFE) and funded by the Department of Energy (DOE), subcontract B524196. This research used resources of the Oak Ridge Leadership Computing Facility at the Oak Ridge National Laboratory, which is supported by the Office of Science of the US DOE under contract DE-AC05-00OR22725 (subaward ENP009). This work also used the Extreme Science and Engineering Discovery Environment (XSEDE), which is supported by NSF grant OCI1053575 (subaward TGMCA08X004).

References

1. S.A. Survey, *Unplanned Explosions at Munitions Sites*, tech. report, Small Arms Survey, Mar. 2013.
2. T.C. Henderson et al., "Simulating Accidental Fires and Explosions," *Computing in Science & Eng.*, vol. 2, no. 2, 2000, pp. 64–76.
3. M. Berzins, *Status of Release of the Uintah Computational Framework*, tech. report UUSCI-2012-001, *Scientific Computing and Imaging (SCI) Inst.*, Univ. Utah, 2012.
4. B.A. Kashiwa, *A Multifield Model and Method for Fluid-Structure Interaction Dynamics*, tech. report LA-UR-01-1136, Los Alamos Nat'l Laboratory, 2001.
5. B.A. Kashiwa et al., *A Cell-Centered ICE Method for Multiphase Flow Simulations*, tech. report LA-UR-93-3922, Los Alamos Nat'l Laboratory, 1994.
6. D. Sulsky, S. Zhou, and H.L. Schreyer, "Application of a Particle-in-Cell Method to Solid Mechanics," *Computer Physics Comm.*, vol. 87, nos. 1–2, 1995, pp. 236–252.
7. J.E. Guilkey, T.B. Harman, and B. Banerjee, "An Eulerian-Lagrangian Approach for Simulating Explosions of Energetic Devices," *Computers and Structures*, vol. 85, nos. 11–14, 2007, pp. 660–674.
8. J. Spinti et al., "Heat Transfer to Objects in Pool Fires," *Transport Phenomena in Fires*, WIT Press, 2008.
9. J. Luitjens and M. Berzins, "Improving the Performance of Uintah: A Large-Scale Adaptive Meshing Computational Framework," *Proc. 24th IEEE Int'l Parallel and Distributed Processing Symp.*, IEEE, 2010; http://ieeexplore.ieee.org/xpl/abstractKeywords.jsp?reload=true&arnumber=5470437.
10. J.U. Brackbill and H.M. Ruppel, "FLIP: A Method for Adaptively Zoned, Particle-in-Cell Calculations of Fluid Flows in Two Dimensions," *J. Computational Physics*, vol. 65, no. 2, 1986, pp. 314–343.
11. S.G. Bardenhagen, "Energy Conservation Error in the Material Point Method for Solid Mechanics," *J. Computational Physics*, vol. 180, no. 1, 2002, pp. 383–403.
12. M. Steffen, R. M. Kirby, and M. Berzins, "Decoupling and Balancing of Space and Time Errors in the Material Point Method (MPM)," *Int'l J. for Numerical Methods in Eng.*, vol. 82, no. 10, 2010, pp. 1207–1243.
13. S.G. Bardenhagen, J.U. Brackbill, and D. Sulsky, "Numerical Study of Stress Distribution in Sheared Granular Material in Two Dimensions, *Physical Review E*, vol. 62, 2000, pp. 3882–3890.
14. A.D. Brydon et al., "Simulation of the Densification of Real Open-Celled Foam Microstructures," *J. Mechanics and Physics of Solids*, vol. 53, no. 12, 2005, pp. 2638–2660.
15. S.G. Bardenhagen, J.A. Nairn, and H. Lu, "Simulation of Dynamic Fracture with the Material Point Method Using a Mixed J-Integral and Cohesive Law Approach," *Int'l J. Fracture*, vol. 170, no. 1, 2011, pp. 49–66.
16. J.R. Peterson and C.A. Wight, "An Eulerian-Lagrangian Computational Model for Deflagration and Detonation of High Explosives," *J. Combustion and Flame*, vol. 159, no. 7, 2012, pp. 2491–2499.
17. M.J. Ward, S.F. Son, and M.Q. Brewster, "Steady Deflagration of HMX with Simple Kinetics: A Gas Phase Chain Reaction Model," *Combustion and Flame*, vol. 114, nos. 3–4, 1998, pp. 556–568.
18. A.I. Atwood et al., "Burning Rate of Solid Propellant Ingredients, Part 1: Pressure and Initial Temperature Effects," *J. Propulsion and Power*, vol. 15, no. 6, 1999, pp. 740–747.
19. C.A. Wight and E.G. Eddings, "Science-Based Simulation Tools for Hazard Assessment and Mitigation," *Advancements in Energetic Materials and Chemical Propulsion*, vol. 114, no. 5, 2008, pp. 921–937.
20. C.M. Tarver and S.K. Chidester, "On the Violence of High Explosive Reactions," *J. Pressure Vessel Technology*, vol. 127, no. 1, 2005, pp. 39–48.
21. P.C. Souers et al., "JWL++: A Simple Reactive Flow Code Package for Detonation," *Propellants, Explosives, Pyrotechnics*, vol. 25, no. 2, 2000, pp. 54–58.
22. H.L. Berghout et al., "Combustion of Damaged PBX9501 Explosive," *Thermochimica Acta*, vol. 384, nos. 1–2, 2002, pp. 261–277.
23. S.G. Parker, J. Guilkey, and T. Harman, "A Component-Based Parallel Infrastructure for the Simulation of Fluid Structure Interaction," *Eng. with Computers*, vol. 22, nos. 3–4, 2006, pp. 277–292.
24. J. Luitjens and M. Berzins, "Scalable Parallel Regridding Algorithms for Block-Structured Adaptive Mesh Refinement," *J. Concurrency and Computation: Practice and Experience*, vol. 23, no. 13, 2011, pp. 1522–1537.
25. M. Berzins et al., "Uintah: A Scalable Framework for Hazard Analysis," *Proc. Teragrid 2010*, ACM, 2010; doi:10.1145/1838574.1838577.
26. Q. Meng, M. Berzins, and J. Schmidt, "Using Hybrid Parallelism to Improve Memory Use in the Uintah Framework," *Proc. Teragrid 2011*, ACM, 2011 doi:10.1145/2016741.2016767.

27. Q. Meng and M. Berzins, *Scalable Large-Scale Fluid-Structure Interaction Solvers in the Uintah Framework via Hybrid Task-based Parallelism Algorithms*, tech. report UUSCI-2012-004, SCI Inst., Univ. of Utah, 2012.
28. R.W. Armstrong, S.G. Bardenhagen, and W.L. Elban, "Deformation-Induced Hot Spot Consequences of AP and RDX Crystal Hardness Measurements," *J. Energetic Materials and Chemical Propulsion*, vol. 11, no. 5, 2012, pp. 413–425.
29. J.R. Peterson et al., "Multiscale Modeling of High Explosives for Transportation Accidents," *Proc. 2012 XSEDE Conf.*, ACM, 2012; http://doi.acm.org/10.1145/2335755.2335828.
30. M. Hall et al., "The Influence of an Applied Heat Flux on the Violence of Reaction of an Explosive Device," *Proc. 2013 XSEDE Conf.*, ACM, to be published, 2013.
31. P.M. Dickson et al., "Thermal Cook-Off Response of Confined PBX 9501," *The Royal Society A*, vol. 460, no. 2052, 2004, pp. 3447–3455.

Jacqueline Beckvermit is a research assistant and PhD candidate in the School of Science at the University of Utah. Her research interests include combustion of energetic materials and high performance computing of energetic materials. Beckvermit has a BS in chemistry from Fort Lewis College. Contact her at beckvermit@gmail.com.

Joseph Peterson is a research assistant in the School of Chemical Sciences and a PhD candidate at the University of Illinois at Urbana-Champaign. His research interests include combustion and energetic materials, microbial regulation and metabolism, and physics simulations. Peterson has a BS in chemistry and a BS in computer science from the University of Utah. Contact him at jrptrsn3@illinois.edu.

Todd Harman is an assistant research professor in the Department of Mechanical Engineering at the University of Utah. His research interests include fluid-structure interaction, computational fluid dynamics, and high-performance computing. Harman has a PhD in mechanical engineering from the University of Utah. Contact him at t.harman@utah.edu.

Scott Bardenhagen is the owner and chief scientist at Mesomechanics. His research interests include the mechanics of mesostructured materials such as composites, foams, and granular materials, as well as bridging material scales (from atomistic through continuum). Bardenhagen has a PhD in aerospace engineering from the University of Michigan. Contact him at bard@mesomechanics.com.

Charles A. Wight is the president of Weber State University and an adjunct professor of chemistry at the University of Utah. His research interests include chemistry of energetic materials and high-performance computer simulations of explosives and explosions. Wight has a PhD in chemistry from the California Institute of Technology. Contact him atpresident@weber.edu.

Qingyu Meng is a research assistant in the Scientific Computing and Imaging (SCI) Institute and a PhD candidate in the School of Computing at the University of Utah. His research interests include parallel computing and distributed runtime systems. Meng has a BS in computer science from the University of Science and Technology of China. Contact him atqymeng@cs.utah.edu.

Martin Berzins is a professor of computer science in both the School of Computing and in the SCI Institute at the University of Utah. He has worked in the fields of mathematical software, numerical analysis, and parallel computing with application to challenging problems in science and engineering. Berzins has a PhD in mathematical software and numerical analysis from the University of Leeds. Contact him at mb@sci.utah.edu.

CHAPTER 3

MODIFIED JWL EQUATION OF STATE FOR NEAR ATMOSPHERIC CONDITIONS

One of the equations of state commonly used for describing the combustion reactants and products of solid explosives is the Jones-Wilkins-Lee Equation of State (JWL EOS). This EOS was first developed to describe the expansion of detonation products,[1] and was later used to describe the reactants in shock-initiated reactions.[2] In our application, simulation of DDT, it is necessary to utilize an EOS that is valid over an extremely wide range of temperatures and pressures where solids and gases are in intimate contact. We have therefore developed a modified version of the JWL EOS in which the high-pressure properties around the Chapman-Jouguet (CJ) state are unchanged, but low-pressure behavior has been modified to be consistent with interactions with gases.

The temperature-dependent JWL EOS uses pressure, volume, and energy to describe the isothermal expansion of an explosive material, and is defined as

$$P_{JWL} = Ae^{-R_1 V_r} + Be^{-R_2 V_r} + \frac{\omega C_v T}{V_r}. \tag{3.1}$$

The equation consists of the temperature, T, relative volume, $V_r = V/V_0 = \rho_0/\rho$, constant specific heat, C_v, the Gruneisen coefficient, ω, and four fit parameters, A, B, R_1, and R_2. The constants A and B were calculated from the total energy available determined from detonation calorimetry experiments, detonation velocity, the CJ pressure, and initial density. R_1 and R_2 are linear coefficients calculated to fit the experimental expansion data of a cylinder test.[1–3] The parameters were chosen to satisfy four conditions: (1) the EOS must follow the measured CJ state, (2) the equation must match the experimentally determined cylinder test expansion behavior, (3) thermodynamic limits for large expansions must be considered, and (4) the equation must maintain hydrodynamic continuity.[1]

The cylinder test is a standard experiment designed to measure the explosives ability to accelerate metal and the expansion of the detonation products. The experiment consists of a cylinder of solid explosive confined by a copper tube and detonated at one end. The deto-

nation is initiated by an exploding bridgewire detonator. This produces a shock, putting the explosive material in compression, and transitions to a detonation. The detonation velocity is measured by fine electrical pin wires placed inside the cylinder, and the displacement of the metal is measured by a streak camera.[4] The validity of the JWL EOS in the Uintah Computational Framework for the reactants and products was examined by reproducing the cylinder test.[5] The simulations resulted in a less then 8%[5] error from experimental results,[6] though there was an overestimation of case expansion at low expansion volumes (early in the simulation). Peterson and Wight[5] concluded this was due to an over estimation of the CJ pressure as a result of a stiff EOS, that is, there is too large of a change in the pressure for small changes in the specific volume. This was also observed by Menikoff,[7] who found inconsistencies at pressures greater than 10 GPa, including lower than expected particle velocities. A full description of Uintah's validated EOS can be found in.[5]

3.1 Problem with JWL EOS in Tension

The JWL EOS is graphically described in Figure 3.1 using the constants for the unreacted PBX-9501 stated in Table 3.1. The first term on the right hand side of Equation 3.1 dominates at high pressures as seen by the red line, the second term at intermediate pressures (the green line), and the last term at low pressures and large expansions (the blue line).[8] This EOS was developed to represent the relationship between pressure and volume of a solid explosive when the material is under compression. Therefore the JWL EOS has only been validated for relative volumes less than one. As a consequence of fitting the curve to match cylinder case expansion data at high densities and pressure, the JWL equation results in negative pressures at low relative volumes. This is a problem when modeling deflagration, which places the material in tension, resulting in negative pressures.

Though negative pressures are physical and have been observed in solid materials, many computational codes, including the Uintah Computational Framework, are unable to simulate negative pressures. This results in catastrophic algorithm errors when attempting to simulate an unconfined deflagration. Uintah places an infinitesimally small amount of mass of every material in every grid cell. This allows MPMICE to not track the boundaries of a material, enabling the solid reactant to convert to product gas. The ICE component calculates the pressure of a grid cell by analyzing all materials in the cell. Since negative pressures are nonphysical for gases, Uintah has determined negative pressures are nonphysical in all MPMICE simulations. This has lead to the modification of the JWL EOS for the solid explosive material, eliminating the possibility of negative pressures.

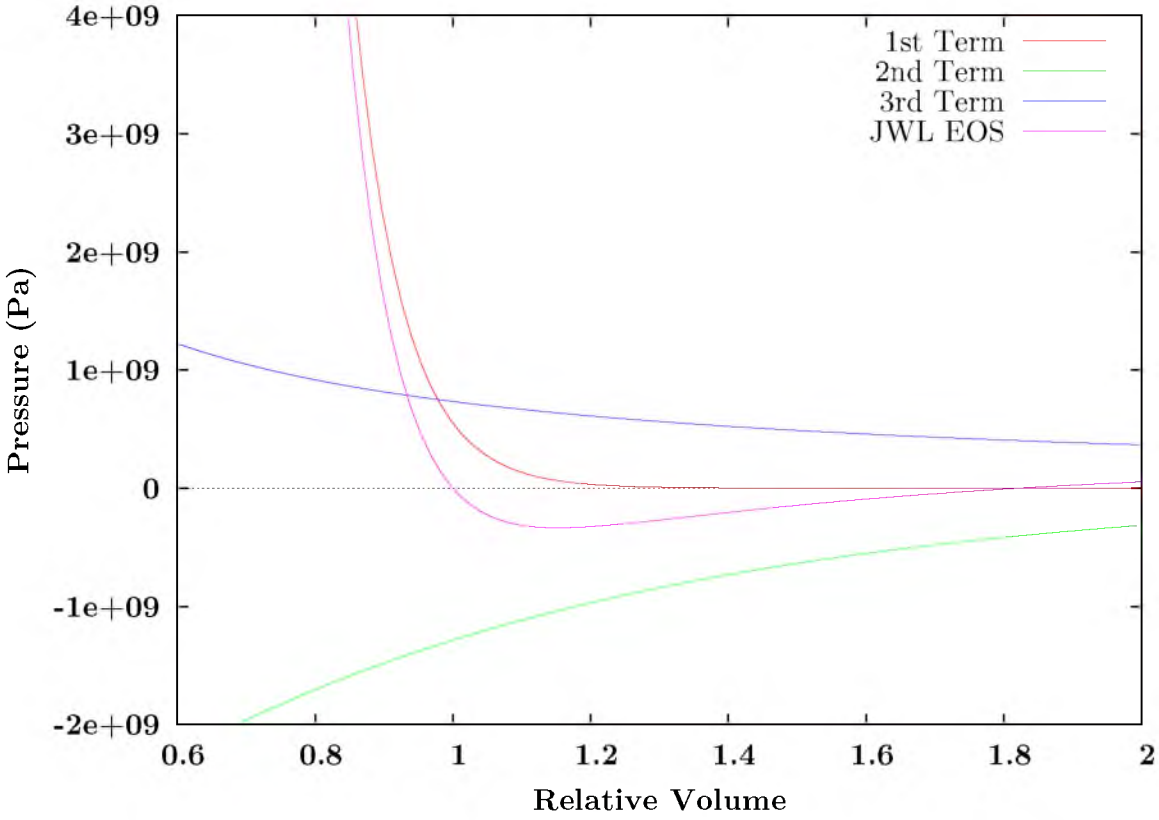

Figure 3.1: JWL Equation of State.

Table 3.1: JWL Constants.[3]

Variable	Solid PBX-9501	Product Gas
A	732000 GPa	1668.9 GPa
B	-5.2654 GPa	59.69 GPa
R_1	14.1	5.9
R_2	1.41	2.1
ω	0.8867	0.45
C_v	2.7806e-3 GPa/K	1.0e-5 GPa/K
P_{ref}	101325 Pa	
ρ_0	1832 Kg/m^3	1832 Kg/m^3

3.2 Modifications to the JWL EOS

The modified JWL EOS for the reactant uses the original form, Equation 3.1, for compression of the material above the reference pressure, P_{ref}, typically 1 atm. When the JWL EOS calculates a pressure $\leq P_{ref}$, the modified EOS is used:

$$P_{MOD} = P_{ref}(\frac{1}{V_r})^{\frac{K_0}{P_{ref}}} \tag{3.2}$$

where $K_0=\rho c^2$. This equation originated from an altered solid phase equation of state implemented in many of the MPM constitutive models to ensure a positive equilibration pressure.[9] To keep the EOS continuous, a reference density, ρ_{ref}, at the current temperature and a reference pressure are iteratively solved for, as described in Appendix B. Since the temperature in the cell is constantly changing, the reference density is calculated every timestep. The reference density is the density at the reference pressure, and current temperature used in place of ρ_0. Because the density is determined at every timestep, the derivative of the EOS equations can be determined at the reference pressure, where $\rho=\rho_{ref}$. The first derivatives of the original EOS and modified EOS,

$$\frac{\delta P_{JWL}}{\delta \rho} = \frac{AR_1\rho_0}{\rho^2}e^{-R_1\frac{\rho_0}{\rho}} + \frac{BR_2\rho_0}{\rho^2}e^{-R_2\frac{\rho_0}{\rho}} + \frac{C_vT\omega}{\rho_0} \tag{3.3}$$

$$\frac{\delta P_{MOD}}{\delta \rho} = \frac{K_0}{\rho}(\frac{1}{V_r})^{\frac{K_0}{P_{ref}}-1} \tag{3.4}$$

respectively, are inherently equal to each other at the reference pressure. This ensures that the EOS functionality is continuous over the transition from expansion to compression.

The modified EOS is illustrated in Figure 3.2 with P_{ref}=101325 Pa. Notice the compression behavior above 1 atm is the same as the original JWL EOS; below the pressure exponentially decays to zero but is never negative. With these modifications, tension and compression can occur in the reactant material without outputting negative pressures or changing the detonation-expansion profile.

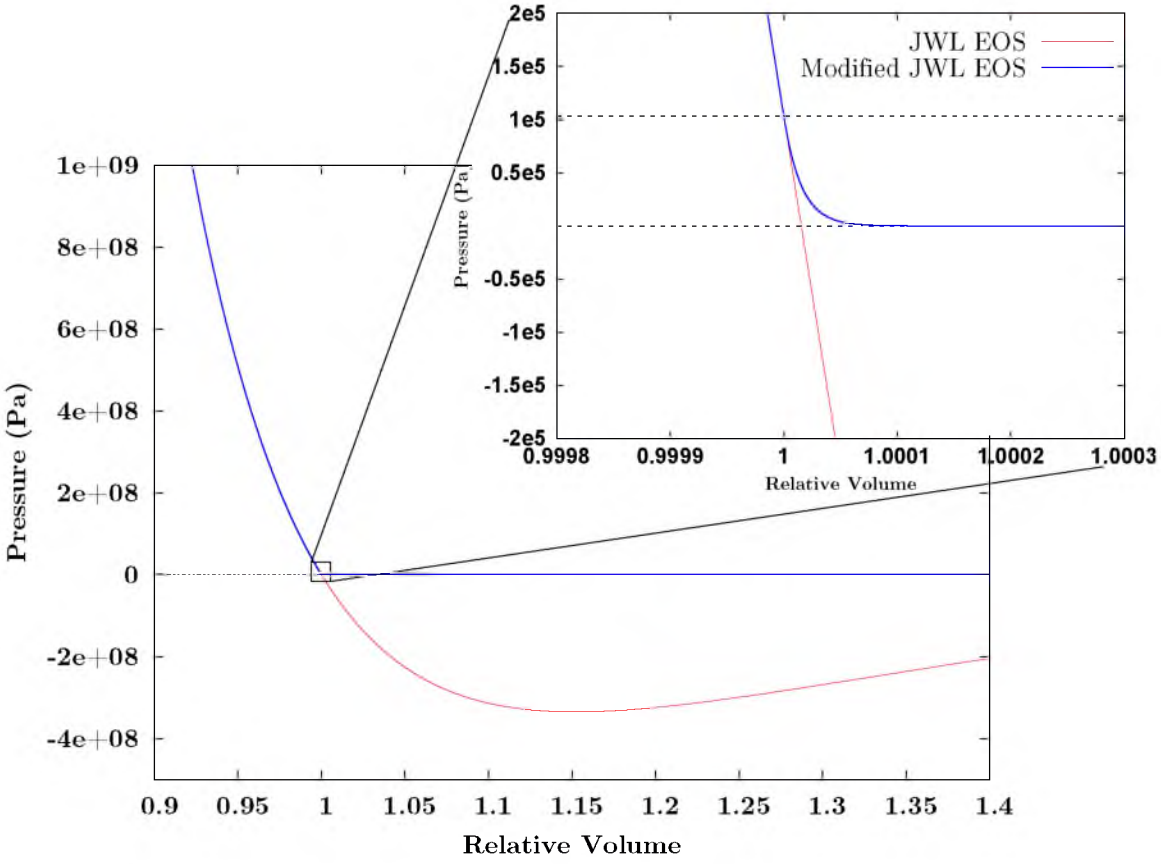

Figure 3.2: JWL Equation of State and Modified Equation of State.

3.3 References

[1] E. L. Lee, H. C. Hornig, J. W. Kury, *Adiabatic Expansion of High Explosive Detoantion Products*, Tech. Report TID-450, UC-4, Lawrence Radiation Lab, University of California, **1968**.

[2] E. L. Lee, C. M. Tarver. Phenomenological Model of Shock Initiation in Heterogeneous Explosves. *Phys. of Fluids* **1980**, *23*, 2362–2372.

[3] K. S. Vandersall, C. M. Tarver, F. Garcia, S. K. Chidester. On the Low Pressure Shock Initiation of Octahydro-1,3,5,7-tetranitro-1,3,5,7-tetrozocine Based Plastic Bonded Explosives. *J. App. Phys.* **2010**, *107*, 094906–0–11.

[4] R. Catanach, L. Hill, H. Harry, E. Aragon, D. Murk, *Cylinder Test Specification*, Tech. Report LA-13643-MS, Los Alamos Natl. Lab., **1999**.

[5] J. R. Peterson, C. A. Wight. An Eulerian-Lagrangian Computational Model for Deflagration and Detonation of High Explosives. *Combust. Flame* **2012**, *159*, 2491–2499.

[6] T. R. Gibbs, A. Popolato (Eds.), *LASL Explosive Property Data*, University of California Press, Berkely and Los Angeles, California, **1980**.

[7] R. Menikoff. Comparison of Constitiutive Models for Plastic-Bonded Explosives. *Combust. Theory Model.* **2008**, *12*, 73–91.

[8] W. Weseloh, *JWL in a Nutshell*, Tech. Report LA-UR-14-24318, Los Alamos Natl. Lab., **2014**.

[9] J. E. Guilkey, T. B. Harman, B. Banerjee. An Eulerian-Lagrangian Approach for Simulating Explosions of Energetic Devices. *Comput. Struct.* **2007**, *85*, 660–674.

CHAPTER 4

MULTISCALE MODELING OF HIGH EXPLOSIVES FOR TRANSPORTATION ACCIDENTS

Joseph R. Peterson, Jacqueline C. Beckvermit, Todd Harman, Martin Berzins, and Charles A. Wight. 2012. Multiscale modeling of high explosives for transportation accidents. In Proceedings of the 1st Conference of the Extreme Science and Engineering Discovery Environment: Bridging from the eXtreme to the campus and beyond (XSEDE '12). ACM, New York, NY, USA, , Article 32 , 8 pages. DOI=10.1145/2335755.2335828 http://doi.acm.org/10.1145/2335755.2335828

Multiscale Modeling of High Explosives for Transportation Accidents

Joseph R. Peterson
Department of Chemistry
University of Utah
Salt Lake City, Utah
joseph.peterson@utah.edu

Jacqueline C. Beckvermit*
Department of Chemistry
University of Utah
Salt Lake City, Utah
j.beckve@chem.utah.edu

Todd Harman
Department of Mechanical Engineering
University of Utah
Salt Lake City, Utah
t.harman@utah.edu

Martin Berzins
Scientific Computing and Imaging Institute
University of Utah
Salt Lake City, Utah
mb@sci.utah.edu

Charles A. Wight
Department of Chemistry
University of Utah
Salt Lake City, Utah
chuck.wight@utah.edu

ABSTRACT

The development of a reaction model to simulate the accidental detonation of a large array of seismic boosters in a semi-truck subject to fire is considered. To test this model large scale simulations of explosions and detonations were performed by leveraging the massively parallel capabilities of the Uintah Computational Framework and the XSEDE computational resources. Computed stress profiles in bulk-scale explosive materials were validated using compaction simulations of hundred micron scale particles and found to compare favorably with experimental data. A validation study of reaction models for deflagration and detonation showed that computational grid cell sizes up to 10 mm could be used without loss of fidelity. The Uintah Computational Framework shows linear scaling up to 180K cores which combined with coarse resolution and validated models will now enable simulations of semi-truck scale transportation accidents for the first time.

Keywords

Deflagration, detonation, parallel multi-scale modeling, granular compaction

1. INTRODUCTION

Analyzing risks involved with transporting and storing solid phase propellants, explosives and pyrotechnics involves understanding reactive behaviors of the materials used in the device. In such analyses, the ability to model the underlying physics of rapid reaction scenarios over large spatial and temporal scales is paramount. Motivation for this work is the 2005 incident in Utah's Spanish Fork Canyon, where a truck containing seismic booster explosives overturned, caught fire and unexpectedly detonated with violence attributed to "sympathetic" reaction of multiple explosive devices reacting in tandem [11]. A number of milestones towards predictive solution on the length scales of interest have been achieved. The scale of the problem is sufficiently large that utilizing supercomputing resources is essential to capture the physical behavior of the array of explosives. The Uintah Computational Framework [15] provides the means to both model and compute the simulation scenario on supercomputers [28, 26]. Both modeling techniques and computing resources are sufficiently mature to address tens-of-meter-scale simulations of explosions.

An energetic material model capable of accurately predicting the physics of a reaction over time scales from microseconds to minutes is desirable. Previous research in the field of granular compaction of the explosive octahydro-1,3,5,7-tetranitro-1,3,5,7-tetrazocine (HMX) beds has led to the development of several bulk-scale analytical models that are able to predict the qualitative behavior of compaction and the resulting reaction [4, 16]. These modeling efforts have examined the behavior of materials with varying porosity, particularly noting that large differences between bulk averaged quantities of interest and micro-scale heterogeneities. This is especially relevant for temperature, which drives the decomposition of solid reactants leading to deflagration-to-detonation transition (DDT) in granular, porous, and/or damaged explosives, or shock-to-detonation transition (SDT) in solid and plastic bonded explosives (PBX). In DDT and SDT the transient energetic extremes are attributed to frictional heating, plastic flow, crystal fracture [1] and grain/binder de-bonding [35], which create hot-spots that act as nucleation sites for reaction. When enough hot-spots are formed, a self-sustaining combustion occurs that can cause a DDT or SDT. These events are extremely dangerous and damaging. A number of works in this field have highlighted the need for mesoscale simulations (micrometer scale) for the validation of bulk scale models [29, 7, 17, 3]. A conclusion from these studies is that mesoscale simulations are useful not only for validation, but also in inspirirng physically based bulk models. Mesoscale simulations of compaction have been used to validate the burning behavior of a model [32] for bulk

XSEDE12, July 16 - 20 2012, Chicago, Illinois, USA

reactions over the range of deflagration and detonation phenomena.

Validation is necessary as the predictability of many bulk-scale models is subject to large uncertainty associated with the applied boundary conditions, limiting the applicability of the model to conditions used for calibration. In many cases these models are limited by the range over which the reaction equations have been calibrated. This brings into question whether the model can accurately capture the physics outside this calibration range. Thus as models are extended beyond their calibration regions, careful consideration must be taken in analyzing the physical results on that temporal and spatial scale, to understand the effect on the primary metric of interest. In addition, the levels of uncertainty in the model must be addressed at a given scale in order to have confident analysis of results and observations.

Section 2 describes, very generally, the approach taken in simulating these multi-scale problems. Sections 3-5 describe modeling advancements that enable large-scale simulation of the energetic arrays found in the Spanish Fork accident. Section 6 concludes with a discussion of the current outlook of large scale accident simulations along with recommendations for further study.

2. SIMULATION METHODOLOGY

All simulations made use of a fluid-structure interaction algorithm, based on the combination of the particle-based Material Point Method (MPM) and the cell-based Implicit Continuous Eulerian (ICE) compressible multi-material CFD, known as MPMICE [21, 19]. The ICE algorithm, originally formulated by Kashiwa et al. at LANL [24, 22, 23], is capable of simulating flow scenarios with any number of materials in the compressible or incompressible regime while conserving mass, momentum and energy. ICE is necessary for solving the complex flow behavior of combustion gas interactions in surface flames, convective flames and high-density detonation product gas expansion. MPM is a Lagrangian method based on the particle-in-cell method from LANL, first described by Sulsky, et al. [37, 5, 6]. MPM excels in modeling of solid material mechanics, including large deformations [5], complex geometries [12], fracture [25], material contact [6] and even biological constructs [20]. MPMICE leverages the strengths of both methods to solve high deformation rate fluid-structure interactions (the flow field, deformation of the solid, etc.) [18]. The use of MPMICE allows simulations of flow, deformation and fluid-solid interactions at micro- to deka-meter length scales.

Simulations were performed in one, two or three dimensions. Adaptive mesh refinement was used when parts of the domain where relatively dormant to reduce computational cost. A recently developed decentralized scheduling model including on-node threading and intra-node message-passing-interface (MPI) communications was used to achieve appropriate utilization of XSEDE resources [28, 27]. Typical three dimensional problems utilized between 512 and 49,152 cores for the validation and production simulations. The largest influence on solution accuracy, aside from the particular material models used, was the grid resolution for ICE and number of particles for MPM. All validation simulations for both micro-scale compaction and bulk-scale compaction were examined for convergence. An extension of the various models to coarser resolutions was performed with a relative error bound between 5% and 10% compared with converged resolution. The limits for which the models can perform under this error bound were identified for the metric of interest (detonation velocity, burn rate, etc.) in the particular simulation.

3. MESOSCALE COMPACTION SIMULATIONS

A number of shock impact experiments on granular explosive beds have been reported [33]. The experiments consisted of a column of explosive granules packed to different extents of porosity. These granular beds are then impacted at several hundred meters per second and investigated with stress and velocity gauges at the top and bottom of the column. Experiments provided validation data for bulk scale reaction and sub-grid-scale model; reactions did not occur in every case. A modeling approach inspired by a number of other studies of mesoscale compaction of porous beds was adopted [29, 7, 17]. Simulations of randomly generated sphere packings of experimentally determined HMX distributions [14, 7] were run with a model including a Steinberg-Cochran-Guinan [36, 13] viscoelastic response of the explosive material. Melting temperature and specific heat models for HMX were taken from Menikoff and Sewell [31]. Simulation cell sizes were 5 μm with 9 particles per cell making them computationally intensive, requiring thousands of processors even in two dimensions. The model was validated against experimentally determined stress and velocity profiles for non-reactive cases. A typical example of these granular compaction simulations, excluding reaction, can be seen in Figure 1 demonstrating both the behaviors of the temperature and the stress. Features such as the compaction wave, plastic yield, work heating and frictional heating can all be seen along with a few hot-spots. The model was found to have similar behavior to previously validated non-reactive models [33, 30].

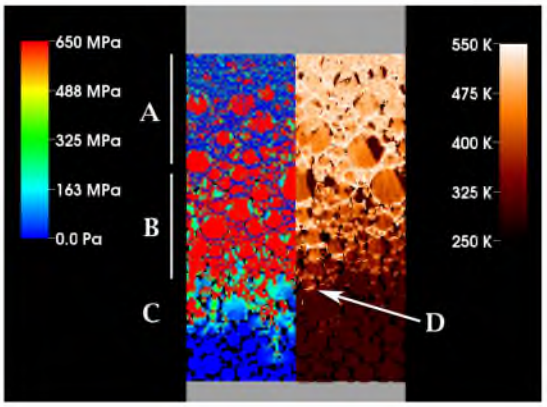

Figure 1: Stress and temperature distributions in a granular bed after being impacted from the top at 288 m/s. A plastic flow zone (A), a compaction zone (B), stress fingers (C), and friction and plastic flow induced hot-spots (D) can be seen.

A comparison of temperatures for a non-reactive case for particles and fluids is shown in Figure 2. The left image depicts the particle temperature while the right image shows

fluid temperatures. The Uintah implementation of the reaction model uses the cell centered temperatures in the determination of the burn rate while the particle temperatures are used for for determining the solid's mechanical behavior. High temperatures of gas in void spaces can enhance reaction rates and must be represented accurately to ensure the correct burn rate. These comparisons underscore the need for accurately modeling both gas and solid phases and their interactions, as gas temperatures in void spaces can be seen to be near the ignition temperature in a number of places.

Of particular interest in the granular compaction of HMX is the initiation of sustained reaction. This is important for this study as the heterogeneous nature of the bed allows for transient energy extremes, as seen in hot-spots. The decomposition of HMX was modeled using the Ward, Son, Brewster (WSB) model [39] with a decomposition temperature threshold of 450 K. While validation of the reaction model against experimental data continues, the utility of being able to model mesoscale phenomena in heterogeneous condensed explosives becomes ever more apparent. Some studies have been performed on the effects of frictional heating, melting, discretization strategies and geometries [7, 35, 29, 31, 38, 17], but relatively little work has been performed with respect to surface area, porosity and gas permeability. Bulk-scale models may be developed based on the simulations of these effects since currently some may not be probed or validated experimentally; hence our development of mesoscale models. Congruent to the development of mesoscale models is the progression of the bulk-scale material models towards correct behavior in both compaction for porous explosives and damage in solid explosive. Results from these mesoscale simulations are utilized as a validation source for bulk-scale models.

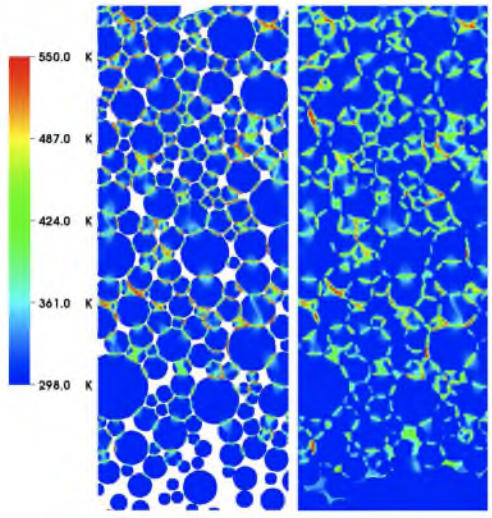

Figure 2: Temperature distribution in a granular compaction after 5 microseconds. The left image shows particle temperature and the right images shows gas temperature. The same color scale is used for both plots.

4. BULK-SCALE COMPACTION SIMULATIONS

When simulating the transportation of explosives it is important to model accurately bulk-scale compaction, since the surface area, gas confinement and damage from both mechanical and thermal insult are directly affected by porosity. For this study a new compaction model was implemented to represent a heterogeneous compaction of energetic materials. This model uses previously implemented isotropic damage model for full density explosive, ViscoScram [9], merged with an accurate representation of bulk compaction, P-α [40]. The P-α model allows a quantitative extent of porosity that is used to determine whether convective burning can occur in a material. Similarly, ViscoScram has a variable that represents the extent of cracking in the explosive material. By using these quantities, a relationship presented by Belyaev et al. [8], and a fit by Berghout et al. [10] for a PBX of interest, the WSB burn model [39] allows burning inside materials. This allows pressurization and continued damage of HMX, which can cause self-accelerated sub-sonic reactions that may undergo DDT or SDT.

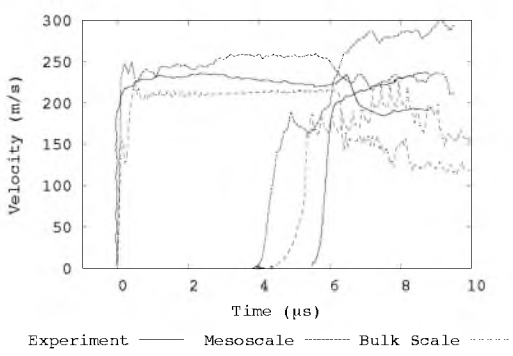

Figure 3: A comparison of bulk scale and mesoscale simulations of experimental Shot 912 [33] where the HMX bed is impacted at 288 m/s. Lines on the left are from experimental velocity gauges at the top of the bed, and those on the right are from gauges on the bottom of the bed.

To validate the compaction behavior of the P-α modified ViscoScram, a homogenized version of the simulation presented in Section 3 was run. The results have been compared to the mesoscale simulations presented in the previous section and the experimental data. Velocity profile comparisons can be seen in Figure 3. Agreement to within 10% can be seen for the velocities at the top and bottom of the specimen for Shot 912 [33]. Stress profile comparisons can be seen in Figure 4. The P-α modified ViscoScram model has larger error in stress than in velocity. Figure 5 demonstrates the utility of mesoscale simulations in that temperatures on the timescale of microseconds are difficult or impossible to obtain experimentally. The temperature computed by the bulk-scale model is larger than the average temperature for the mesoscale simulation, however it is within one standard

deviation of the averaged mesoscale temperature. By incorporating this bulk-scale compaction model, the deflagration to detonation phenomenon can be more accurately represented in porous or damaged materials. What then remains is extension of simulations to a length scale of tens-of-meters.

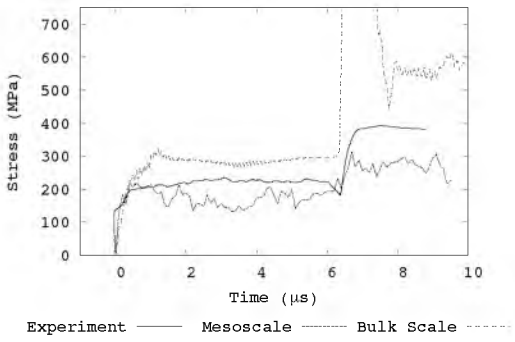

Figure 4: A comparison of bulk scale and mesoscale simulations of experimental Shot 2477 [33] where the HMX bed is impacted at 288 m/s. Lines are from experimental stress gauges at the top of the bed.

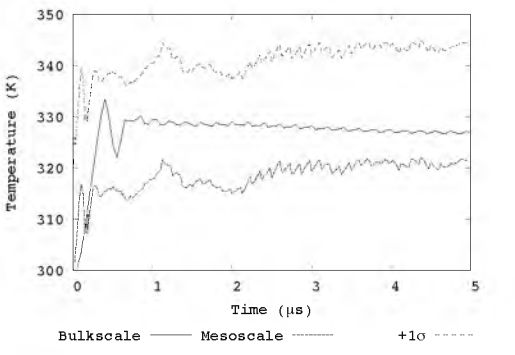

Figure 5: A comparison of temperatures computed by the mesoscale simulation and the bulk scale simulation measured at the top of the granular column. The mesoscale temperature was averaged laterally across the simulation domain and a standard deviation computed. The line marked "$+1\sigma$" has the standard deviation of the temperature added to the average for the mesoscale simulation.

5. COARSE RESOLUTION MODELS

Despite the availability of petascale machines such as NSF's Kraken, considerations must be made when weighing the accuracy of solution against the time, power and expense of the simulation. The complexity of the modeling approach and the grid cell size must be selected to maximize the accuracy while minimizing computational cost. It is desirable to extend the models to the largest cell size possible while maintaining a target level of error. The model used by Uintah to simulate multiple reaction phenomena, such as deflagration and detonation, is DDT1 [32]. Both deflagration and detonation are subject to grid cell size dependence but are barely seen to have particle density dependence [32]. The more resolution dependent model will limit the extension to coarser grid cell sizes and dictate computational costs. To extend the deflagration and detonation models used in DDT1 to regions outside the range in which they are calibrated, a metric of interest must be identified, and a convergence study performed.

Work has begun in extending the WSB model [39, 41] and the JWL++ [34] model used in the previous validation study [32] beyond their calibration ranges. In the WSB model, the metric of interest is the burn rate which often has the largest effect in the moderate strain rate region of material deformation. In the case of detonation the metric of interest is the affect of the transient pressure wave and subsequent release wave on materials close to the blast wave. These materials are accelerated and become dangerous projectiles, which is why they are of interest.

Coarsening the grid cell size will potentially allow for larger scale simulations with similar accuracies as mesoscale simulations. The burn rate is determined both experimentally and computationally by a strand burner test [2]. Experimentally a stick of explosive is confined and lit at one end. Pressurization occurs due to confinement that causes the burn rate to increase. The burn rate is measured by the time of arrival at a number of measurement gauges placed in the explosive. This allows the burn rate to be determined as a function of pressure. In many cases the initial temperature of the bulk explosive was changed to investigate the temperature dependence of the burn rate [2].

Computationally the same data can be collected by enclosing a stick of explosive in symmetric boundaries, allowing for the pressure to rise as burning occurs. These simulations were run in one dimension for simplicity and speed. Here the pressure in the gas cells were averaged, giving the simulated pressure, and the mass burned was measured. These computational experiments were used to determine the grid cell size dependence of the burn rate computed by the WSB model. The results in Figure 6 show minimal grid dependence on the burn rate for the resolutions studied. The initial bulk temperature of the HMX was 373 K. It was also observed that the burn rate was slightly overestimated at higher initial bulk temperatures and slightly underestimated at room temperature (298 K). However, at most the error was no larger than 10% of the experimental burn rate. The region of interest is dependent upon the specific explosive and our focus was on the validation of the WSB reaction model for HMX. For this simulation it is important to look at elevated pressure and temperatures, for this is where convective burning and transitions to detonations occur. The same simulation was run at initial bulk temperatures of 298 K and 423 K, which produce similar grid dependence results.

When looking at the cell size effects on detonation, the

main metric of interest is the effect of the expansion wave on other objects in the domain. For instance, if a detonation wave accelerates a piece of steel, it is desirable to know, to high accuracy, the velocity of the steel. Similarly, once the explosive material is consumed, the blast wave is largely supported by expansion of gases without the reaction to sustain the peak. This expansion wave begins at the sonic plane. The sonic plane is the point at which material behind the lead pressure wave no longer affects the detonation front. The release wave, seen in Figure 7 at the end of the plateau as the pressure begins to drop, is the main factor in the velocity of the steel plate. The release wave can effect objects on the length scale of a few millimeters while the reaction peak has a much smaller effect on the velocity of an object. Simulations were performed at various grid cell sizes showing the effect of cell size on the velocity of the steel. In these simulations a small piece of explosive was collied with a one dimensional stick of explosive causing detonation to occur. At the end of the explosive rod is a steel plate. As the detonation consumes the explosive, the pressure wave accelerates the steel plate. The velocity of the steel plate was computed and compared against a converged resolution simulation, determining the error in the velocity. With increased cell size the pressure spike due to reaction encroaches on the sonic plane affecting the amount of energy that is transferred to the steel. With increasing the grid cell size, the rate parameters for the JWL++ model had to be reduced to keep the detonation velocity constant at 8800 m/s.

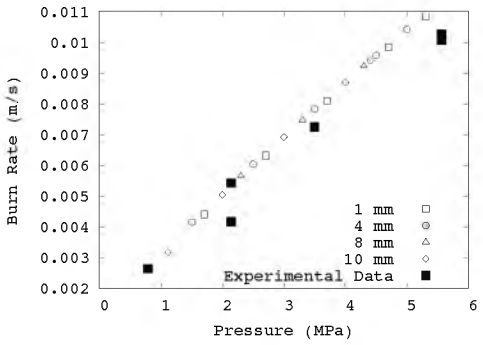

Figure 6: Resolution dependence of burn rate of WSB model at a bulk temperature of 373 K. Simulated data was compared against data from Atwood et al. for the explosive HMX [2].

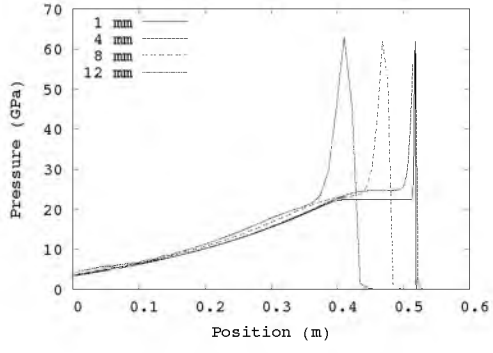

Figure 7: Pressure profiles for detonation simulations at various cell sizes.

Within the studied cell sizes, the differences in velocity of the steel was less than 8%. At larger grid cell sizes the reaction constant is seen to decrease more rapidly, and the velocity difference changes considerably, likely due to the reaction peak falling inside the expansion region. This changes the sonic plane and hence the amount of material that can affect the reaction front, effectively increasing the reaction rate. The shift in the reaction peak is demonstrated in Figure 7. Note the reaction peak migrates back with increased cell size, encroaching slightly on the release wave at cell sizes larger than about 10 mm. Therefore, a cell size larger than 10 mm will effect the sonic plane. A consequence of the shift due to larger cell size is that the reaction wave will reach a position slightly later in time than the more finely resolved simulations, but by no more than 10 microseconds behind the converged wave. However, this is partially offset by the fact that the interpolated pressure of the shock is felt at an earlier time because of the coarser mesh resolution. With little error associated with larger resolutions in both the burn rate and detonation propagation the capability to move up to 10 mm grid cell size while keeping the same accuracy now seems feasible.

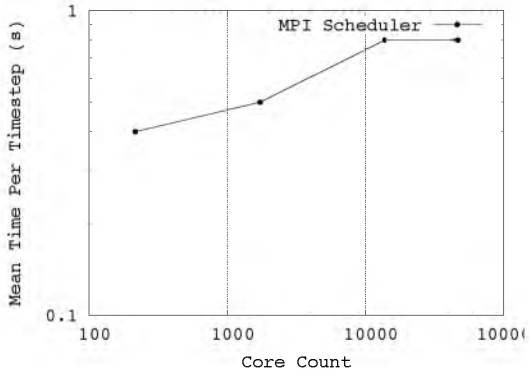

Figure 8: Weak scaling of the Uintah framework.

In addition to a grid cell size study, a scaling study was performed showing the capability of the Uintah framework to model high particle density MPMICE simulations characteristic of those seen in the trucking accident on a large number of cores. The study simulated detonation of HMX at various domain sizes ranging from 10^3 mm^3 to 360^3 mm^3 at 1 mm grid cell size. Simulations were run with 1000 grid cells/patch and 1 patch/core. The results can be seen in

Figure 8. These results can be improved upon with recent advancements made in improving memory use for the Uintah framework, allowing for linear scalablility up to 180K cores. [28, 27]. Increased zoning, along with the relaxation of the time stepsize due to the larger cell size will allow simulations of semi-truck sized explosions.

6. CONCLUSIONS

For many different reasons the safe transportation of explosives is essential. Models designed to analyze potential accident scenarios must accurately capture the relevant physics over a wide range of spatial and temporal ranges. Utilizing mesoscale results in validating bulk-scale models has proven to be useful for improving predictive capability. Furthermore, a physical quantity that is difficult to measure experimentally may be analyzed by mesoscale simulations and used to inspire bulk-scale models. A bulk-scale model for the compaction of a porous explosive, and damage evolution of fully densified material has been validated with mesoscale results. Good agreement has been shown between the simulated and experimental stress profiles for both mesoscale and bulk scale simulations. Good agreement has also been seen between temperatures in mesoscale and bulk-scale simulations, highlighting the utility of the mesoscale modeling.

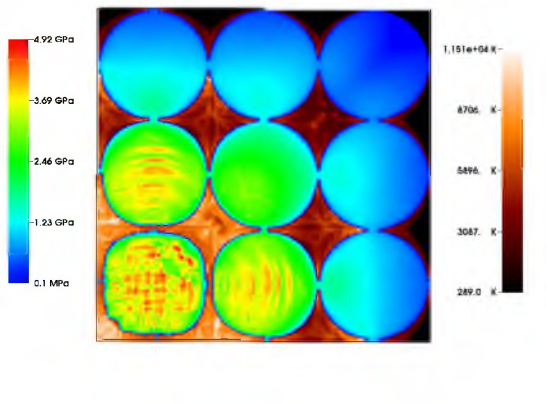

Figure 9: Demonstration of combustion in an array of explosives. The left colormap shows the pressure inside the explosive cylinders, while the right colormap shows the temperature of the product gas. The array was ignited in the lower left corner.

Using validated bulk-scale models, our studies have shown that extension of these models to larger cell sizes can capture, without significant loss of fidelity, the metric of interest. Both detonation and deflagration reactions were found to extend reasonably well to larger cell sizes. The detonation model was found to be the limiting factor with maximum cell sizes on the order of 10 mm, due to the reaction peak encroaching on the sonic plane effecting blast wave pressure and imparted kinetic energy.

Complex geometries such as those seen in the 2005 truck accident are of high interest for their potential of being a "sympathetic" explosion. For example, the 2005 accident involved 18,500 small explosive cylinders packaged in an array similar to that seen in Figure 9. The preliminary modeling efforts of this explosive array show deflagration to detonation transition in agreement with the violence of the truck explosion. This simulation will provide the benchmark needed to validate a bulk-scale array. We have shown that the current Uintah code can move to much coarser grid cell sizes, allowing accurate modeling of arrays orders of magnitude larger. The coarsened resolution, combined with Uintah's linear scalability up 180K cores [27] will allow for full-scale simulations of transportation accidents on the length scale of tens of meters.

7. ACKNOWLEDGMENTS

Monica Hall, Qingyu Meng, Alan Humphrey and James Guilkey are especially thanked. This work was supported by the National Science Foundation under subcontract No. OCI0721659. Uintah was developed by the University of Utah's Center for the Simulation of Accidental Fires and Explosions (C-SAFE) and funded by the Department of Energy, subcontract No. B524196. We would also like to thank TACC and NICS for access to computing resources.

8. REFERENCES

[1] R. Armstrong. Dislocation mechanics aspects of energetic material composites. *Reviews on Advanced Material Science*, 19:13–40, 2009.

[2] A. I. Atwood, T. L. Boggs, P. O. Curran, T. P. Parr, and D. M. Hanson-Parr. Burning rate of solid propellant ingredients, part 1: Pressure and initial temperature effects. *Journal of Propulsion and Power*, 15(6):740–747, November-December 1999.

[3] M. Baer. Modeling heterogeneous energetic materials at the mesoscale. *Thermochim. Acta*, 384:351 367, 2002.

[4] M. Baer and J. Nunziato. A Two-Phase Mixture Theory for the Deflagration-to-Detonation Transition in Reactive Granular Materials. *International Journal of Multiphase Flow*, 12:861–889, 1986.

[5] B. Banerjee. Material point method simulations of fragmenting cylinders. In *Proceedings of the 17t ASCE Engineering Mechanics Conference*, Newark, DE, June 2004.

[6] S. Bardenhagen, J. Guilkey, K. Roessig, J. Brackbill, W. Witzel, and J. Foster. An improved contact algorithm for the material point method and application to stress propagation in granular material. *CMES*, 2:509 522, 2001.

[7] A. Barua and M. Zhou. A Lagrangian framework for analyzing microstructural level response of polymer-bonded explosives. *Modelling and Simulation in Materials Science and Engineering*, 19(5):61 68, 2011.

[8] A. Belyaev, A. Korotkov, A. Sulimov, M. Sukoyan, and A. Obmenin. Development of combustion in an isolated pore. *Combustion, Explosion and Shock Waves*, 5:4–9, 1969.

[9] J. Bennett, K. Haberman, J. Johnson, and B. Asay. A constitutive model for the non-shock ignition and

mechanical response of high explosives. *Journal of the Mechanics and Physics of Solids*, 46(12):2303–2322, 1998.

[10] H. L. Berghout, S. F. Son, and B. W. Asay. Convective burning in gaps of pbx 9501. *Proceedings of the Combustion Institute*, 28:911–917, 2000.

[11] M. Berzins, J. Luitjens, Q. Meng, T. Harman, C. Wight, and J. Peterson. Uintah - a scalable framework for hazard analysis. In *Proceedings of Teragrid 2010*, page (published online), 2010.

[12] A. Brydon, S. Bardenhagen, E. Miller, and G. Seidel. Simulation of the densification of real open-celled foam microstructures. *Journal of the Mechanics and Physics of Solids*, 53:2638–2660, 2005.

[13] P. Conley, D. Benson, and P. Howe. Microstructural effects in shock initiation. In *11th International Detonation Symposium*, page 768, Snowmass, CO, 1998.

[14] J. Dick. Measurement of shock initiation sensitivity of low density hmx. *Combustion and Flame*, 54:121–129, 1983.

[15] J. Germain, A. Morris, S. Parker, A. Malony, and S. Shende. Performance analysis integration in the uintah software development cycle. *International Journal of Parallel Programming*, 31:35–53, 2003.

[16] K. Gonthier, R. Menikoff, S. Son, and B. Asay. Modeling Energy Dissipation Induced by Quasi-Static Compaction of Granular HMX. In *Shock Compression of Condensed Matter*, pages 289–292, 1997.

[17] K. Gonthier, R. Menikoff, S. Son, and B. Asay. Direct Numerical Simulation of Weak Shocks in Granular Material. In *12th International Detonation Symposium*, San Diego, California, USA, August 11-16 2002.

[18] J. Guilkey, T. Harman, and B. Banerjee. An Eulerian-Lagrangian approach for simulating explosions of energetic devices. *Computers and Structures*, 85:660–674, 2007.

[19] J. Guilkey, T. Harman, B. Kashiwa, J. Schmidt, and P. McMurtry. An eulerian-lagrangian approach for large deformation fluid-structure interaction problems, part 1: Algorithm development. In *Fluid Structure Interactions II*, Cadiz, Spain, 2003. WIT Press.

[20] J. Guilkey, J. Hoying, and J. Weiss. Computational modeling of multicellular constructs with the material point method. *Journal of Biomechanics*, 39:2074–2086, 2006.

[21] T. Harman, J. Guilkey, B. Kashiwa, J. Schmidt, and P. McMurtry. An eulerian-lagrangian approach for large deformation fluid-structure interaction problems, part 2: Multi-physics simulations within a modern computational framework. In *Fluid Structure Interactions II*, Cadiz, Spain, 2003. WIT Press.

[22] B. Kashiwa. A multimaterial formalism. Technical Report LA-UR-94-771, Los Alamos National Laboratory, Los Alamos, 1994.

[23] B. Kashiwa. Fluid-structure interaction modeling. Technical Report LA-UR-13111-RP, Los Alamos National Laboratory, Los Alamos, 1996.

[24] B. Kashiwa. A multi field model and method for fluid-structure interaction dynamics. Technical Report LA-UR-01-1136, Los Alamos National Laboratory, Los Alamos, 2001.

[25] R. B. Leavy, R. M. Brannon, and O. E. Strack. The use of sphere indentation experiments to characterize ceramic damage models [uintah-related publication]. *International Journal of Applied Ceramic Technology*, 7(5):606–615, 2010.

[26] J. Luitjens and M. Berzins. Scalable parallel regridding algorithms for block-structured adaptive mesh refinement. *Concurrency And Computation: Practice And Experience*, 2011.

[27] Q. Meng and M. Berzins. Scalable large-scale fluid-structure interaction solvers in the uintah framework via hybrid task-based parallelism algorithms. Sci tech report uusci-2012-004, University of Utah.

[28] Q. Meng, M. Berzins, and J. Schmidt. Using hybrid parallelism to improve memory use in the uintah framework. In *Proceedings of Teragrid 2011*, page (published online), July 2011.

[29] R. Menikoff. Compaction wave profiles: Simulations of gas gun experiments. *Journal of Applied Physics*, 90:61–68, 2001.

[30] R. Menikoff, J. Dick, and D. Hooks. Analysis of wave profiles for single-crystal cyclotetramethylene tetranitramine. *Journal of Applied Physics*, 971:023529, 2005.

[31] R. Menikoff and T. Sewell. Constituent properties needed for mesoscale simulations of hmx. *Combustion Theory and Modeling*, 6:103, 2002.

[32] J. Peterson and C. Wight. An Eulerian-Lagrangian computational model for deflagration and detonation of high explosives. *Combustion and Flame*, page in Press, 2012.

[33] S. Sheffield, R. Gustavsen, and R. Alcon. Shock initiation studies of low density hmx using electromagnetic particle velocity and pvdf stress gauges. In *10th International Detonation Symposium*, Boston, MA, July 1993.

[34] P. Souers, S. Anderson, J. Mercer, E. McGuire, and P. Vitello. JWL++: A Simple Reactive Flow Code Package for Detonation. *Propellants, Explosives, Pyrotechnics*, 25:54–58, 2000.

[35] H. Springer, E. Glascoe, J. Reaugh, J. Kercher, and J. Maienschein. Mesoscale modeling of deflagration-induced deconsolidation in polymer-bonded explosives. In *17th APS SCCM Conference*, Chicago, IL, June 26-July 1 2011.

[36] D. Steinberg, S. Cochran, and M. Guinan. A constitutive model for metals applicable at high-strain rate. *Journal of Applied Physics*, 51(3):1498–1504, 1980.

[37] D. Sulsky, S. Zhou, and H. Schreyer. Application of a particle-in-cell method to solid mechanics. *Computer Physics Communications*, 87:236–252, 1995.

[38] W. Trott, M. Baer, J. Castaneda, L. Chhabildas, and J. Asay. Investigation of the mesoscopic scale response of low-density pressings of granular sugar under impact. *Journal of Applied Physics*, 101:024917, 2007.

[39] M. Ward, S. Son, and M. Brewster. Steady Deflagration of HMX With Simple Kinetics: A Gas Phase Chain Reaction Model. *Combustion and Flame*, 114:556–568, 1998.

CHAPTER 5

MODELING DEFLAGRATION IN ENERGETIC MATERIALS USING THE UINTAH COMPUTATIONAL FRAMEWORK

 Jacqueline Beckvermit, Todd Harman, Andrew Bezdjian, Charles Wight, Modeling Deflagration in Energetic Materials using the Uintah Computational Framework, Procedia Computer Science, Volume 51, 2015, Pages 552-561, ISSN 1877-0509, http://dx.doi.org/10.1016/j.procs.2015.05.321.

Procedia Computer Science

Volume 51, 2015, Pages 552–561

ICCS 2015 International Conference On Computational Science

Modeling Deflagration in Energetic Materials using the Uintah Computational Framework

Jacqueline Beckvermit[1]*, Todd Harman[1], Andrew Bezdjian[1], and Charles Wight[2]

[1] University of Utah, Salt Lake City, Utah, U.S.A
[2] Weber State University, Ogden, Utah, U.S.A.

Abstract

Predictive computer simulations of highly resolved large-scale 3D deflagrations and detonations are dependent on a robust reaction model embedded in a computational framework capable of running on massively parallel computer architectures. We have been developing such a model in the Uintah Computational Framework, which has exhibited good strong and weak scaling characteristics up to 512K cores[16]. Our focus is on predicting a Deflagration to Detonation Transition (DDT) when a large number of energetic devices are present. An example of this is a semi-tractor-trailer loaded with thousands of mining boosters that rolled over, ignited and went through a DDT. Our current reaction model adapts components from a) Ward, Son and Brewster[22] which incorporates the effects of pressure and initial temperature on deflagration, b) Berghout et al.[9] to model burning in cracks of damaged explosives, and c) Souers[20] for describing fully developed detonation. The reaction model has been subjected to extensive validation against experimental tests. Current efforts are focused on the effects of varying the grid resolution on multiple aspects of deflagration and the transition to detonation.

Keywords: Detonation, DDT, Deflagration, Multiscale Modeling, Deflagration Propagation

1 Introduction

In August of 2005, a truck carrying 16,000 kilograms of seismic boosters overturned, caught fire and detonated in Spanish Fork Canyon, Utah. The damage was catastrophic, causing a crater 10 meters deep by 24 meters wide with burning debris found up to a quarter of a mile away. It was apparent by the size of the crater that the explosion transitioned from a deflagration into a fully developed detonation. This research focuses on developing a science based reaction model incorporated into the Uintah Computational Framework[1] to simulate large scale transportation accidents. Our model captures the appropriate chemistry and physics, including the temperature and pressure sensitivity of the burn rate, detonation propagation, Shock to Detonation Transition (SDT) and Deflagration to Detonation Transition (DDT). Using

*j.beckve@chem.utah.edu

Selection and peer-review under responsibility of the Scientific Programme Committee of ICCS 2015

doi:10.1016/j.procs.2015.05.321

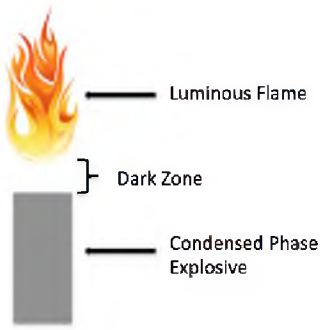

Figure 1: Schematic showing the three regions involved in the combustion of solid explosives.

this advanced computational framework, we can simulate the conditions necessary for a DDT to occur in much larger systems. With this computational tool, packaging protocols can be simulated to decrease the probability of detonation while transporting explosives.

The Uintah Computational Framework, developed at the University of Utah, is a collaborative effort within the Chemistry, Mechanical Engineering and Computer Science departments. The framework contains algorithms for modeling fluid structure interactions with MPM, ICE, and MPMICE[11, 12, 13], involving multiple materials, solid $\rightarrow$ gas exothermic reactions and a variety of constitutive models and equations of state. MPMICE solves the mass, momentum and energy conservation equations for the fluids and solids. Our reaction model is a source term in these equations, specifically the amount of converted mass. The solid $\rightarrow$ gas reaction models, which utilize the fluid structure interactions of MPMICE, have been validated for the explosives 1,3,5,7-octahydro-1,3,5,7-tetranitro-1,3,5,7-tetrazocine (HMX) and PBX-9501 (95 percent HMX with 5 percent of a plastic bonding agent). In this paper we have focused on these explosives due to the abundance of experimental data available. This paper describes a reaction model which is used within Uintah's MPMICE component to calculate the propagation of conductive and convective deflagration needed to simulate a DDT.

2 Deflagration in Solid Explosives

With the combustion of explosives there are three reaction zones/regions. The first is the condensed phase, where there is a large temperature increase from the luminous flame and where intermediates species are formed. The second is the dark zone as illustrated in Figure 1. Within this zone, the intermediate products are comparatively unreactive, causing a time delay for the radicals to build up in concentration before ignition in the luminous flame[3]. The height of the dark zone above the condensed phase is very important in determining the flame structure at low pressures and the burn rate at high pressure. This height is known as the flame standoff distance, which plays a large role in the transition into convective deflagration. As intermediate product gas concentrations and relative pressures are increased, the luminous flame moves closer to the condensed phase, decreasing the flame standoff distance and increasing the burn propagation and solid $\rightarrow$ gas mass conversion rate (burn rate). The third region is the bright zone, known for its luminous flame. This region is characterized by a large temperature increase, resulting from HCN and NO reacting to final products. The temperature in this zone can approach the adiabatic limit[3].

In the combustion of high explosives, there are two types of deflagration: conductive and convective. In a conductive deflagration, heat is transferred between the products of reaction and the surface of the explosive. This deflagration is observed to have relatively slow flame propagation velocity. For PBX-9501 undergoing a conductive deflagration the flame propagation

speed is a few cm/s, varying slightly with pressure[19]. As the pressure of the system increases the flame standoff distance will decrease, increasing the propagation speed of the deflagration. At relatively high pressures the flame standoff distance will decrease to a point that the flame can propagate into the cracks and pores of the solid material, transitioning into convective deflagration. This pressure is known as the critical pressure[9], and is inversely dependent on the porosity of the material. Convective deflagration is a very important mode in the combustion of high explosives because of its tendency to transition into a detonation. Above the critical pressure, hot product gases propagate into the damaged solid, igniting the material within. This results in significantly faster burning velocities. For PBX-9501 the convective deflagration velocities have been measured between 400 m/s to 1500 m/s[8].

Convective deflagration is very important to understanding a Deflagration to Detonation Transition (DDT). It has been observed that in a monolithic condensed phase explosive, a DDT occurs from the coalescence of pressure waves formed from convective deflagration. As burning occurs within the material, pressure waves propagate outward and grow in strength until a shock to detonation transition occurs[4]. This phenomena, in solid explosives, has been observed experimentally[4, 21] and in computational experiments[4, 15]. Understanding and accurately modeling conductive/convective deflagration is required to predict the behavior of 10s-1000s of reacting explosive devices.

3 Modeling Deflagration of HMX Based Explosives

Within Uintah, multiple reaction models have been combined with various constitutive material models to represent many aspects of combustion. Uintah's Deflagration to Detonation model, DDT1, is a multi-material, multiphase model used to describe the slow propagations of deflagration and the high energy release rates of detonation. We use the ViscoSCRAM[6] constitutive model to describe crack development or material damage in the condensed phase with respect to pressure, allowing for convective deflagration. The Ward, Son and Brewster (WSB)[22] burn rate model describes the mass flux of combustion, this is coupled with a reactive flow model, JWL++[20], to model detonation.

The WSB model[22] utilizes simple kinetics and is a commonly used approach to model steady combustion of explosive materials. It utilizes an iterative solution to determine the rate of mass conversion and is dependent on the pressure and temperature, while assuming global kinetic reactions. The WSB model was derived out of Los Alamos National Labratory to define the steady deflagration rate of HMX and similar explosives, in one dimension. This model assumes a high activation energy with unimolecular, irreversible, zeroth order thermal decomposition of the condensed phase. The gas phase reactions are considered second order with negligible activation energy. Good agreement is shown in the gas phase temperature between HMX undergoing a conductive deflagration and self deflagrating nitramines, when the activation energy is assumed to be negligible. With this model the flame standoff distance, pressure and temperature dependence on the burn rate agree well with experimental data[22]. The assumption that the gas phase has a negligible activation energy is justified by the gas phase reactions being radical chain reactions. This chemistry is easily explained with a hydrogen/oxygen combustion system. In these systems there is an activation energy associated with the initiation/branching step but the recombination/termination step is temperature insensitive, resulting in a negligible activation energy. This is similar to the chemistry seen with radical gas phase reactions in the steady combustion of HMX. The main assumptions in the WSB model are 1) the specific heat of the gas phase and the condensed phase are equal, 2) there is no mass diffusion assumed in the condensed phase, 3) the gas phase follows the ideal gas law,

4) the condensed phase is considered incompressible and 5) there is no pressure dependence associated with the heat release of the condensed phase, only the gas phase.

The WSB model uses a simplified two phase chemistry model, in which the solid explosive (A) is converted to gas phase intermediates (B) which react to form the final products (C). A(solid) $\rightarrow$ B(gas) $\rightarrow$ C(gas). Therefore only two phases of the combustion are modeled; the condensed and gas phases. The melt layer present in many explosives is assumed to have little impact on the overall combustion and is therefore ignored. This model has a large pressure dependence associated with the conductive heat transfer; as mentioned before, this greatly affects the rate of gas phase reactions. The mass burn flux is computed using Equations 1 and 2, where m_b is the rate of mass converted in $kg/(m^2 s)$, and T_s is the calculated condensed phase surface temperature.

$$m_b(T_s) = \left[\frac{\kappa_c \rho_c A_c R T_s^2 exp(-E_c/RT_s)}{C_p E_c [T_s - T_0 - Q_c/2C_p]}\right]^{1/2} \tag{1}$$

$$T_s(m_b, P) = T_0 + \frac{Q_c}{C_p} + \frac{Q_g}{C_p(1 + \frac{x_g(m_b,P)}{x_{cd}(m_b)})} \tag{2}$$

The surface temperature of the solid is dependent on the initial bulk solid temperature, T_0. An increase in the surface temperature is a result of the condensed phase reacting to intermediates, and the conductive heat transfer from the luminous flame reactions. In determining the mass burn flux and surface temperature the flame standoff distance, x_g, convective-diffusive length, x_{cd}, and the Damkohler number, D_a, must be determined as seen in Equations 3,4, and 5. Equations 1 and 2 are solved iteratively until a convergence criteria is met. For use in Uintah, this model has been modified to include three dimensional effects by including the surface area of a cell and the total mass within the cell[23], see Equations 6, and 7. This model has been validated against experimental data for a wide range of pressures at initial solid temperatures of 273K, 298K and 423K[18].

$$x_g(m_b, P) = \frac{2x_{cd}(m_b)}{\sqrt{{m_b}^2 + 4D_a(m_b, P)} - m_b} \tag{3}$$

$$x_{cd}(m_b) = \frac{\kappa_g}{m_b C_p} \tag{4}$$

$$D_a(m_b, P) = \frac{B_g MW^2 C_p P^2}{R^2 \kappa_g} x_{cd}(m_b)^2 \tag{5}$$

$$MB = \Delta t * BFA * m_b \tag{6}$$

$$BFA = \frac{\Delta x * \Delta y * \Delta z}{(\Delta x|g_x| + \Delta y|g_y| + \Delta z|g_z|)\frac{1}{max(g^{(1/3)})}} \tag{7}$$

The WSB model utilizes the crack propagation results from the ViscoSCRAM constitutive evaluation to model the transition into convective deflagration as defined by Berghout[9]. The critical pressure, P_c, is dependent on the crack radius or porosity, w, and computed using Equation 8.

$$P_c^{2.84} w^2 = 8x10^8 \tag{8}$$

The ViscoSCRAM constitutive model was developed for the explosive PBX-9501 to describe crack development and the formation of hot spots in damaged materials. It is a combination

of Maxwell's visco-elastic model developed by Addessio et al.[2] and the Statistical Crack Mechanics model[10], developed at Los Alamos National Laboratory. ViscoSCRAM was developed to model the mechanical behavior of brittle explosives under non-shock conditions accounting for the viscoelastic response, statistical fracture mechanics and hot spot ignition. The growth of the cracks in a solid explosive are dependent on the initial crack radius, crack growth rate, five Maxwell elements and other parameters allowing for random distribution of cracks[6]. This model has been fit to match experimental relaxation times as determined by the visco-elastic response[6]. More about Uintah's validated reaction and material models can be found at[18].

3.1 Conductive Deflagration Model

The WSB model, described in Section 3.0, shows good agreement with experimentally measured mass burn rates over a wide range of initial solid temperatures[18]. Before Equations 1-5 are solved, certain conditions in the computational cells need to be satisfied. Those conditions include:

- The computational cell must be on the surface of the explosive, or the product gas pressure in a surrounding cell must be above the critical pressure for convective deflagration.
- There must be a surrounding cell with a significant amount of material above the ignition temperature. For PBX-9501 the ignition temperature is 550 K.

Once these criteria are satisfied, the cell will react converting solid HMX $\rightarrow$ gas via Equations 1-5.

As discussed above the original one dimensional WSB model was extended to three dimensions, allowing for Equations 1-5 to be calculated over a finite cell of reactant[23]. This extension introduced a grid resolution dependence. The WSB model computes the mass converted during a finite amount of time using Equations 1, and 2. This rate is then multiplied by the burn front area of the cell, BFA, and the change in time, Δt, using Equation 6. For conductive deflagration the burn front area is calculated by the surface of the cell exposed to air using Equation 7. Where Δx, Δy, and Δz are the length of the finite volume grid cell in the x, y, and z directions and g_x, g_y, and g_z are the components of the normalized density gradient[23]. This allows for only the surface of the explosive to deflagrate, making the burn rate of conductive deflagration independent of the cell size.

The WSB Equations 1-5, and the criteria for burning initiation has been shown to compute the correct conductive mass burn rate, however the propagation velocity of the deflagration front was orders of magnitude faster than the measured velocities. This overdriven velocity was due to the discretization of the domain into cells of a finite size and the cell ignition criteria described above. We discovered that cells adjacent to a burning cell could ignite before the deflagration traversed across the burning cell. This "skipping" or "jumping" of the reaction was dependent on cell spacing and timestep size.

To mitigate this non-physical propagation we added an "induction period" before mass could be consumed. This "induction period" is meant to emulate the amount of time needed for the hot gases to flow through the cell before igniting the next one. In doing so the propagation of deflagration will be constant for all cell sizes, eliminating a resolution dependence. The length of the "induction period" is dependent on the product gas pressure in the surrounding cells and the grid resolution. Son et al.[19] experimentally measured the propagation velocity of a flame on the surface of PBX-9501 and found it to follow Equation 9, where P_d is the dimensionless pressure (P/P_0, P_0 =0.1 MPa). This equation was used in the determination of the "induction

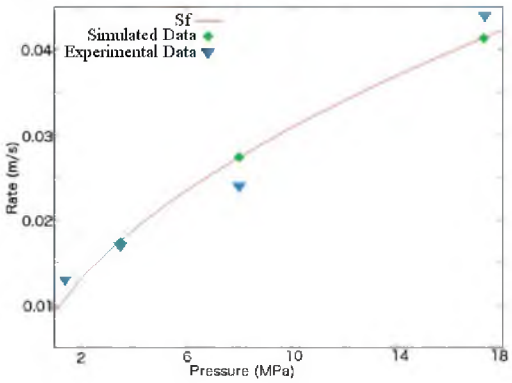

Figure 2: Pressure dependence of the conductive deflagration propagation. Simulated two dimensional results (diamonds) compared to experimental data (triangles) determined by Son et al.[19].

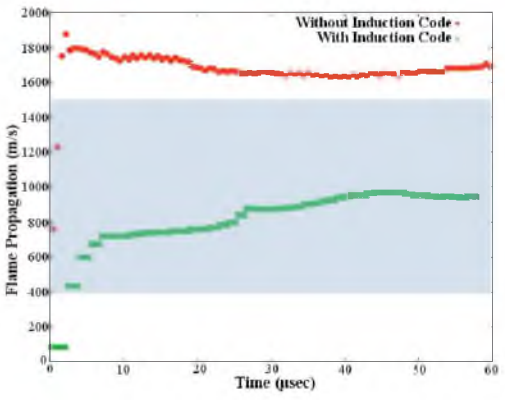

Figure 3: Instantaneous convective deflagration propagation vs time for a 1 dimensional simulation. This plot shows the large decrease in propagation velocity with the "induction period" correction seen by the green points. The blue shaded region is experimentally determined propagation of convective deflagration for PBX-9501[8].

period", Equation 10, where Δx is the average length of the cell and A is a constant used to control the propagation velocity. For conductive deflagration A=1, following the equation determined by Son et al.[19]. The addition of an "induction time" corrected the deflagration propagation velocity on the surface of PBX-9501 as shown in Figure 2.

$$S_f = 0.259 P_d^{0.538} \tag{9}$$

$$\tau = \frac{\Delta x A}{S_f} \tag{10}$$

3.2 Convective Deflagration Model

The propagation of a convective deflagration is a complex phenomena and there is no empirical correlation to describe the flame propagation into cracks or pores. For PBX-9501 the propagation velocity in cracks has been experimentally measured to be between 400 and 1500 m/s[8]. Our model for deflagrating PBX-9501 has been validated against experimental data for multiple pressures, initial temperatures and grid resolutions for conductive deflagration[18, 17]. An abundance of research has been directed at understanding convective deflagration[14, 5, 7], but there are still many unknowns and no empirical correlations similar to Equations 1-5 and 9 to evaluate the mass burn rate and propagation velocity. We therefore assume that the WSB model is valid in this regime and compute the mass burn rate and propagation velocity using Equations 1-6, 9 and 10. The constant A was determined using a one dimensional simulation where a stick of PBX-9501 was thermally ignited at elevated pressures, to ensure convective deflagration. The propagation of the deflagration was measured by the amount of time it took for the burn front to travel a known distance through the material. A was varied until simulation results matched the experimental data to within the bounds of uncertainty. In our simulations

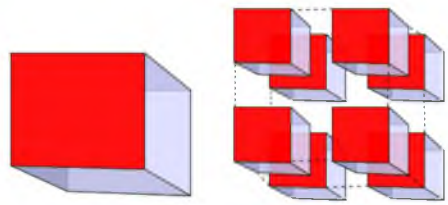

Figure 4: Illustration of a grid cell doubling in resolution resulting in the surface area doubling seen by the red cell faces.

using Δx = 2 mm, A = 0.0002 gave the most accurate convective deflagration propagation velocity. This constant will change with each explosive and has only been determined for PBX-9501. Figure 3 shows the decrease in propagation velocity with the addition of an "induction period" correction, as shown by the green line. The blue shaded region are the experimental results of Berghout et al.[8].

With convective deflagration the reaction occurs inside the reactant, therefore the burn front area was assumed to be one sixth of the surface area of the cell, introducing a resolution dependence. By calculating the burn front area this way, the total mass burned for a given volume would double when increasing the resolution of a cell by two. Figure 4 illustrates this phenomena as seen by the area of the red cell faces doubling. To account for this, the burn front area for convective deflagration is calculated using Equation 11, where BFA_{ref} is the reference burn front area. The elimination of the normalized density gradient was attributed to the fact that convective deflagration occurs in cells which are not on the surface, therefore the normalized density gradient in a homogenous material will cause the denominator of Equation 7 to equal Δx for a square cell. By evaluating the burn front area of convective deflagration with respect to a reference resolution the grid dependence was eliminated. The reference resolution of $2mm$ was chosen for our simulations because the flame propagation and conductive burn rates for this resolution lie within the experimental data and the resolution is large enough to run petascale simulations without loss of fidelity[17]. Until further experimental research is done to fully understand the mass burn rate with convective deflagration this approach, to the best of our knowledge, accurately represents convective deflagration and decreases the non-linearity in the simulations.

$$BFA_{new} = \frac{\Delta x * \Delta y * \Delta z}{BFA_{ref}} \tag{11}$$

3.3 Grid Convergence Study

A grid convergence study was performed to ensure that the time to detonation of deflagrating PBX-9501 was no longer exhibiting a resolution dependence. This study utilized all reaction models, equations of state, and material models needed to represent a DDT. For this study a 2D stick of PBX-9501 was thermally activated at ambient pressure with a bulk temperature of 298K; 5 different grid resolutions were examined ranging from $4mm$ to $0.25mm$. The time from thermal activation to detonation for each resolution was analyzed. Clear convergent behavior can be seen in Figure 5 as resolutions approached $0.5mm$. Although convergence criteria can be met at a $0.25mm$ resolution, running large 3D simulations at a fine mesh size can be very computationally expensive. Thus, all of the simulations for this research used a resolution of $2mm$. By increasing the grid resolution from $0.25mm$ to $2mm$ large 3D simulations can be run using 512 times less computing power with only a 8% error associated with the time to detonation. Extensive research has been done on the effects of increasing the resolution on the burn rate and the detonation propagation[17]. We have determined that the rate of reaction for conductive[17] and convective deflagration have no dependence on the resolution and the denotation velocity is not affected by the increase of resolution until cells are $8mm$ or larger[17].

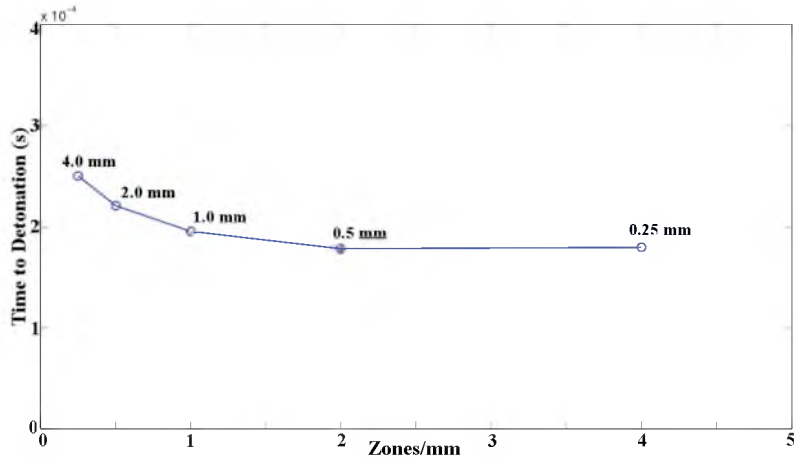

Figure 5: Convergence study results on the time to denotation as a function of the resolution.

4 Conclusion

Modeling the Deflagration to Detonation Transition in solid explosives is very difficult. The addition of an "induction period" to the Uintah DDT1 model has allowed for a more accurate representation of the flame propagation velocity for conductive and convective deflagration. The new burn front area calculation has eliminated the resolution dependence of the mass burn rate for convective deflagration. With these changes Uintah accurately predicts a Deflagration to Detonation Transition in solid PBX-9501 and HMX. Large scale simulations would not be possible without the use of the global kinetic reaction model and a non-resolution dependent burn model.

Current efforts are focused on analyzing a large scale 3D simulation run on 64,000 cores on DOE's Mira. This simulation consists of 968 million particles in 206 million cells representing 1/8th of the semi-tractor-trailer involved in the 2005 accident. These results will give us a better understanding into the physical mechanisms of DDT in large arrays of explosives and will be used to determine a safer packaging configuration to suppress the probability of transportation accidents in the future.

Acknowledgments

Uintah was developed by the University of Utah's Center for the Simulation of Accidental Fires and Explosions (C-SAFE) and funded by the Department of Energy, subcontract No. B524196. This work was supported by the National Science Foundation under subcontract No.OCI0721659. An award of computer time was provided by the Innovative and Novel Computational Impact on Theory and Experiment (INCITE) program. This research used resources of the Argonne Leadership Computing Facility at Argonne National Laboratory, which is supported by the Office of Science of the U.S. Department of Energy under contract DE-AC02-06CH11357 (sub-award Uintah_Safety) . This research used resources of the Oak Ridge Leadership Computing Facility at the Oak Ridge National Laboratory, which is supported by the Office of Science of the US DOE under contract DE-AC05-00OR22725 (sub-award ENP009). This work also used the Extreme Discovery Environment (XSEDE), which is supported by NSF

grant OCI1053575 (sub-award TGMCA08X004).

References

[1] http://www.uintah.utah.edu.

[2] F. Addessio and J. Johnson. A Constitutive Model for the Dynamic Response of Brittle Materials. *Journal of Applied Physics*, 67:3275–3286, 1990.

[3] W. R. Anderson, N. E. Meagher, and J. A. Vanderhoff. Dark Zones of Solid Propellant Flames: Critically Assessed Datasets, Quantitative Model Comparision, and Detailed Chemical Analysis. *Combustion and Flame*, 158:1228–1244, 2011.

[4] B. Asay, editor. *Shock Wave Science and Technology Reference Library*, volume 5 pages 483-489. Springer, 2010.

[5] B. W. Asay, S. F. Son, and J. B. Bdzil. The Role of Gas Permeation in Convective Burning. *International Journal of Multiphase Flow*, 22(5):923–952, 1996.

[6] J. G. Bennett, K. S. Haberman, J. N. Johnson, B. W. Asay, and B. F. Henson. A Constitutive Model for the Non-Shock Ignition and Mechanical Response of High Explosives. *Journal of the Mechanics and Physics of Solids*, 46(12):2303–2322, 1998.

[7] H. L. Berghout, S. F. Son, and B. W. Asay. Convective Burning in Gaps of PBX 9501. In *Procceedings of the Combustion Institute*, volume 28, pages 911–917, 2000.

[8] H. L. Berghout, S. F. Son, L. G. Hill, and B. W. Asay. Flame Spread Through Cracks of PBX 9501 (a Composite Octrahydro-1,3,5,7-Tetranitro-1,3,5,7-Terazocine-Based Explosive). *Journal of Applied Physics*, 99:114901–7, 2006.

[9] H. L. Berghout, S. F. Son, C. B. Skidmore, D. J. Idar, and B. W. Asay. Combustion of Damaged PBX 9501 Explosive. *Thermochimica Acta*, 384(261-277), 2002.

[10] J. K. Dienes, J. Middleditch, J. D. Kershner, Q. H. Zuo, and A. Starobin. Progress in Statistical Crack Mechanics: An Approach to Initiation. In *12th International Detonation Symposium*, San Diego, CA, August 2002.

[11] J. E. Guilkey, T. B. Harman, and B. Banerjee. An Eulerian-Lagrangian Approach for Simulating Explosions of Energetic Devices. *Computers and Structures*, 85:660–674, 2007.

[12] J. E. Guilkey, T. B. Harman, B. A. Kashiwa, J. Schmidt, and P. A. McMurtry. An Eulerian-Lagrangian Approach for Large Deformation Fluid-Structure Interaction Problems, part 1: Algorithm Development. In *Fluid Structure Interactions II*, pages 143–156, Cadiz, Spain, 2003. WIT Press.

[13] T. Harman, J. E. Guilkey, B. A. Kashiwa, J. Schmidt, and P. A. McMurtry. An Eulerian-Lagrangian Approach for Large Deformation Fluid-Structure Interaction Problems, Part 2: Multi-Physics Simulations within a Modern Compuational Framework. In *Fluid Structure Interactions II*, pages 157–166, Cadiz, Spain, 2003. WIT Press.

[14] K. K. Kuo, A. T. Chen, and T. R. Davis. Convective Burning in Solid-Propellant Cracks. *AIAA Journal*, 16(6):600–607, 1978.

[15] A. Macek. Transition from Deflagration to Detonation in Case Explosives. *Journal of Chemical Physics*, 31(1):162–167, 1959.

[16] Q. Meng, A. Humphrey, J. Schmidt, and M. Berzins. Investigating Applications Portability with the Uintah DAG-based Runtime System on PetaScale Supercomputers. In *Procceedings of SC13: International Conference for High Performance Computing, Networking, Storage and Analysis*, pages 96:1–96:12, 2013.

[17] J. R. Peterson, J. Beckvermit, T. Harman, M. Berzins, and C. A. Wight. Multiscale Modeling of High Explosives for Transportation Accidents. In *XSEDE '12: Proceedings of 2012 XSEDE Conference*, New York, NY, 2012. ACM.

[18] J. R. Peterson and C. A. Wight. An Eulerian-Lagrangian Computational Model for Deflagration and Detonation of High Explosives. *Combustion and Flame*, 159:2491–2499, 2012.

[19] S. F. Son and H. L. Berghout. Flame Spread Across A Surface of PBX 9501. In *American Institute of Physics*, pages 0–7354–0341–4, 2006.

[20] P. C. Souers, S. Anderson, J. Mercer, E. McGuire, and P. Vitello. JWL++: A Simple Reactive Flow Code Package for Detonation. *Propellants, Explosives, Pyrotechnics*, 25:54–58, 2000.

[21] C. M. Tarver, T. C Goodale, R. Shaw, and M. Cowperthwaite. Deflagration-to-Detonation Transition Studies for Two Potential Isomeric Cast Primary Explosives. In *6th Symposium (International) on Detonation*, Coronado, CA, 1976.

[22] M. Ward, S. F. Son, and M. Brewster. Deflagration of HMX with Simple Kinetics: A Gas Phase Chain Reaction Model. *Combustion and Flame*, 114:556–568, 1998.

[23] C. A. Wight and E. Eddings. Science-Based Simulation Tools for Hazard Assessment and Mitigation. *International Journal of Energetic Materials and Chemical Propulsion*, 8(373-389), 2009.

A Nomenclature

A	Induction time coefficient			
A_c	Condensed phase frequency factor	$1.637\text{x}10^{15}$	$1/s$	[23]
B_g	Gas phase frequency factor	$1.6\text{x}10^{-3}$	$m^3/(kg \cdot K^2 \cdot s)$	[23]
BFA	Burn front area		m^2	
BFA_{new}	New burn front area		m^2	
BFA_{ref}	Reference burn front area	0.002	m	
C_p	Specific heat of the condensed phase	$1.4\text{x}10^{3}$	$J/(kg \cdot K)$	[23]
D_a	Damkohler number			[22]
E_c	Condensed phase activation energy	$1.76\text{x}10^{5}$	J/mol	[23]
g_x	x component of the normalized density gradient			[23]
g_y	y component of the normalized density gradient			[23]
g_z	z component of the normalized density gradient			[23]
m_b	Mass flux		$kg/(m^2 \cdot s)$	[22]
MB	Mass burned per timestep		kg/s	
MW	Molecular weight	$3.42\text{x}10^{-2}$	kg/mol	[23]
P	Pressure		Pa	
P_c	Critical pressure		Pa	[9]
P_d	Dimensionless pressure	P/P_0 P_0= $0.1MPa$		[8]
Q_c	Chemical heat release from condensed phase reaction	$4.0\text{x}10^{5}$	J/kg	[23]
Q_g	Chemical heat release from gas phase reaction	$3.018\text{x}10^{6}$	J/kg	[23]
R	Ideal gas constant	8.314	$J/(K \cdot mol)$	[22]
S_f	Flame propagation		cm/s	[8]
T_s	Surface temperature of the condensed phase		K	[22]
T_0	Initial temperature of condensed phase		K	[22]
w	Crack radius		m	[9]
x_{cd}	Convective-diffusive length		m	[23]
x_g	Gas phase flame thickness		m	[22]
κ_c	Condensed phase thermal conductivity	0.2	$W/(m \cdot K)$	[23]
κ_g	Gas phase thermal conductivity	0.07	$W/(m \cdot K)$	[23]
ρ_c	Density of condensed phase	$1.34\text{x}10^{3}$	kg/m^3	[23]
τ	Induction time		s	
Δt	Change in time		s	
Δx	Length of cell in the x direction		m	[23]
Δy	Length of cell in the y direction		m	[23]
Δz	Length of cell in the z direction		m	[23]

CHAPTER 6

PHYSICAL MECHANISMS OF DDT IN AN ARRAY OF PBX 9501 CYLINDERS

This chapter has been submitted to Combustion and Flame, Jacqueline Beckvermit, Todd Harman, Chuck Wight and Martin Berzins, "Physical Mechanisms of DDT in an Array of PBX 9501 Cylinders," January 2016.

The Deflagration to Detonation Transition (DDT) in large arrays (100s) of explosive devices is investigated using large-scale computer simulations running the Uintah Computational Framework. Our particular interest is understanding the fundamental physical mechanisms by which convective deflagration of cylindrical PBX 9501 devices can transition to a fully developed detonation in transportation accidents. The simulations reveal two dominant mechanisms, inertial confinement and Impact to Detonation Transition. In this study we examined the role of physical spacing of the cylinders and how it influenced the initiation of DDT.

6.1 Introduction

In 2005 a semi-tractor-trailer carrying 8,400 seismic boosters on US Route 6 in Spanish Fork Canyon, Utah overturned and ignited. Within three minutes, the deflagration caused by the fire transitioned into a fully developed detonation. The detonation produced a crater approximately 24 m wide and 10 m deep; hot metal shards from the trailer started small fires a quarter of a mile away. From the size of the crater it is clear that the explosive underwent a Deflagration to Detonation Transition (DDT). This research is focused on determining the physical mechanisms of a DDT in large arrays of explosive cylinders. This research is significant since the reaction rates of the two modes of combustion (deflagration and denotation) differ by roughly five orders of magnitude, and similar accidents could occur in the future in populated areas.

Many scientists have studied how a subsonic reaction, controlled by heat transfer (deflagration), transitions into a fully developed, highly energetic detonation in a single device.

Previous research determined that the different mechanisms for this transition depended, in part, on the porosity and phase of the monolithic solid in a highly confined environment. The mechanisms were studied experimentally[1–4] and computationally.[5,6] The physical experiments consist of a condensed phase explosive, packed at various fractions of Theoretical Maximum Densities (TMD), confined in a steel tube. The explosive was ignited by a combustion-driven piston moving at low velocities to avoid a shock to detonation transition.[1] Diagnostic probes were placed throughout the steel tube to measure the response of the explosive bed, including but not limited to the velocity of the piston, the velocity of the pressure waves and the onset of convective deflagration. For explosives near the TMD, the mechanism for DDT was the coalescence of pressure waves. In highly confined experiments as described above, the deflagration produces pressure waves which propagate through the material, in front of the reaction zone. At some distance the waves coalesce forming a shock discontinuity. This shock continues to grow in strength until the pressure rise causes a transition to detonation.[2,5,7] In monolithic solid explosives convective deflagration plays a very important role in the transition because the pressure waves are generated within the material. Convective deflagration occurs in the cracks and pores of the solid material and is controlled by the convective heat transfer of the penetrating gases.[8] As a result of the pressure waves, the explosive undergoes deformation and is damaged allowing the flame to penetrate deeper.

The mechanism for DDT in lower density condensed phase explosives (50-70% TMD) is similar. In the experiments of[1,4,7] a porous bed of explosive was ignited by a slow-moving piston. The initial compaction wave from the piston traveled through the explosive bed, compressing the porous material to around 90% TMD. The frictional hot spots and shear caused by the initial compaction wave ignited the explosive material. Pressure waves formed behind the initial compaction wave, further compressing the explosive bed, forming a $\sim$100% TMD high-density plug. This plug was formed in front of the burn front and behind the compaction wave. As the convective deflagration traveled towards the plug, the size of the plug grew. Once the burn front reached the back of the high-density plug, it behaved as a second piston, causing a shock to detonation transition in the remaining unburnt explosive.[1,4,7]

Though the mechanisms for DDT are understood and accepted for highly confined monolithic solids, to our knowledge no research has examined how the shape of the explosive or how the interactions with other explosives influences the transition to detonation. Here we examine arrays of explosive cylinders, specifically those present in the 2005 transportation

accident. The explosive of interest is PBX 9501 (95% 1,3,5,7-octahydro-1,3,5,7-tetranitro-1,3,5,7-tetrazocine (HMX) and 5% of a plastic binder) due to the abundance of experimental data and previously validated numerical models for describing DDT.[9,10] These arrays have gaps between the cylinders providing a pathway for products of reaction to escape and space for cylinders to accelerate and collide with each other, unlike a monolithic solid. We therefore expect some similarities to the observed mechanism of porous explosives, with differences due to the interactions with other explosives and the unconfined nature of this problem. The aim of this paper is to present two physical mechanisms for a DDT in multiple large arrays of PBX 9501 cylinders. The two mechanisms are inertial confinement and Impact to Detonation Transition. Section 6.2 will describe the computational domain and initial conditions, numerical models and present results showing justification for performing 2D simulations. Section 6.3 will describe the two dominant DDT mechanisms.

6.2 Computational Methods

To investigate the mechanisms for initiating a DDT in an array of explosives, large-scale simulations were conducted. These simulations were performed in two and three dimensions. The array consisted of PBX 9501 cylinders, with dimensions similar to those in the 2005 trucking accident, (0.054 m in diameter and 0.33 m long). The sizes of the cylinders were fixed and the packing configuration was varied see Figure 6.1. Table 6.1 describes the different initial configurations for each simulation presented. The compaction and displacement of the explosive cylinders which would be seen in a transportation accident was not examined. This research was focused on determining the initiation mechanism for DDT in an ordered array of explosive cylinders to understand how deflagration transitions to detonation in the transportation and storage of explosive cylinders. It is understood the movement of the cylinders in the truck rolling over would effect the placement of the cylinders and ultimately the initiation mechanism. The two-dimensional simulations were run with the $x-, y-, z-$and $z+$ boundaries closed (planes of symmetry), prohibiting gases or explosive particles from escaping. On the $x+$ and $y+$ boundaries we assumed a zero gradient for temperature, pressure, density, and velocity. These boundaries were positioned $>$0.5 m from the reactive explosive to minimize any nonphysical boundary condition effects. The initial temperature of the cylinders and surrounding gas was 300 K, and the pressure was 1 atm. To initiate the reactions, the gas temperature in a few computational cells on the $x-$ boundary was set to 2500 K. Adaptive Mesh Refinement and a grid resolution of 2 mm was used to decrease computational costs without loss of fidelity of the results.[9–11]

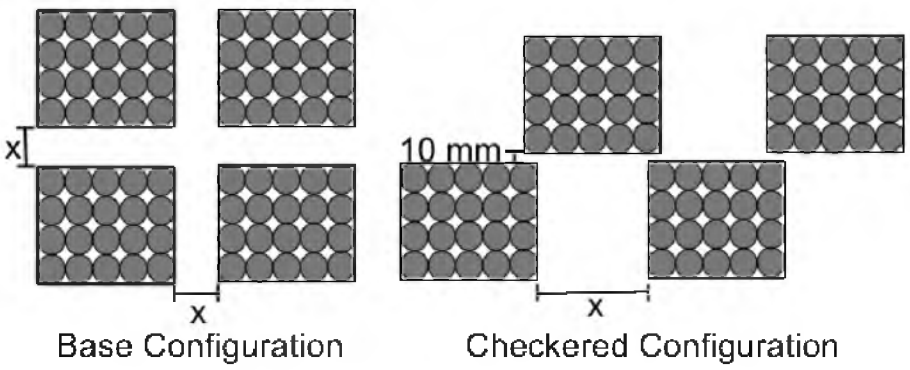

Figure 6.1: Initial configurations of explosive boxes. Both configurations have 20 cylinders per box.

Table 6.1: Initial Conditions

Simulation Name	# of Cylinders per box	Spacing between boxes (x)	Configuration (Described in Figure 6.1)
Transportation Accident	20	10 mm	Base
Base_20_190mm	20	190 mm	Base
Checkered_20_220mm	20	250 mm	Checkered
Base_16_120mm	16	120 mm	Base
Base_12_90mm	12	90 mm	Base
Base_4_14mm	4	14 mm	Base
Base_1_6mm	1	6 mm	Base

Resolution studies previously showed that 2 mm grid resolution could be used without degradation to the results.[10,11]

The simulations were all run using the Uintah Computational Framework[12,13] developed at the University of Utah. This framework utilizes the fluid-structure interaction algorithm of MPM, ICE and MPMICE[14–16] to solve for the conservation of mass, momentum and energy. The Material Point Method (MPM) is used to evaluate the evolution of the solid material. MPM allows the solid field (Lagrangian points) to distort,[15,17–19] then they are interpolated back to the cell center in order to be incorporated into the CFD multimaterial model (MPMICE). This allows for simulations consisting of multiple-phase materials to use the same Eulerian background mesh with no issues related to the laws of conservation. The development and methods for solving the governing multimaterial CFD model equations are found in.[14–16,20,21] Embedded within MPMICE is a DDT reaction model. The reaction model has been validated for multiple initial temperatures (273, 298, and 423 K), pressures

(0.5-60 MPa) and grid resolutions.[9–11,22] The model utilizes a modified Ward, Son and Brewster (WSB) burn model[10,22,23] to evaluate the mass conversion rate, the ViscoSCRAM constitutive model[24] to model the damage in the solid, and the JWL++ simple reactive flow model[25] to describe detonation. The DDT model implemented in Uintah does not use the JWL++ model to determine the onset of detonation, it is used to determine the mass conversion rate once detonation is reached. Uintah's DDT model determines when detonation is reached by exceeding a pressure threshold of 5.3 GPa. As described by Peterson et al.,[9] this approach gave reasonable run distance to detonation results for shock-initiated detonation. The commonly used JWL equation of state[25,26] was used for the solid explosive and the product gases. A full description of the models used and their limitations can be found in.[9]

Substantial changes in the Uintah infrastructure were required in order to run these numerical experiments at the scales required. The MPMICE component, which produces a graph of tasks to be executed, is now done dynamically[27] by using message passing to communicate between nodes.[13,28] This method has been shown to be portable across a number of different supercomputers, and has been applied to early simulations of the DDT problem considered here.[29,30] More recently, substantial changes were required to the Uintah infrastructure to allow the large-scale simulations described in Section 6.2.1.[31] Once these changes were in place, Uintah demonstrated that it is possible to model the 2005 transportation accident.[31]

6.2.1 Dimensional Effects

In this section we provide justification for using low-cost 2D computational domains for our investigations, as was done in.[31] Highly resolved 3D simulations are computationally expensive and require tens of thousands of computing cores, running for hundreds of wall clock hours to complete a single simulation. To reduce these costs the effect of the length of the computational domain in the z direction was investigated. Three simulations were performed with z = 3 m (full 3D), 0.33 m (highly confined 3D), and 2 mm (2D). The explosive packing configuration of the 2005 transportation accident, consisting of 20 explosive cylinders packaged in a fiberboard box, was used. For simplicity the fiberboard was not modeled, instead 10 mm gaps filled with air separated the "boxes." In the 2D and highly confined small 3D simulations the $x-, y-, z-$ and $z+$ boundaries were symmetric walls while the $x+$ and $y+$ boundary conditions were a zero gradient for the primitive variables $[T, p, v, \rho]$. Figure 6.2 shows three domain sizes.[31] The small, highly confined 3D domain, yellow region, includes the addition of a 10 mm gaps between the boxes in the z

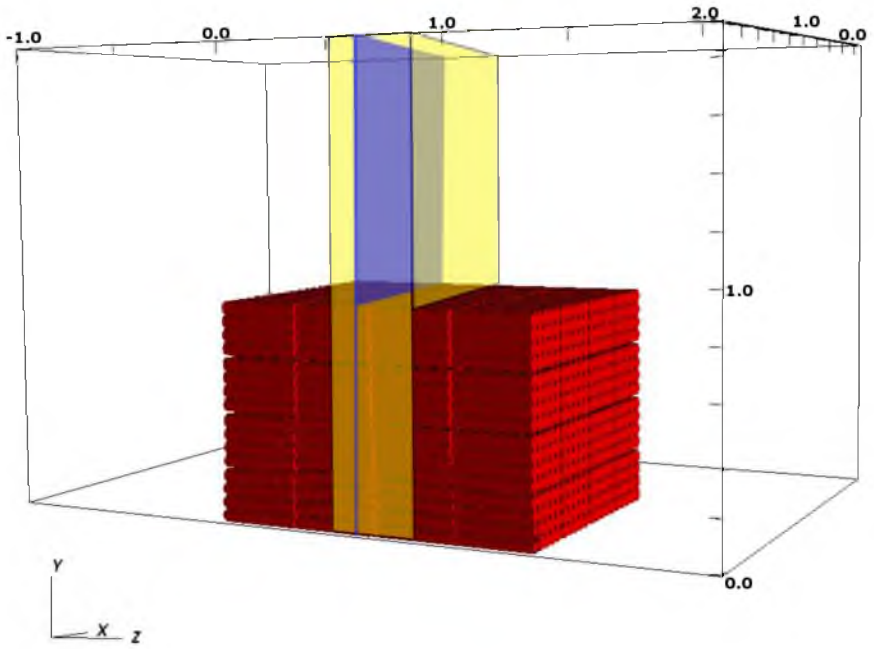

Figure 6.2: Image illustrating the initial conditions of the 2D (blue), small 3D (yellow) and full 3D (whole image) simulations. The cylinders, red, are packaged in the Transportation Accident configuration, consisting of 20 cylinders per "box".

direction. The gap is critical since it allows the hot product gases to expand, similar to the full 3D simulation. Finally, the boundary conditions in the full 3D simulation were planes of symmetry on the $x-$ and $y-$ boundaries, acting as the ground and the back of the truck. All other boundaries conditions were set to a zero gradient for the primitive variables, and the edge of the domain was far from the area of interest to minimize nonphysical boundary condition effects.

All three simulations were ignited on the $x-$ axis by hot product gas, and they exhibited similar behavior until detonation occurred. We concluded that the DDT resulted from inertial confinement, which will be discussed in Section 6.3. Figure 6.3 shows the maximum pressure in the computational domain as a function of time.[31] Note the good qualitative agreement between the three experiments. The oscillations in the pressure profile are due to the deflagration encountering the open space surrounding each cylinder as it traversed through the cylinders. As expected, the large 3D simulation took longer to detonate due to the additional escape routes for expanding product gases. By increasing the length of the$z$dimension the product gases could expand, slowing the rate of pressurization in the domain and increasing the time to detonation. Not only do the three pressure profiles show similarities, the physical location where the DDT took place and the physical mechanism were very similar, as shown in Figures 6.4, 6.5 and 6.6. Note that detonation occurred in

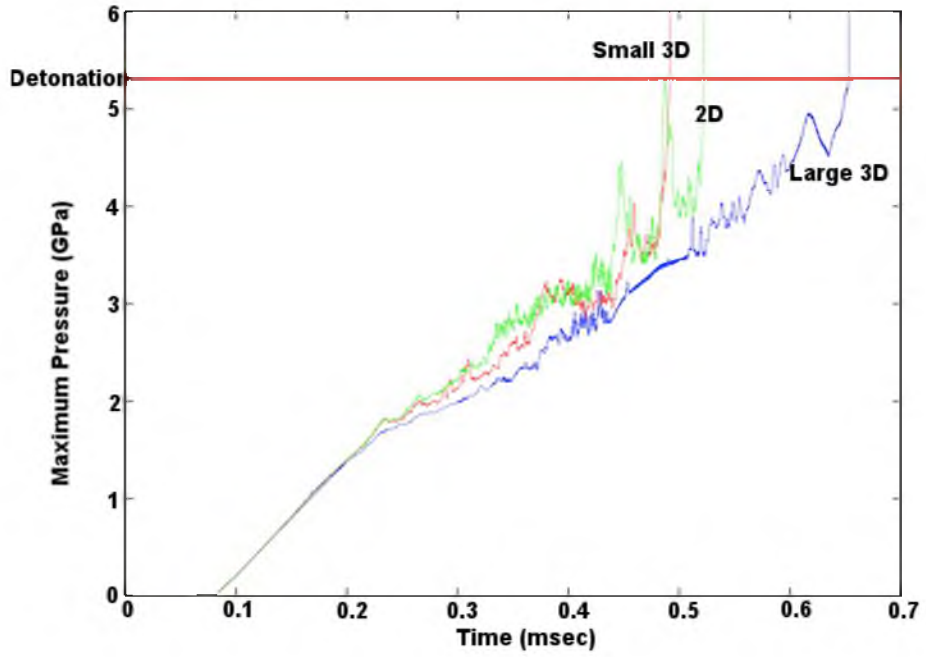

Figure 6.3: Maximum pressure in the domain versus time for the different-sized computation domains.

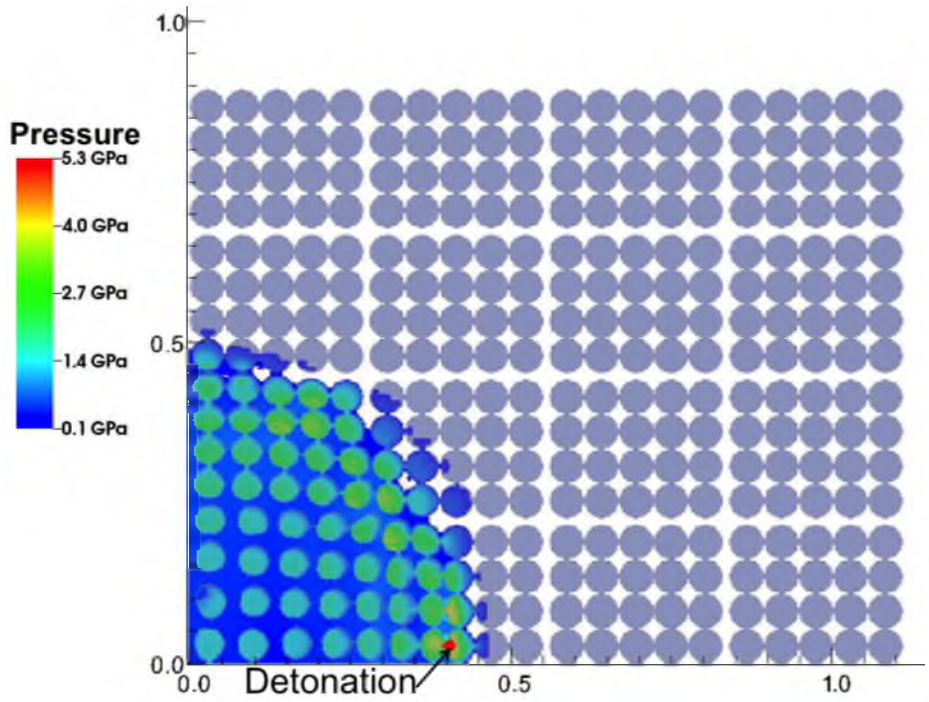

Figure 6.4: Contour plot of pressure and shadow of explosive cylinders in the 2D simulation (Transportation Accident).

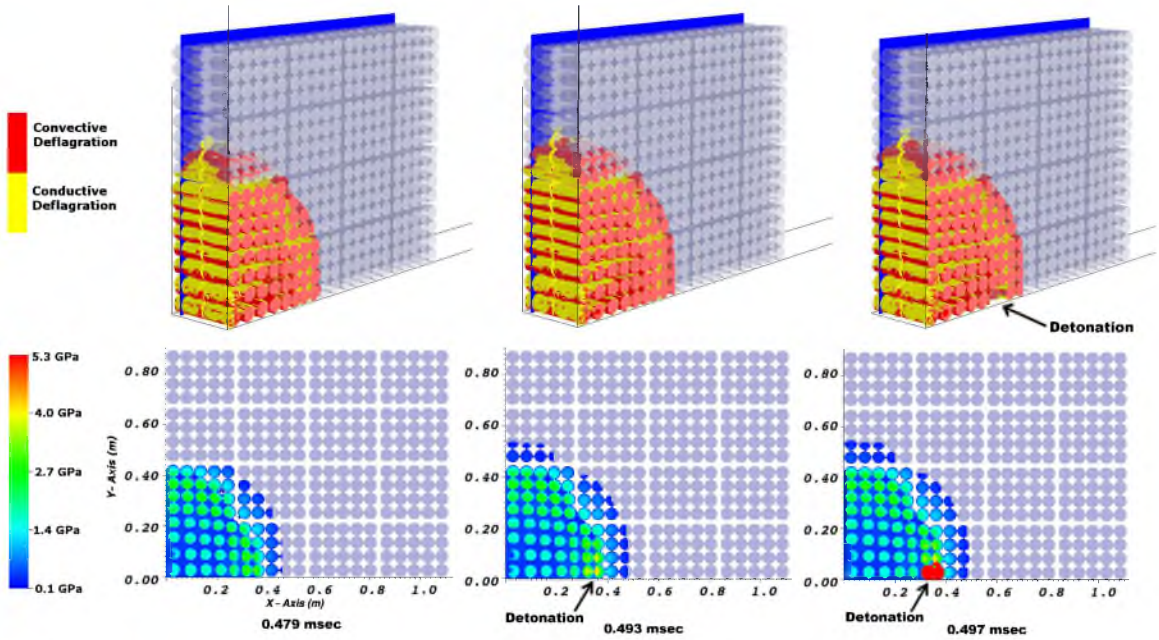

Figure 6.5: The top figure shows the progression of deflagration through the explosives (light blue). The dark blue slice shows the location of the pressure contour plot (shown below). The bottom plot shows the contour plot of pressure of DDT over time in the small 3D simulation used in.[31]

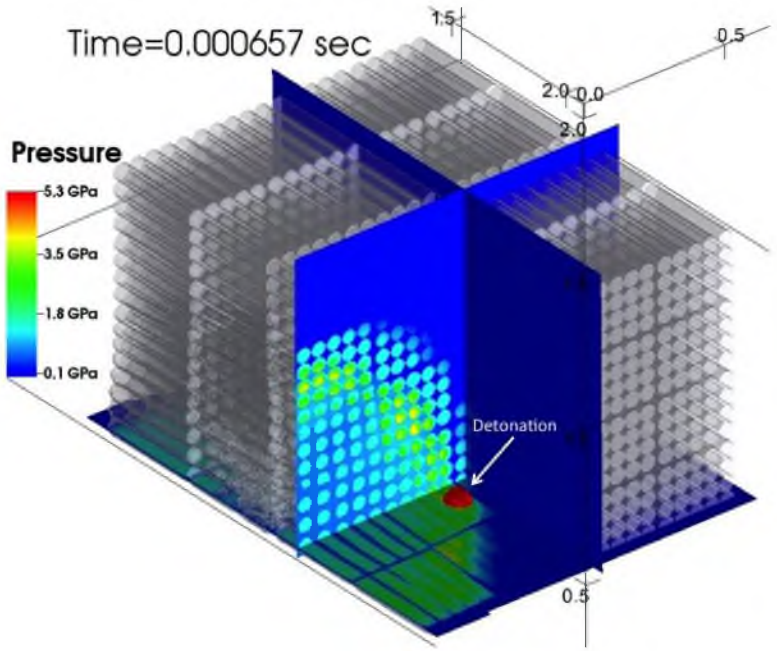

Figure 6.6: Contour plot of pressure and shadow of the explosive cylinders, in the full 3D simulation.

the same "box" of explosives for all three simulations, though in a slightly different position. This is due to the close proximity of the domain walls, preventing product gases from leaving the domain in the 2D and small 3D simulations.

The high computation cost of performing a full 3D simulation and the good quantitative and qualitative agreement in the detonation location and maximum pressure profile justifies using low-cost 2D computational domains in this study. The full 3D simulation cost 24M service units (SU's) while the small 3D and 2D simulations only cost 215K and 10K SU's, respectively.

6.3 Results and Discussion

The main objective of this paper is to understand the physical mechanisms for a DDT in an array of solid explosives. Two mechanisms were predominantly observed over a wide range of initial conditions, inertial confinement and Impact to Detonation Transition. All simulation results presented used the same-sized PBX 9501 cylinders, but the initial spacing between the cylinders and "boxes" was varied, as described in Table 6.1 and Figure 6.1.

6.3.1 Inertial Confinement

Inertial confinement occurs when the inertial mass of the cylinders surrounding a deflagration is greater than the pressure forces exerted on the cylinders. These cylinders move relatively slowly away from the reaction zone and as they move, the cylinders collide and deform, filling in the gaps between the cylinders, trapping the product gases. The deformation and expansion of the explosives is limited due to the close spacing of the cylinders. As deflagration and deformation continues, a high-density barrier is formed, trapping the product gases and increasing the local pressure. The increase in localized pressure causes a positive feedback, increasing the reaction rate until 5.3 GPa is reached and detonation occurs. This phenomenon is shown in Figure 6.7, which shows the volume fraction of PBX 9501 after multiple cylinders have deflagrated and deformed. Figure 6.8 shows the pressure as a function of time and position along the white line in Figure 6.7. As specified by the reaction model, detonation occurs at 5.3 GPa, the red dotted line. Notice that in front of the barrier (0-350 mm) the pressure slowly increases, plateaus, then sharply decreases. In these cylinders the product gases flow unimpeded from the burn front, resulting in a relatively low pressure. The decrease in pressure in these cylinders is sharper than expected due to the cylinders moving through space. Therefore the cylinders from 0-350 mm are slowly decreasing in pressure due to expanding gases and the cylinders moving from the initial position through space while the data is collected at the same point

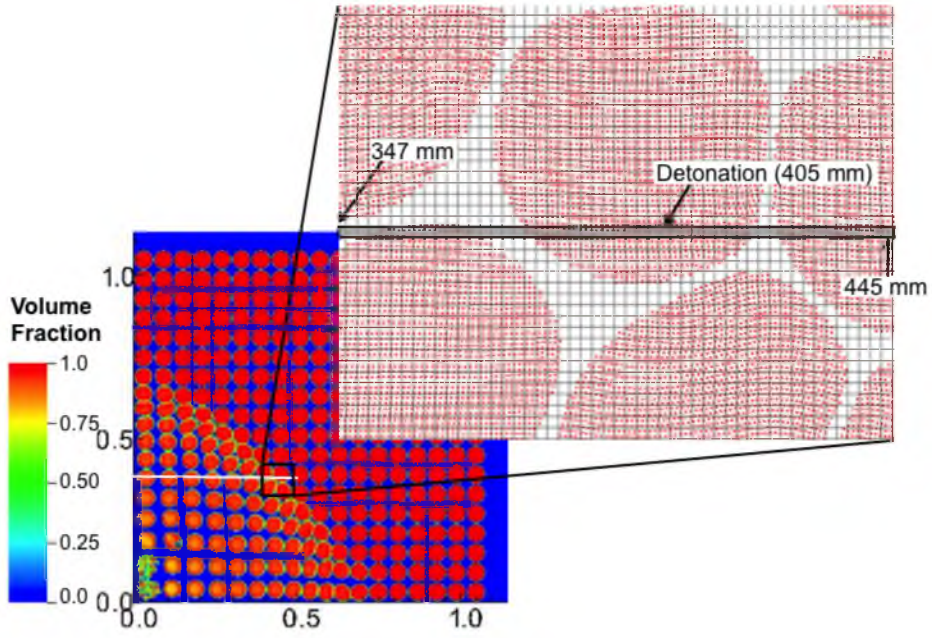

Figure 6.7: Volume Fraction of PBX 9501 cylinders forming a high-density barrier leading to the inertial confinement mechanism in the Base_1_6mm simulation.

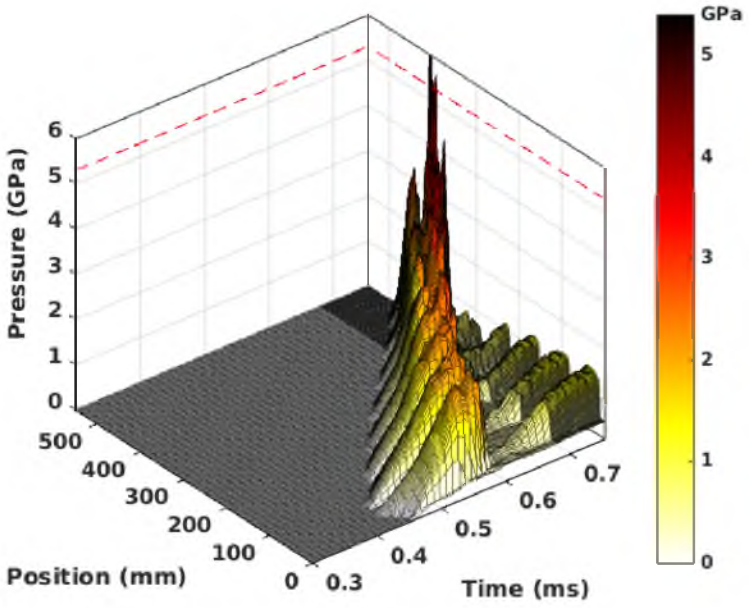

Figure 6.8: Pressure profile versus position and time. The red dotted line represents detonation. Position of data is shown in Figure 6.7.

in space. Between 350-480 mm the high-density barrier begins to form, restricting the flow field and causing an increase in pressure until detonation is reached at 0.753 msec. In this region of the domain we observed the explosive cylinders to be moving at approximately 300 m/s as the barrier is being formed, trapping and compressing the gases between the cylinders. A combination of the pressure wave formed from the compression of the gas and the high-density barrier restricting the expansion of product gases is thought to raise the localized internal pressure of the cylinders from 2-3 GPa to detonation. Beyond 480+ mm the cylinders are at ambient pressure and temperature since hot gases cannot flow beyond the barrier.

The inertial confinement mechanism was also observed when 20 cylinders were placed in a "box" and spaced to reproduce the 2005 Transportation Accident, see Figures 6.4, 6.5 and 6.6. Even though the initial layout of the cylinders is different between these simulations, the same mechanism to initiate DDT was observed. Visually the barrier is not as pronounced for simulations with 20 cylinders per "box" when compared to simulations consisting of one explosive cylinder per "box." However, in both numerical experiments the explosive material and product gases did not have room to expand, thus the cylinders collided and deformed, forming a high-density barrier.

Another way of analyzing the inertial confinement mechanism is looking at the pressure profile in the cell where detonation first occurs, Figure 6.9. This figure shows the pressure profile for many simulations with varying initial cylinder configurations. For inertial confinement the idealized pressure profile is a monotonic raise in pressure after burning first begins in the cell. The Transportation Accident is a perfect example of this. Notice the pressure in the cell where detonation first occurs gradually increases to 5.3 GPa after ignition, without any sharp transitions. The increase in pressure occurs very quickly after the cell is ignited (less than 1 msec). The Base_1_6mm and Base_4_14mm simulations also exhibit this behavior.

With the inertial confinement mechanism the global maximum pressure slowly increases as the barrier is formed. This is illustrated in Figure 6.3, which shows a fairly linear increase in the maximum pressure in the domain until detonation is reached. The amount of time needed to form this barrier depends on the original configuration of the explosives. As expected, the closer the explosives are packaged together, the less time it takes to form the barrier. Inertial confinement has only been observed when the explosives are closely packed together. As the explosives are separated there is more room for the explosive material and gases to expand.

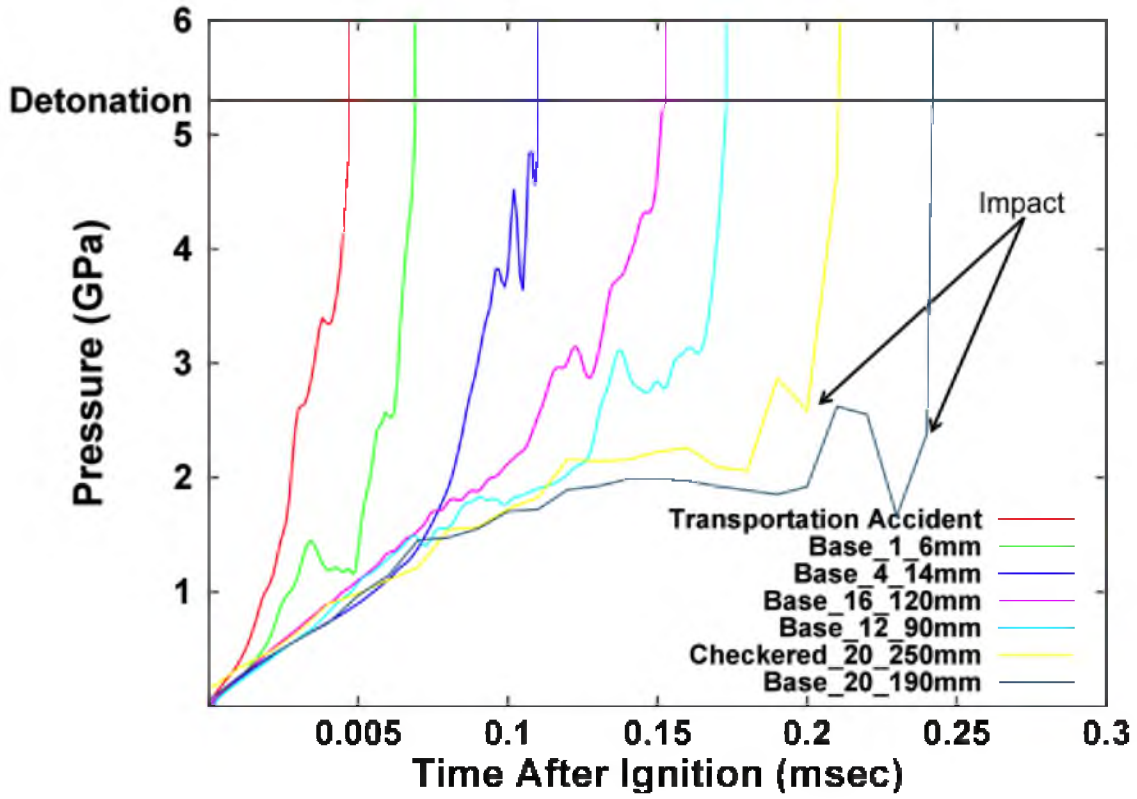

Figure 6.9: Pressure in cell of detonation after time of ignition.

6.3.2 Impact to Detonation Transition

The second mechanism for initiating a DDT in an array of explosive cylinders is an Impact to Detonation Transition (IDT). This occurs when a deflagrating cylinder is impacted by either a) another cylinder or b) by a large pressure wave. When the deflagrating cylinders are at an elevated pressure, the external force can be relatively small to initiate a DDT.

The IDT mechanism was observed in simulations where the cylinders were spaced further apart, allowing gases or solids to accelerate before impacting surrounding cylinders. An example of an IDT is shown in Figure 6.10. The blue region represents surrounding gas and the orange region shows high-density explosive. As the deflagration moved radially through the domain, deflagrating cylinders began deforming and compacting into one another as seen at point A, forming the "jet" shown at point B. The impact of the solid "jet" caused the transition to detonation. The impact generated stress waves in the explosive that reflected, amplified, and accelerated the burn rate to the point of detonation.

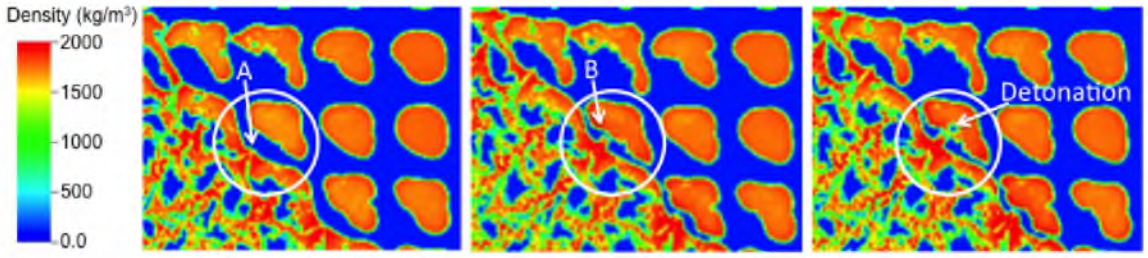

Figure 6.10: Formation of PBX 9501 "jet" leading to a DDT.

Another example of the IDT mechanism was observed when the explosives were packaged 20 (5x4) to a "box." The boxes were evenly spaced 190 mm from one another and separated by ambient gas (Base_20_190 mm simulation). As the deflagration progressed outward from the $x-$ corner of the domain, the deflagrating cylinders moved outward accordingly. As shown in Figure 6.11, the explosive material and gases had ample room to expand. Due to the increased spacing, more cylinders had time to deflagrate before the transition to detonation, increasing the overall time to detonation. This simulation detonated 1.55 msec after ignition, more than double the amount of time observed for an inertial confinement DDT. In this simulation the external force or impact was from a pressure wave produced from the deflagration of surrounding explosives. At each cell, shown by the shaded line in Figure 6.11, a time series of the computed pressure was plotted in Figure 6.12. Notice the pressure in the deflagrating cylinder, 1630-1644 mm, plateaus around 2 GPa before rapidly increasing to detonation, seen by the red dotted line. This phenomenon is evident in Figure 6.9, which shows the pressure in the cell where detonation initiated versus time. The pressure profile for this cell, navy blue line, shows the cell deflagrating for a long period of time (2 GPa), before the impact occurred at t=0.24 msec after ignition of the cell. After the impact there is a sharp increase in pressure, and detonation occurs.

A third example of the IDT mechanism is shown with 20 cylinders packaged to a "box" arranged in a checkerboard configuration, with 0.25 m gaps between each "box," see Figure 6.13 (Checkered_20_250mm simulation). As the deflagration progressed outward, the product gases and explosive moved away from the origin. At 1.73 msec DDT occurred due to an impact event. Close examination of pressure contour plots and particle visualization showed the impact was a pressure wave and high-velocity explosive projectile. Figure 6.14 shows the pressure profile of this simulation as a function of time and position. In this simulation the pressure in the explosive cylinders was approximately 2 GPa before the impact, at which point it rapidly increased to greater than 5.3 GPa. In Figure 6.9 the

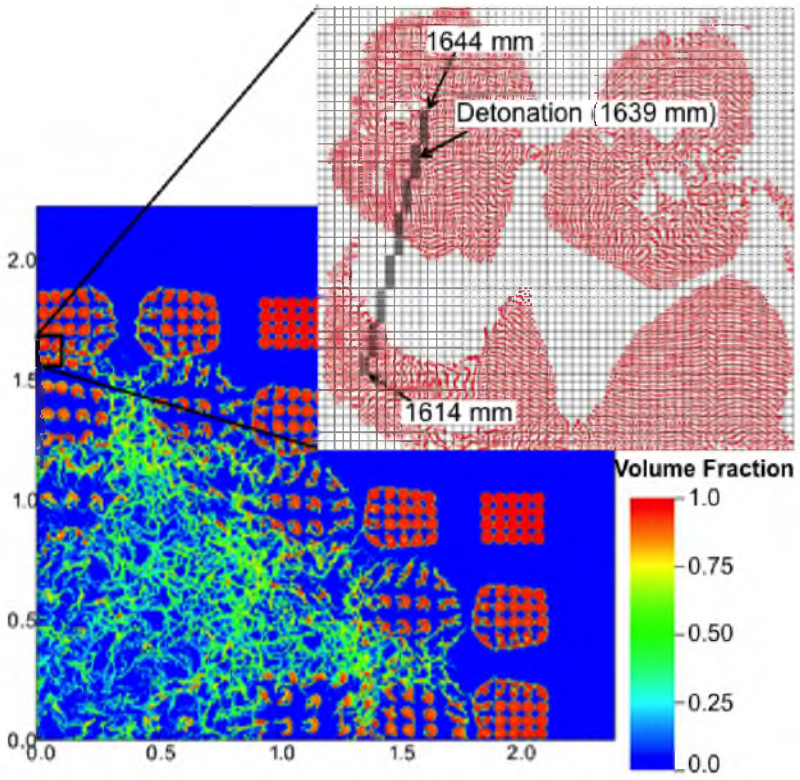

Figure 6.11: Volume fraction of PBX 9501 in the Base_20_190mm simulation exhibiting IDT mechanism behavior.

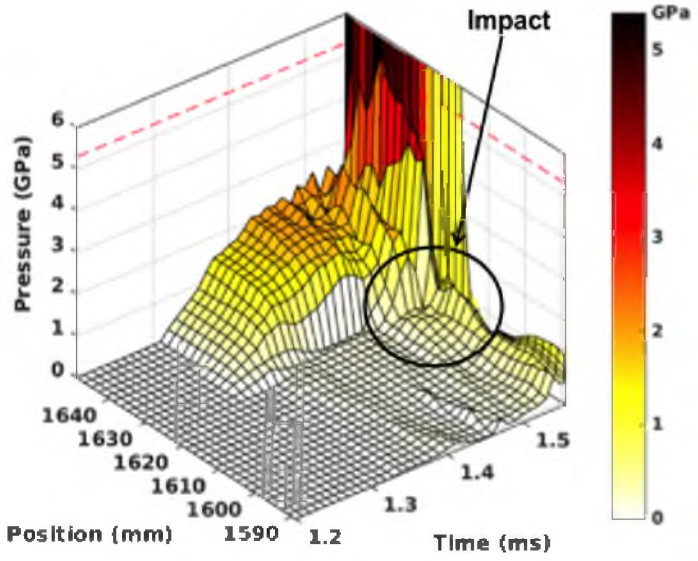

Figure 6.12: Pressure profile versus time and position for an IDT in Base_20_190mm simulation. Position of data extraction is shown in Figure 6.11 by the grey region.

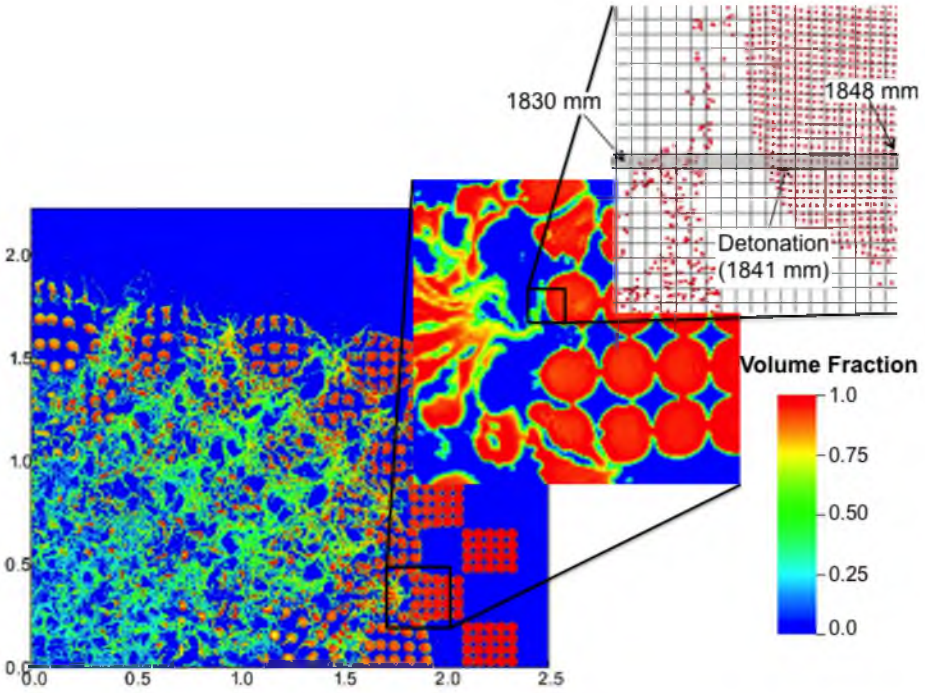

Figure 6.13: Volume fraction of PBX 9501 in Checkered_20_250mm simulation exhibiting IDT mechanism behavior.

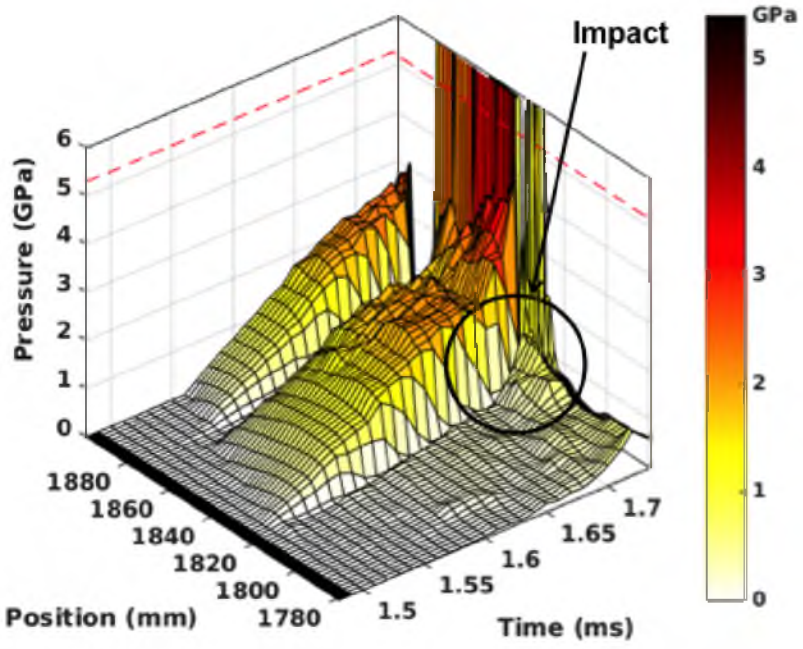

Figure 6.14: Pressure profile verses time and position for an IDT in the Checkered_20_250mm simulation. Position of data extraction is shown in Figure 6.13 by the grey region.

yellow line shows the pressure profile in the cell where detonation occurred. It is qualitatively similar to the other experiments with IDT symptoms prior to a DDT.

The Impact to Detonation mechanism was observed in a variety of array layouts. Each experiment exhibited similar traits, a deflagrating cylinder at elevated pressure reaching detonation by an impact. This mechanism was only observed when there was substantial spacing between the boxes or cylinders.

6.4 Conclusion

Two physical mechanisms for DDT in an array of explosive cylinders were presented, inertial confinement and Impact to Detonation Transition. Inertial confinement occurs when the cylinders are packed closely together, allowing for a high-density barrier to form and trapping the product gases. Impact to Detonation occurs when deflagrating cylinders at high pressures (1-2 GPa) undergo a mechanical insult. The differences between these two mechanisms are very subtle and depend on the ability of the product gases to expand. In both mechanisms two conditions are required. First, the cylinders must be at an elevated pressure. For inertial confinement this elevated pressure is much higher than observed in an IDT due to the confinement made from the high-density barrier. Second, there needs to be an external force on the cylinders. With inertial confinement this external force is the compression of trapped gases between the cylinders. For an IDT the force originates from either the impact of pressure waves or fast-moving explosive material. The inertial confinement mechanism is easy to identify since the global maximum pressure gradually increases and the cylinders compact together.

6.5 References

[1] J. M. McAfee, B. W. Asay, et al. Deflagration to detonation in granular HMX. *9th Int. Detonation Symp.* **1989**, 265–279.

[2] A. Macek. Transition from Deflagration to Detonation in Case Explosives. *J. Chem. Phys.* **1959**, *31*, 162–167.

[3] A. Campbell, *Deflagration-to-Detonation Transition in Granular HMX* in *JANNAF Propulsion Systems Hazards Subcommittee Meeting*, Monterey, CA, 1980, pp. 105–130.

[4] S. F. Son, B. W. Asay, J. B. Bdzil. Inert Plug Formation in the DDT of Granular Energetic Materials. *Am. Inst. Phys.* **1996**, 441–444.

[5] C. M. Tarver, T. C. Goodale, et al., *Deflagration-to-Detonation Transition Studies for Two Potential Isomeric Cast Primary Explosives* in *6th Symp. (Int.) Detonation*, Coronado, CA, 1976.

[6] R. Gipdon, A. Macek, *Flame Fronts and Compression Waves During Transition from Deflagration to Detonation in Solids* in *8th Symp. (Int.) on Combus.*, Baltimore, MD, 1962.

[7] B. Asay (Ed.), *Shock Wave Science and Technology Reference Library, Vol. 5*, Springer, **2010**.

[8] B. W. Asay, S. F. Son, J. B. Bdzil. The Role of Gas Permeation in Convective Burning. *Int. J. Multiphase Flow* **1996**, *22*, 923–952.

[9] J. R. Peterson, C. A. Wight. An Eulerian-Lagrangian Computational Model for Deflagration and Detonation of High Explosives. *Combust. Flame* **2012**, *159*, 2491–2499.

[10] J. Beckvermit, T. Harman, A. Bezdjian, C. Wight. Modeling Deflagration in Energetic Materials using the Uintah Computational Framework. *Procedia Comput. Sci.* **2015**, *51*, 552–561.

[11] J. R. Peterson, J. Beckvermit, T. Harman, M. Berzins, C. A. Wight, *Multiscale Modeling of High Explosives for Transportation Accidents* in *XSEDE '12: Proc. of 2012 XSEDE Conference*, ACM, New York, NY, 2012.

[12] **2015**. `http://www.uintah.utah.edu`.

[13] Q. Meng, M. Berzins, J. Schmidt, *Using Hybrid Parallelism to Improve Memeory use in Uintah* in *TeraGrid 2011 Conference, 2011*, Salt Lake City, UT, 2011, p. 24.

[14] J. E. Guilkey, T. B. Harman, B. A. Kashiwa, J. Schmidt, P. A. McMurtry, *An Eulerian-Lagrangian Approach for Large Deformation Fluid-Structure Interaction Problems, part 1: Algorithm Development* in *Fluid Struct. Interact. II*, WIT Press, Cadiz, Spain, 2003.

[15] J. E. Guilkey, T. B. Harman, B. Banerjee. An Eulerian-Lagrangian Approach for Simulating Explosions of Energetic Devices. *Comput. Struct.* **2007**, *85*, 660–674.

[16] T. Harman, J. Guilkey, B. A. Kashiwa, J. Schmidt, P. A. McMurtry, *An Eulerian-Lagrangian Approach for Large Deformation Fluid-Structure Interaction Problems, Part 2: Multi-Physics Simulations within a Modern Computational Framework* in *Fluid Struct. Interact. II, 2003*, pp. 157–166.

[17] D. Sulsky, Z. Chen, H. L. Schreyer. A Particle Method for History Dependent Materials:Dynamic Prioritation of Material Ineterfaces. *Comput. Methods Appl. Mech. Eng.* **1998**, *151*, 343–360.

[18] D. Sulsky, S. Zhou, H. L. Schreyer. Application of Particle-in-Cell Method to Solid Mechanics. *Comput. Phys. Commun.* **1995**, *87*.

[19] S. G. Bardenhagen, E. M. Kober. The Generalized Interpolation Material Point Method. *Comp. Mod. Eng. Sci.* **2004**, *5*.

[20] B. A. Kashiwa, *A Multifield Model and Method for Fluid-Stucture Interaction Dynamics*, Tech. Report LA-UR-01-1136, Los Alamos Natl. Lab., **2001**.

[21] B. A. Kashiwa, R. M. Rauenzahn, *A Multimaterial Formalism*, Tech. Report LA-UR-94-771, Los Alamos Natl. Lab., **1994**.

[22] C. A. Wight, E. Eddings. Science-Based Simulation Tools for Hazard Assessment and Mitigation. *Int. J. Energetic Mater. Chem. Propul.* **2009**, *8*, 373–389.

[23] M. Ward, S. F. Son, M. Brewster. Steady Deflagration of HMX with Simple Kinetics: A Gas Phase Chain Reaction Model. *Combust. Flame* **1998**, *114*, 556–568.

[24] J. G. Bennett, K. S. Haberman, J. N. Johnson, B. W. Asay, B. F. Henson. A Constitutive Model for the Non-Shock Ignition and Mechanical Response of High Explosives. *J. Mech. Phy. Solids* **1998**, *46*, 2303–2322.

[25] P. C. Souers, S. Anderson, J. Mercer, E. McGuire, P. Vitello. JWL++: A Simple Reactive Flow Code Package for Detonation. *Propellants Explos. Pyrotech.* **2000**, *25*, 54–58.

[26] P. Souers, R. Garza, P. Vitello. Ignition and Growth and JWL++ Detonation Models in Coarse Zones. *Propellants Explos. Pyrotech.* **2002**, *27*.

[27] Q. Meng, J. Luitjens, M. Berzins, *Dynamic Task Scheduling for the Uintah Framework* in *in Proc. of the 3rd IEEE Workshop on Many-Task Computing on Grids and Supercomputers (MTAS10), 2010*, pp. 1–10.

[28] Q. Meng, M. Berzins. Scalable Large-Scale Fluid-Structure Interaction Solvers in the Uintah Framework via Hybrid Task-Based Parallelism Algorithms. *Concurr. Comput.* **2014**, *26*, 1388–1407.

[29] M. Berzins, J. Luitjens, Q. Meng, T. Harman, C. A. Wight, J. R. Peterson, *Uintah: A Scalable Framework for Hazard Analysis* in *Proc. Teragrid 2010 Conf., TG 10, 2010.*

[30] J. Beckvermit, J. Peterson, T. Harman, S. Bardenhagen, C. Wight, Q. Meng, M. Berzins. Multiscale Modeling of Accidental Explosions and Detonations. *Comp. Sci. Eng.* **2013**, *15*, 76–86.

[31] M. Berzins, J. Beckvermit, T. Harman, A. Bezdjian, A. Humphrey, Q. Meng, J. Schmidt, C. Wight. Extending the Uintah Framework to Enable Petascale Modeling of Detonation in Arrays of High Explosive Devices. *Accepted SIAM J. Sci. Comput.* **2015**.

CHAPTER 7

PACKING CONFIGURATIONS OF PBX 9501 CYLINDERS TO REDUCE THE PROBABILITY OF A DDT

This chapter has been provisionally accepted to Propellants, Explosives, Pyrotechnics, Jacqueline Beckvermit, Todd Harman, Chuck Wight and Martin Berzins, "Packing Configurations of PBX 9501 Cylinders to Reduce the Probability of a DDT," February 2016.

The detonation of hundreds of explosive devices from either a transportation or storage accident is an extremely dangerous event. This paper focuses on identifying ways of packing/storing arrays of explosive cylinders that will reduce the probability of a Deflagration to Detonation Transition (DDT). The Uintah Computational Framework was utilized to predict the conditions necessary for a large-scale DDT to occur. The results showed that the arrangement of the explosive cylinders and the number of devices packed in a "box" greatly affects the probability of a detonation.

7.1 Introduction

In August of 2005, a tractor-trailer carrying 16,000 kg of seismic boosters overturned, caught fire, and detonated in Spanish Fork Canyon, Utah. The damage was catastrophic, creating a crater 10 m deep by 24 m wide with burning debris found up to 400 m away. It was apparent by the size of the crater that the explosion transitioned from a deflagration into a fully developed detonation. Though these accidents are rare, the damage caused by the detonation of thousands of kilograms of explosives can be extremely detrimental. The focus of this research is to mitigate the risk of detonation of solid class 1.1 explosives in either a transportation or storage accident.

The results from this paper showed that the way the explosives are packed is important in mitigating this risk. To the best of the authors' knowledge the probability of DDT as a function of packaging arrangement has not been studied. Here we describe spatial layouts of

the devices which were computationally tested to determine which would reduce the probability of a denotation. Two hypotheses were tested in these computational experiments:

1. How does the number of explosive cylinders in a "box" contribute to the propensity for a detonation?

2. Does changing the arrangement of the "boxes" filled with explosives alter the propensity for a detonation?

To analyze these hypotheses four variables were examined: (1) the spacing between the boxes, (2) the arrangement of the boxes, (3) the number of cylinders in each box, and (4) the arrangement of cylinders in the box. The Uintah computation tool was used to simulate these different configurations. Once simulated, the configurations were visually examined to determine if a detonation occurred. Section 7.2 discusses the computational framework used to model the DDT scenario and previously identified DDT initiation mechanisms in an array of cylinders. Section 7.4.1 discusses how changing the number of cylinders in a box effects the deflagration to transition to a detonation. Section 7.4.2 examines different packing configurations to reduce the probability of a detonation.

7.1.1 Current Packaging and Storage Protocol

In the 2005 transportation accident, 8,400 seismic boosters were being transported according to the existing U.S. government regulations. Each booster was filled with Pentolite, an equal part mixture of PETN and TNT, which is commonly used for underground oil and gas exploration. Two sizes of cylindrical boosters were on board and were enclosed in open-ended plastic tubes. There were 5,000 large boosters, each containing 2.5 kg of explosive. Each one was 0.737 m long and they were packaged 10 to a box. The smaller boosters weighed 1.13 kg each and were 0.33 m in length and were packaged 20 to a box. All of the seismic boosters were packaged in fiberboard 4G boxes in accordance to the Code of Federal Regulations (CFR) Title 49 §173.62 instruction 132. The CFR states that boosters must only be packaged with materials of the same classification, meaning no detonators can be transported in the same load. They must also be packaged in boxes made of steel, aluminum, wood, plywood, reconstituted wood, fiberboard, or solid plastics. The mass of the explosives in a box or their spatial arrangement is not defined in the regulations and is at the discretion of the manufacturer.[1] The only limitation on the quantity of explosives transported is the maximum weight limit set by each state. For Utah, where the 2005 accident occurred, regulation 23 CFR §658.17 defines a maximum of 36,000 kg, well above the weight in the accident.

The regulations for storing high explosives are defined by the United States Bureau of Alcohol, Tobacco, Firearms, and Explosives (ATF), Title 27 of CFR §555. It describes the ventilation system requirements, permits, required markings, and what material each component of the storage facility can be constructed from. It also states the required spatial separation from surrounding buildings, roadways, and highways. According to Title 27 CFR §555.213 the maximum quantity of high explosives allowed in a building is 136,000 kg. Similar to the transportation regulations, detonators cannot be in the same building as Class 1.1 explosives. There are no regulations on how the explosives are packed or stored inside the building. Boxes can be stacked side by side and on top of one another.

7.2 Computational Methods

The Uintah Computational Framework,[2,3] developed at the University of Utah, was utilized to predict a DDT in large arrays of explosive cylinders in a variety of spatial arrangements. The framework utilizes the fluid-structure interaction algorithms of the Material Point Method (MPM),[4–7] a low- and high-speed compressible CFD algorithm (ICE),[8] and a fluid-structure interaction algorithm (MPMICE).[4,9,10] ICE is a finite-volume method and uses an adaptive hexahedral mesh. MPM was used to evaluate the evolution of the solid material by using Lagrangian points (particles) and an Eulerian mesh to evolve the governing equations. The particle's state vector is interpolated back to the cell-center, where the exchange of mass, momentum, and energy occurs. This allows multiphase materials to use the same Eulerian mesh. The governing equations and the algorithms to solve them can be found in.[4,9–12] Embedded within the MPMICE component is a validated DDT model to represent the reaction of solid explosive $\rightarrow$ gaseous products at multiple initial temperatures and pressures.[13–16] The DDT model utilizes a modified Ward, Son, and Brewster (WSB) burn model[14,16,17] to evaluate the mass conversion rate, the ViscoSCRAM constitutive model[18] to model the damage in the solid, and the JWL++ simple reactive flow model[19] to describe detonation. The commonly used JWL equation of state[19,20] was used for the solid explosive and the product gases. Detonation occurs in Uintah's DDT model when the localized pressure is greater than the pressure threshold, 5.3 GPa.[13,14] Further details on the model can be found in [4, 9-12]. The Uintah framework has a long history of high performance computing and has shown good strong and weak scaling characteristics up to 512 K cores on DOE's Mira.[22–24] Uintah's strong scalability enabled us to run large 2D and full 3D simulations at high grid resolutions (2 mm). The reaction model has been validated at many resolutions including 2 mm.[15,25] Using this advanced computational tool it was

possible to predict if a thermally ignited array of explosives would undergo a DDT event.

7.2.1 Common Simulation Setup

This research focused on the smaller of the two cylinders involved in the 2005 accident, 0.054 m in diameter and 0.33 m in length. Due to the abundance of experimental data and Uintah's validated DDT model, solid PBX 9501 (95% 1,3,5,7-octahydro-1,3,5,7-tetranitro-1,3,5,7-tetrazocine (HMX) and 5% of a plastic binder) was the explosive examined. For simplicity the fiberboard material was not modeled, instead 10 mm air gaps separated the "boxes." These simulations consisted of only two materials, the solid reactant modeled by MPM particles and the product gas modeled by ICE. The explosives and surrounding gas were initially at ambient pressure and temperature, and the explosives were ignited by hot product gas at 2500 K in the $x-$ corner of the domain. All explosive devices were one to two cells away from the computational boundaries to reduce boundary effects. The 2D simulations were performed using symmetric/reflective boundary conditions for the $x-, y-, z-$, and a wall on the $z+$ face. All other boundaries conditions were set to a zero gradient for the primitive variables (temperature, velocity, density, and pressure) and the edge of the computational domain was positioned far from the area of interest to minimize nonphysical boundary condition effects. The 3D simulations were the same with the addition of the $z-$ and $z+$ boundaries being set to a zero gradient for the primitive variables.

There are two ways to package cylinders in a box, tight packing, where the cylinders are in a hexagonal configuration, or loose packing, where the cylinders are in a square configuration. For this study both configurations were examined and preliminary simulations showed that the loose packing distribution is less likely to transition to a detonation. Therefore we only presented the simulations consisting of explosives loosely packed in a "box."

A large 3D simulation was run with 1280 PBX 9501 cylinders packaged 20 to a "box" and stacked one on top of the other, as shown in Figure 7.1. The simulation consisted of 64 "boxes," 4 in each direction, correlating to 1/8th of the original tractor-trailer in the 2005 accident. The domain for this simulation was 12 m^3, resulting in 350 million cells containing 980 million PBX 9501 particles. This was run on 64 thousand cores on DOE's Mira, costing over 24 million core processing units. Under these conditions our results showed that the array transitioned to a denotation at 0.66 msec. From this simulation there was strong evidence that the packing arrangement used in most storage facilities and during transportation will transition to a DDT. This result provided motivation to study new ways of packing/storing explosive cylinders to prevent a detonation. The level of

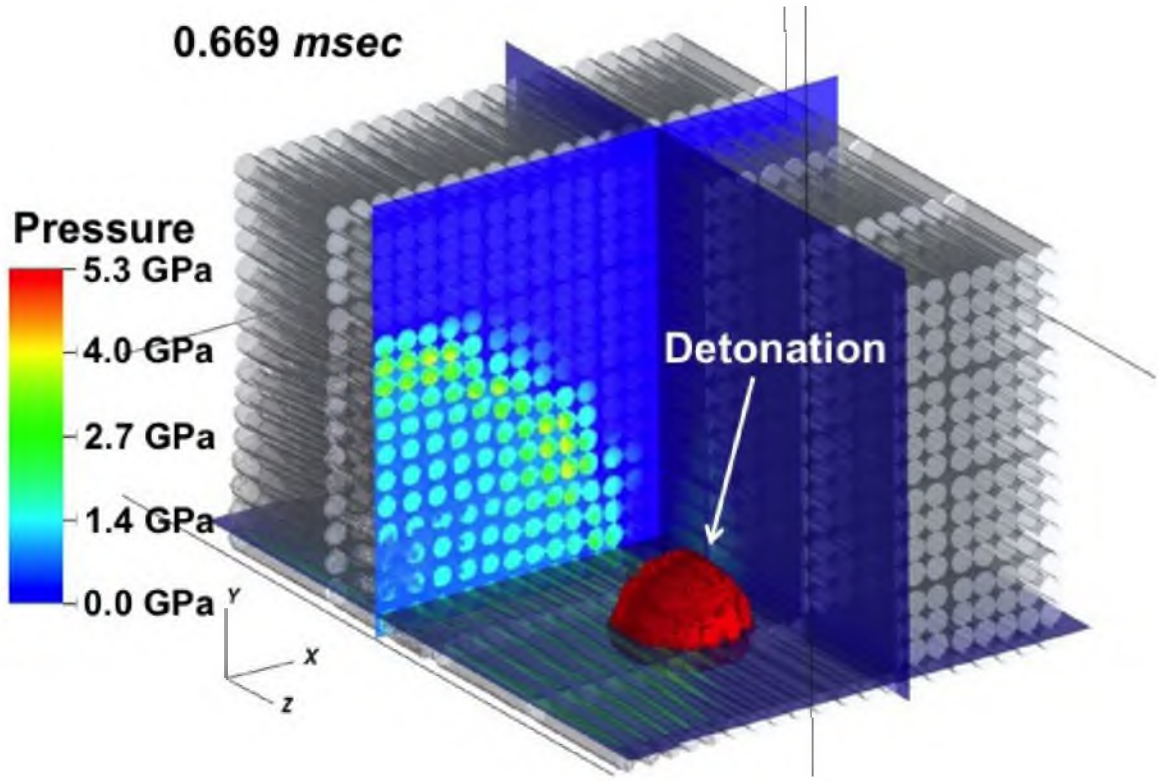

Figure 7.1: Contour plots of the pressure and shadow of the explosive cylinders in the 3D simulation.

computational resources required to preform a parametric study of this type is exceedingly expensive on current computational platforms. We therefore investigated using low-cost, fast running, 2D simulations for our study. We ran a series of 2D simulations and compared the position and time of the detonation against the large 3D results. Analysis of the state of the cylinders at the point of detonation showed that a similar physical mechanism caused the detonation in each simulation.[25] The global maximum pressure in the domain as a function of time was also compared, and good qualitative agreement was observed. The good level of agreement in the main variables of interest justified our use of low-cost 2D simulations for the parametric study.

7.3 DDT Initiation Mechanisms

Previous work on identifying the previously unknown physical mechanisms involved in initiating a DDT in an array of explosive cylinders was presented in.[25] Two dominant mechanisms were identified, inertial confinement and Impact to Detonation Transition (IDT). Inertial confinement only occurs when the explosive cylinders are packaged closely

together. As the deflagration progresses outward, the inertial mass of the surrounding explosives slows the movement of the deforming deflagrating cylinders, causing them to compact into one another. In the compaction zone a high-density barrier forms, trapping the product gases and increasing the local pressure behind the barrier. As the pressure increases, the burn rate accelerates until a detonation is reached.[25] The second mechanism, IDT, was observed when the explosive cylinders were packaged further apart, allowing for the gases and explosive fragments to accelerate to velocities of $\gtrsim$500 m/s before impacting nearby deflagrating cylinders. Due to the deflagration, these nearby explosives are typically at an elevated pressure ($\approx$3 GPa). Once impact occurs the deflagration quickly transitions to detonation. The observations suggested that the mechanical insult generates stress waves in the explosive, that reflect, and produce the pressures required for a detonation. A full discussion of these physical mechanisms can be found at.[25]

7.4 Results and Discussion

This study examined two strategies to reduce the probability of a DDT in packed PBX 9501 cylinders. The first was to change the number of explosives in a "box" and the overall volume or the global Packing Volume Fraction (PVF). The global PVF is the total PBX 9501 volume divided by the total volume that the "boxes" occupy (not the computational domain volume). The second was to change the way in which the "boxes" are organized while keeping the size of the boxes constant. This is referred to as the packing configuration. Figure 7.2 illustrates the four different packing configurations presented.

7.4.1 Critical Packing Volume

This section examines hypothesis one: how the number of explosive cylinders in a "box" contributes to the propensity for a detonation. In these simulations the outer dimensions of the boxes were varied to account for the number of cylinders contained, see Figure 7.2 ((a) compared to (c)). A critical PVF was defined as the maximum global PVF that does not initiate a DDT when thermally ignited. In Section 7.4.2 we show that the initial spatial layout of the explosives greatly influenced the probability of a DDT and that there was not a critical PVF for all packing configurations. This realization led to the hypothesis that varying the number of explosive cylinders in a "box" can increase the critical PVF and decrease the amount of space needed to package 320 PBX 9501 cylinders safely. In this study the only packing configuration examined was the Base configuration, Figure 7.2 (a and c). The number of "boxes" simulated varied in order to contain $\approx$320 cylinders. Two variables were varied in the parametric study: (1) the number of cylinders per box

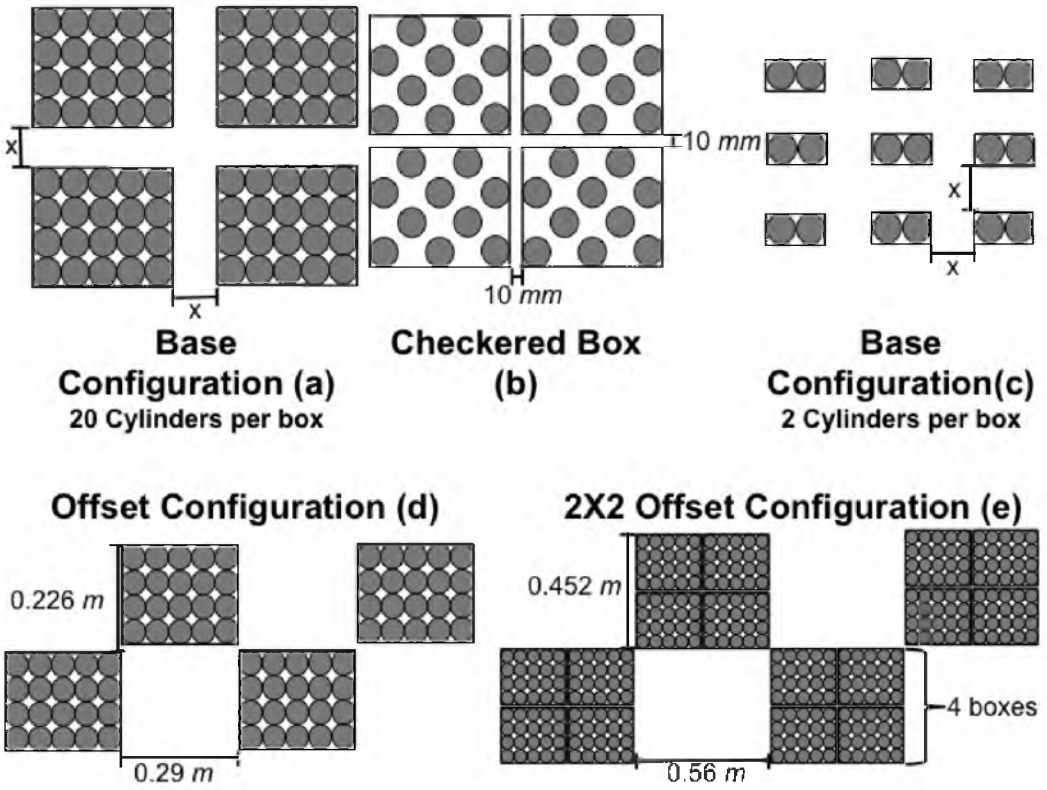

Figure 7.2: Initial packing configurations.

and (2) the distance between the boxes. Table 7.1 shows the simulations nearest to the critical PVF threshold for each configuration. This is a small representation of the >65 simulations examined. Figure 7.3 shows the PVF of all simulations as a function of the number of explosives in a "box." The green line and points show the critical PVF for each configuration and the red points are simulations which resulted in a detonation. Below the critical PVF (blue points) detonation did not occur due to adequate spacing. Above the critical PVF threshold the explosives were too densely packed and resulted in a detonation. This plot illustrates two ideas: (1) the fewer cylinders there were per "box" the larger the critical PVF, (2) there was a threshold at 9 cylinders per "box" where the critical PVF dramatically increases from 0.37 to 0.497.

Table 7.1: Initial conditions for the simulations near the critical packing volume fraction (defined in Section 7.4.1) for each configuration.

Simulation Name	# of Cylinders per box	Spacing between boxes (x)	Configuration (Described in Figure 7.2)	Global Packing Volume Fraction	DDT Initiation Mechanism
Transportation_Accident	20	10 mm	Base	0.739	Inertial Confinement
Base_20_200mm	20	200 mm	Base	0.298	-
Base_20_190mm	20	190 mm	Base	0.31	IDT
Base_20_136mm	20	136 mm	Base	0.387	IDT
Base_16_150mm	16	150 mm	Base	0.26	-
Base_16_120mm	16	120 mm	Base	0.301	IDT
Base_12_104mm	12	104 mm	Base	0.37	-
Base_12_90mm	12	90 mm	Base	0.404	IDT
Base_9_90mm	9	90 mm	Base	0.367	-
Base_9_50mm	9	50 mm	Base	0.497	-
Base_9_40mm	9	40 mm	Base	0.54	IDT
Base_6_34mm	6	34 mm	Base	0.524	-
Base_6_30mm	6	30 mm	Base	0.547	IDT
Base_4_30mm	4	30 mm	Base	0.505	-
Base_4_24mm	4	24 mm	Base	0.548	Inertial Confinement
Base_2_20mm	2	20 mm	Base	0.503	-
Base_2_10mm	2	10 mm	Base	0.62	Inertial Confinement
Base_1_16mm	1	16 mm	Base	0.598	-
Base_1_14mm	1	14 mm	Base	0.615	Inertial Confinement
Offset	20	-	Offset	0.385	-
2X2_Offset	20	-	2X2 Offset	0.375	Inertial Confinement
Checkered_Box	10	-	Checkered Box	0.393	-

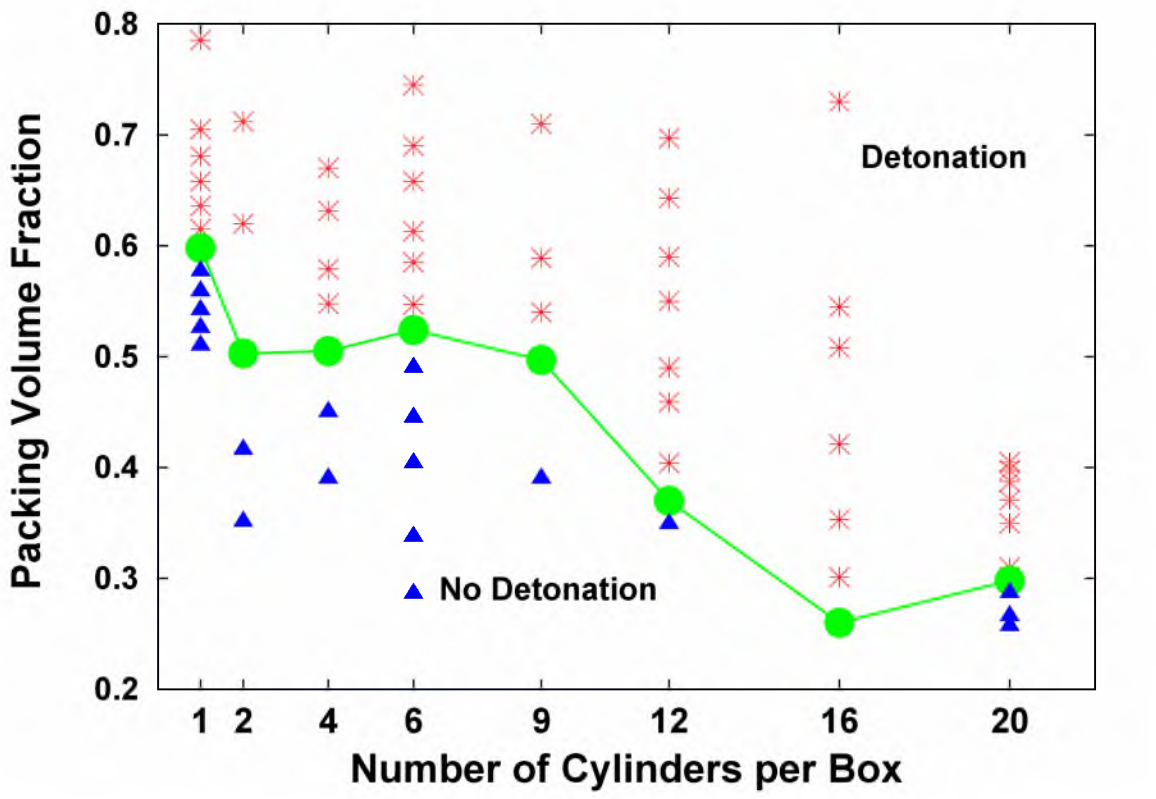

Figure 7.3: The PVF for each of the >65 simulations using between 1 and 20 cylinders per box. The green circles and line represent the critical PVF for each configuration. The red asterisks depict simulations that detonated, while the blue triangles represent simulations that never detonated because they had a PVF below the critical one.

The explanations behind the two postulations illustrated in Figure 7.3 are very similar. The observed average pressure was lower in "boxes" containing fewer cylinders, 2 GPa compared to 3-4 GPa. When more explosives were packaged together the interior devices were "confined" by the surrounding cylinders, thus restricting the expansion of product gases and increasing the localized pressure. When the number of cylinders per box was increased from 9 to 12, in order to ensure safe deflagration the spacing between the "boxes" needed to be doubled, from 50 mm to 104 mm. This was due to a "box" with 12 cylinders reaching a higher pressure, from the confinement of the surrounding cylinders, than was seen in boxes containing 9 cylinders. Figure 7.4 shows that the pressure in the Base_12_90mm simulation was 1-1.5 GPa higher than the pressure reached in the Base_9_90mm simulation, Figure 7.5. Figures 7.6 and 7.7 show the position the data was extracted from, shown by the white line. The only difference between these two simulations was the number of explosives in a "box." A result of the elevated pressure was increased particle velocities. The observed

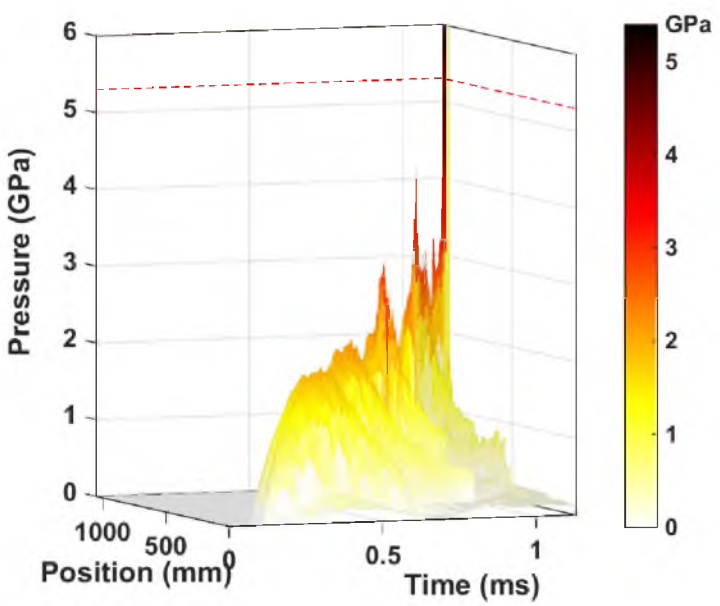

Figure 7.4: Pressure profile verse position and time for the Base_12_90mm simulation. The red dotted line represents the pressure threshold for a detonation. Position of extracted data is shown in Figure 7.6 by the white line.

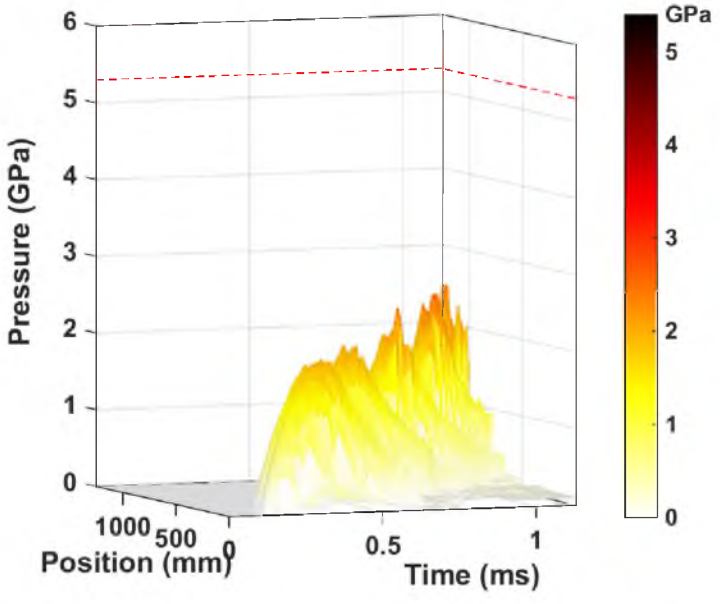

Figure 7.5: Pressure profile verse position and time for the Base_9_90mm simulation. The red dotted line represents the pressure threshold for a detonation. A detonation was not observed in this simulation. Position of extracted data is shown in Figure 7.7 by the white line.

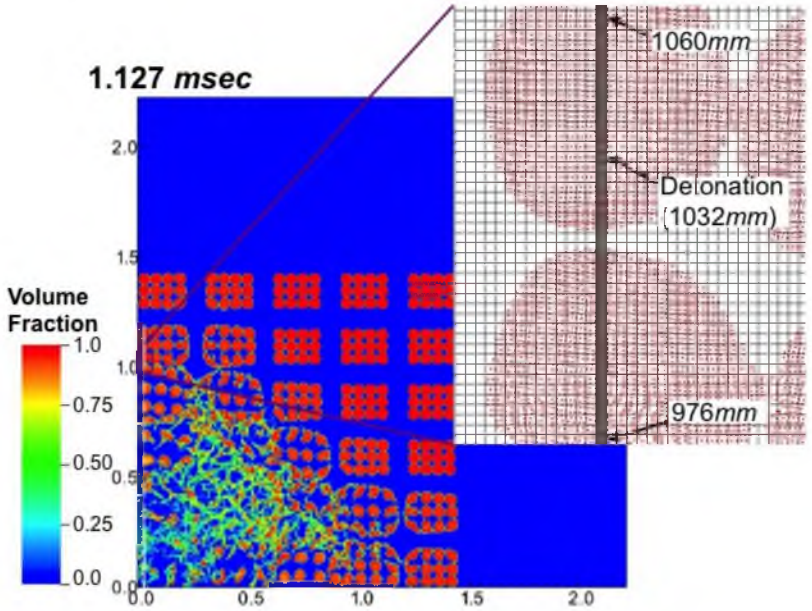

Figure 7.6: The volume fraction of PBX 9501 in each grid cell of the simulation domain, at the timestep at which an IDT initiation of a DDT was detected in the Base_12_90mm simulation. The white line illustrates where the data were extracted for Figure 7.4.

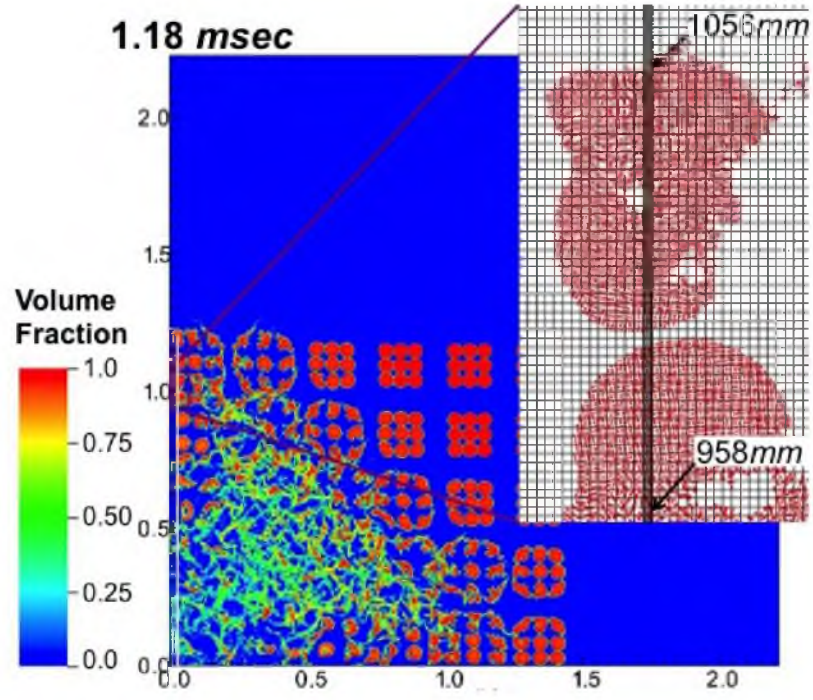

Figure 7.7: The volume fraction of PBX 9501 in each grid cell of the simulation domain in the Base_9_90mm simulation. The white line illustrates where the data were extracted for Figure 7.5.

particle velocities were over 100 m/s faster than those seen in the Base_9 simulation. This forced the boxes to be spaced further apart in order for the impact of deflagrating particles and pressure waves to not initiate an IDT event. Thus the more explosives packed together, the higher the localized pressure, the higher the particle velocity, and the further the boxes must be separated to avoid a detonation.

The same explanation can be used to understand why decreasing the number of cylinders per box resulted in an increase of the critical PVF. It was observed when there were 4 or fewer cylinders per "box" that the gases easily expanded, resulting in low localized pressures. As a result, the only observed DDT mechanism was inertial confinement which occurred when the boxes were packed closely together (<30 mm). For the Base_1 configuration the "boxes" had to be packaged less than 16 mm apart to form inertial confinement. That is less than the space needed for one cylinder (54 mm). Thus packing fewer cylinders in a "box" increased the critical PVF, decreased the space occupied, and decreased the probability of a detonation.

7.4.2 Packing Configuration

The second strategy for safer transportation and storage of explosive devices (hypothesis two) was to change the packaging configuration while holding the global PVF constant. The arrangements are presented in Figure 7.2. In the four configurations considered, the box size was held constant at 0.27 m x 0.216 m, resulting in global PVF ranging from 0.375 to 0.393, see Table 7.1.

The first layout analyzed was the 2X2_Offset configuration, which had a global PVF of 0.375. It contained four boxes packed together surrounded by open space where four other boxes would have been, see Figure 7.2(e). Figure 7.8 shows the progression of deflagration (red) through the explosive cylinders (grey), an enlarged view of the pressure field as the DDT occurred is shown in the upper right corner. These results showed that four "boxes" containing 20 cylinders should not be placed directly next to one another, to avoid a DDT.

The second packing configuration considered was the Base configuration, Figure 7.2(a). Here we present the results from the Base_20_136mm simulation, which had a global PVF of 0.387, similar to the previous test case. This simulation transitioned to detonation due to an IDT mechanism. Figure 7.9 shows a contour plot of the magnitude of the product gas velocities and the pressure field at the time of detonation. The pressure is shown in the upper right corner, focused where the DDT occurred. With this packing arrangement the particles and gases did not have sufficient room to expand, causing the particles to impact surrounding deflagrating cylinders and resulting in a transition to detonation. Figure 7.10

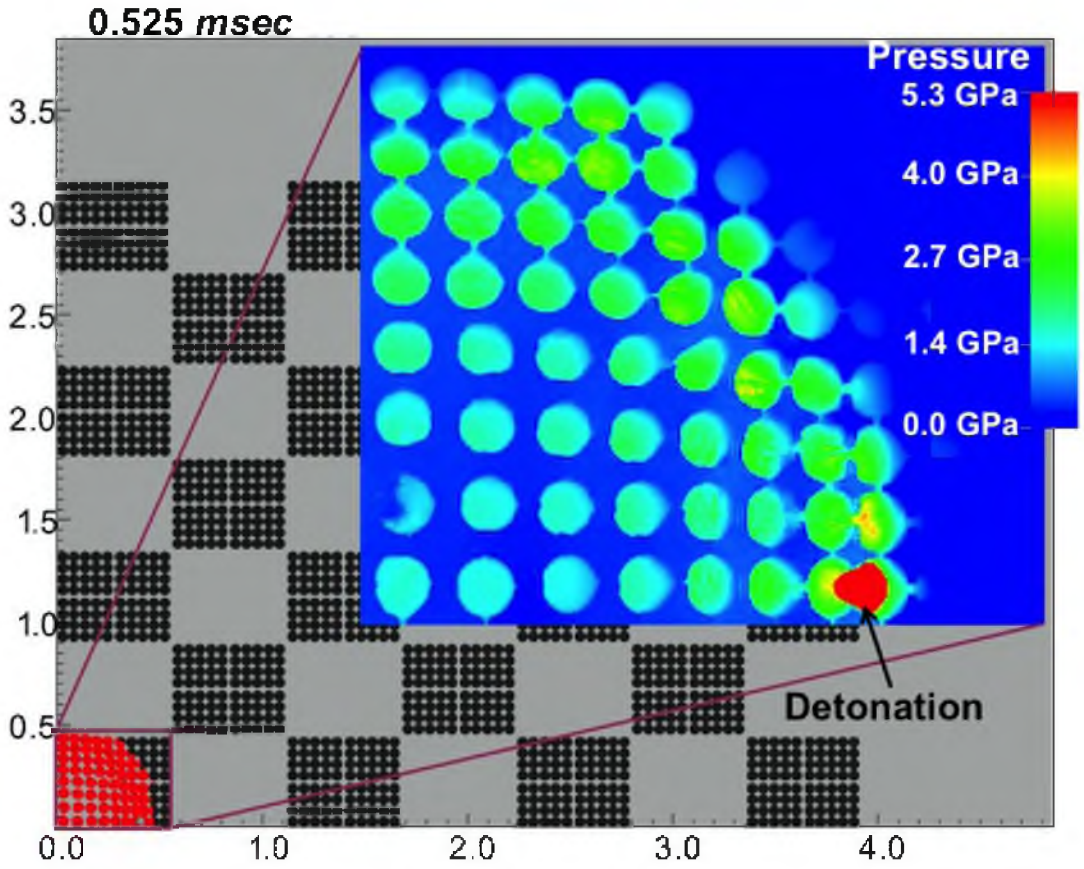

Figure 7.8: Contour plots of the progression of deflagration (red) and the pressure (upper right corner) in the 2X2_Offset configuration. This configuration transitioned to a detonation due to an inertial confinement initiation mechanism.

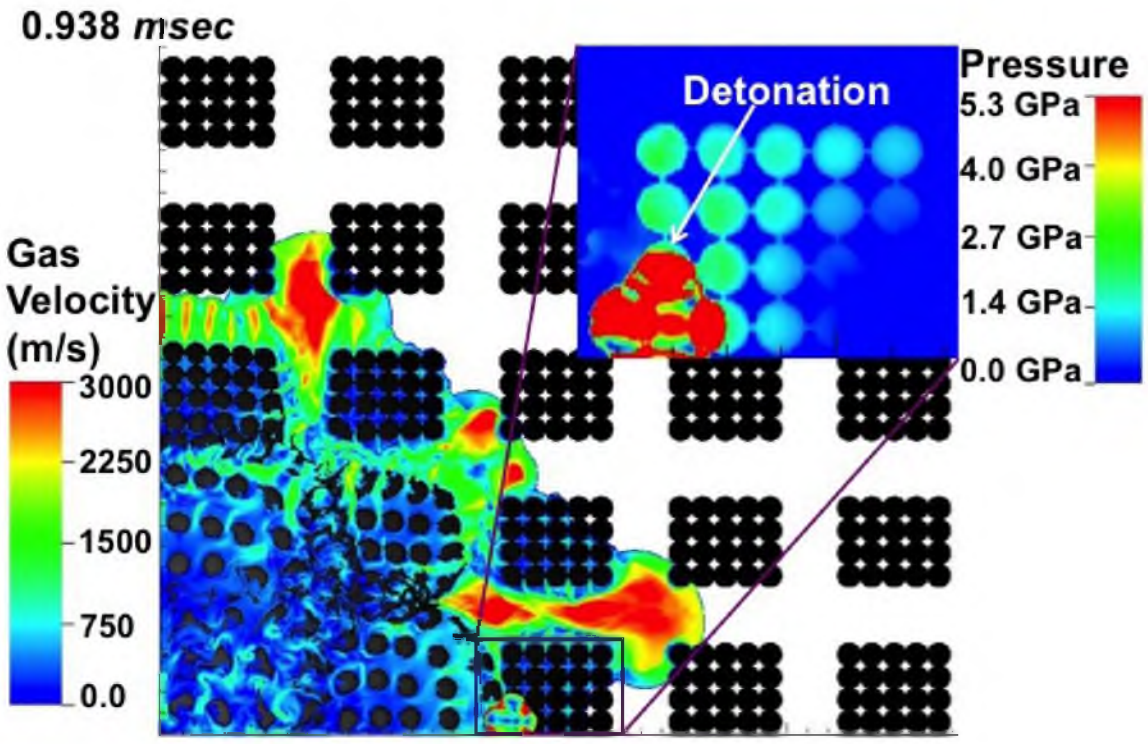

Figure 7.9: Contour plots of the magnitude of the gas velocity and the pressure in the Base_20_136mm configuration. A detonation occurred due to an IDT mechanism.

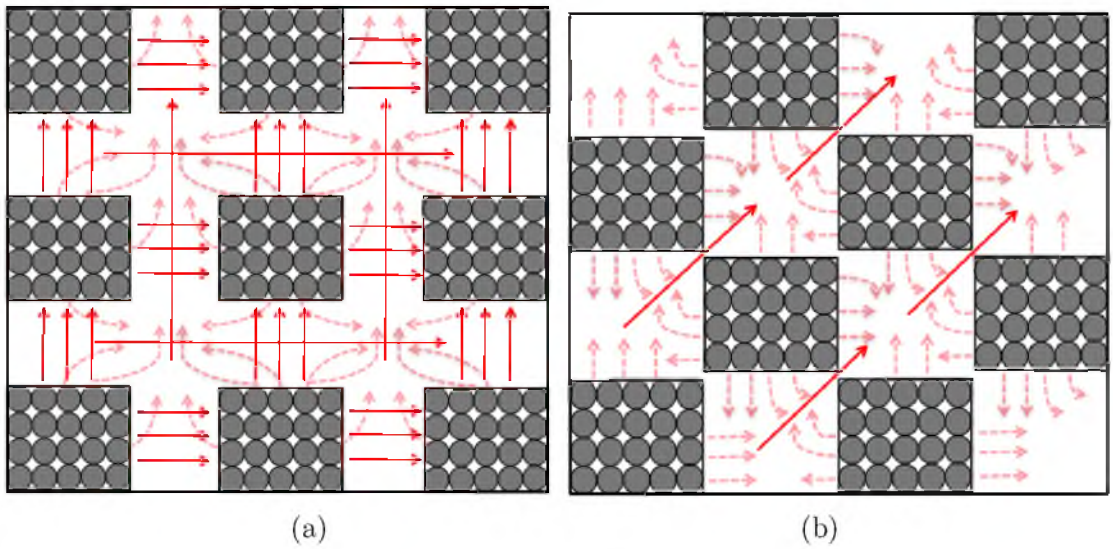

Figure 7.10: Schematic diagram of the idealized undeformed cylinders flow field for the Base_20_136mm (a) and the Offset configuration (b). The solid arrows represent the bulk flow and the dashed arrows the local flow field.

(a) is a schematic diagram of the flow field. Notice there is little impeding the flow of high velocity gases and explosive fragments from impacting the surrounding deflagrating cylinders. As illustrated in Section 7.4.1, in order for this packing configuration of 20 cylinders per box to be effective and not transition to detonation, the "boxes" must be spaced $\geq$200 mm apart.

The next arrangement considered was the Offset configuration, with a global PVF of 0.385. With this spatial layout detonation was not observed. Figure 7.11 shows a contour plot of the magnitude of the gas velocities and pressure. The large open regions allowed the product gases to expand. The pressure in this simulation never reached more than 3 GPa, well below the threshold needed for a detonation. In this configuration an IDT mechanism seemed likely due to the large gaps, allowing gases and particles to accelerate as was seen in the Base_20_136mm configuration. We hypothesize that this did not occur due to the arrangement of the boxes, allowing for the higher gas velocities to redirect the particles and pressure waves away from the deflagrating cylinders and into the small gaps between the

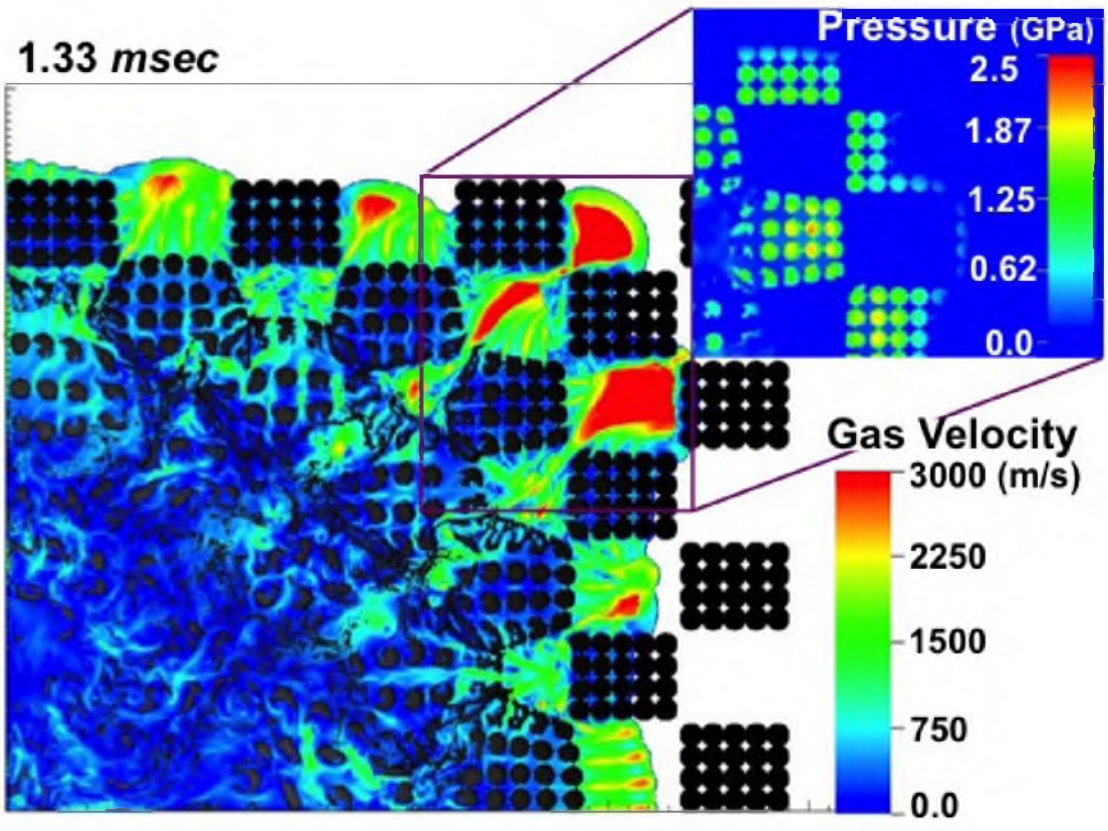

Figure 7.11: Contour plots of the magnitude of the gas velocity and the pressure in the Offset configuration. A detonation did not occur.

corners of the boxes, as shown in Figure 7.11. This gas movement redirects the particles and pressure waves, which could cause an IDT, to an open area. Figure 7.10 (b) illustrates a schematic of how we believe the gas flow is altered by packing the "boxes" in an Offset configuration rather than the Base configuration. This configuration shifted the flow of gas and particles from directly toward the deflagrating cylinders 7.10(a) to in-between the "boxes" 7.10(b), preventing a detonation.

The last packing configuration considered was the Checkered_Box configuration, Figure 7.2(b). In this loading arrangement every other cylinder was removed from the box, and the remaining cylinders were positioned in a checkered configuration so no explosives were directly on top of one another. Figure 7.12 shows the pressure field and magnitude of the gas velocity at t= 0.8 msec. The simulation results showed product gases easily expanded with minimal impedance, resulting in relatively low pressures. Since the pressures were low the particle velocities were ≈300 m/s, much lower than the ≥500 m/s seen in an IDT event. Inertial confinement was also not a possible mechanism for this distribution because

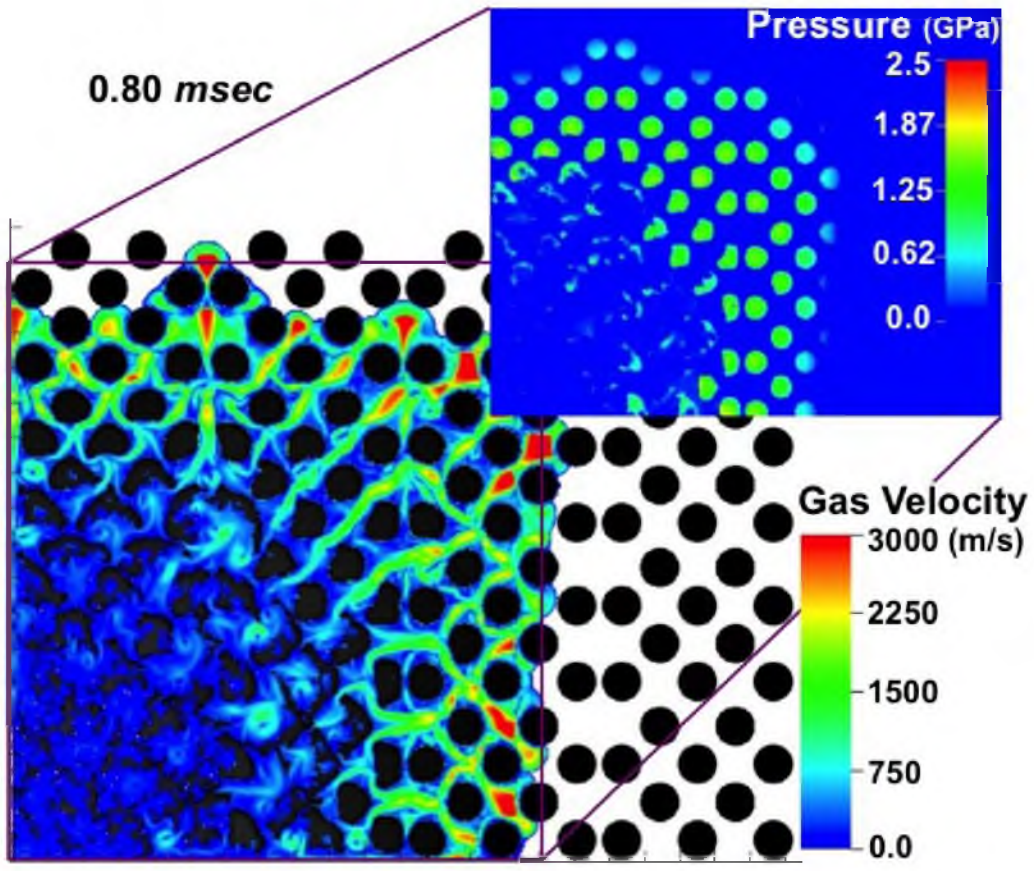

Figure 7.12: Contour plots of the magnitude of the gas velocity and the pressure in the Checkered_Box configuration. A detonation did not occur.

there was substantial distance between each cylinder (>54 mm), making it difficult for them to compact into one another and form a barrier. Similar to the Offset configuration, the pressure in the deflagrating cylinders never reached more than 3 GPa. An enlarged view of the pressure field is seen the upper right corner. This result suggests that this configuration has a low probability of a detonation.

7.4.3 Comparison of 2D versus 3D Computational Domain

A 3D simulation was run to confirm the results of the 2D Offset configuration. The 3D initial setup was the same as the 2D with the addition of 4 rows of "boxes" in the z dimension, giving more space for the product gases to expand, making it more difficult to build to the pressures needed for a detonation. Due to the configuration of the boxes, Adaptive Mesh Refinement[26] could not be utilized, drastically increasing the computational costs. Figure 7.13 shows a contour plot of the pressure and the magnitude of the gas velocity. Notice the pressure was well below 5.3 GPa. The pressure and gas velocities were qualitatively similar to those found in the 2D simulation, Figure 7.11. In both simulations we observed high velocity gases flowing between the corners of the boxes. Even though the 3D simulation did not run to completion, due to lack of resources, the similarities between the 2D and 3D simulations suggest that a detonation would not occur in this configuration.

7.5 Conclusions

The results from numerical experiments described here have shown that the number of cylinders packed in a "box" effected the probability of a detonation. An important factor in the Base configuration not leading to a detonation was adequate space for the explosive fragments and gases to expand. As fewer explosives were packaged together, the mechanism for a DDT switched from IDT to inertial confinement. This allowed the cylinders to be packed closer together without transitioning to a detonation. IDT was less probable with fewer cylinders packed in a "box" because the explosives could not sustain the elevated pressures needed. Strong evidence also suggested that while holding the global PVF constant the packing configuration changes the probability of a detonation along with the DDT mechanism. Two configurations showed that detonation can be avoided while sustaining a global PVF $\approx$0.39, the Offset and Checkered_Box configurations. The 2X2_Offset and Base_20_136mm configurations, on the other hand, exhibited two different mechanisms for DDT and quickly transitioned to a detonation.

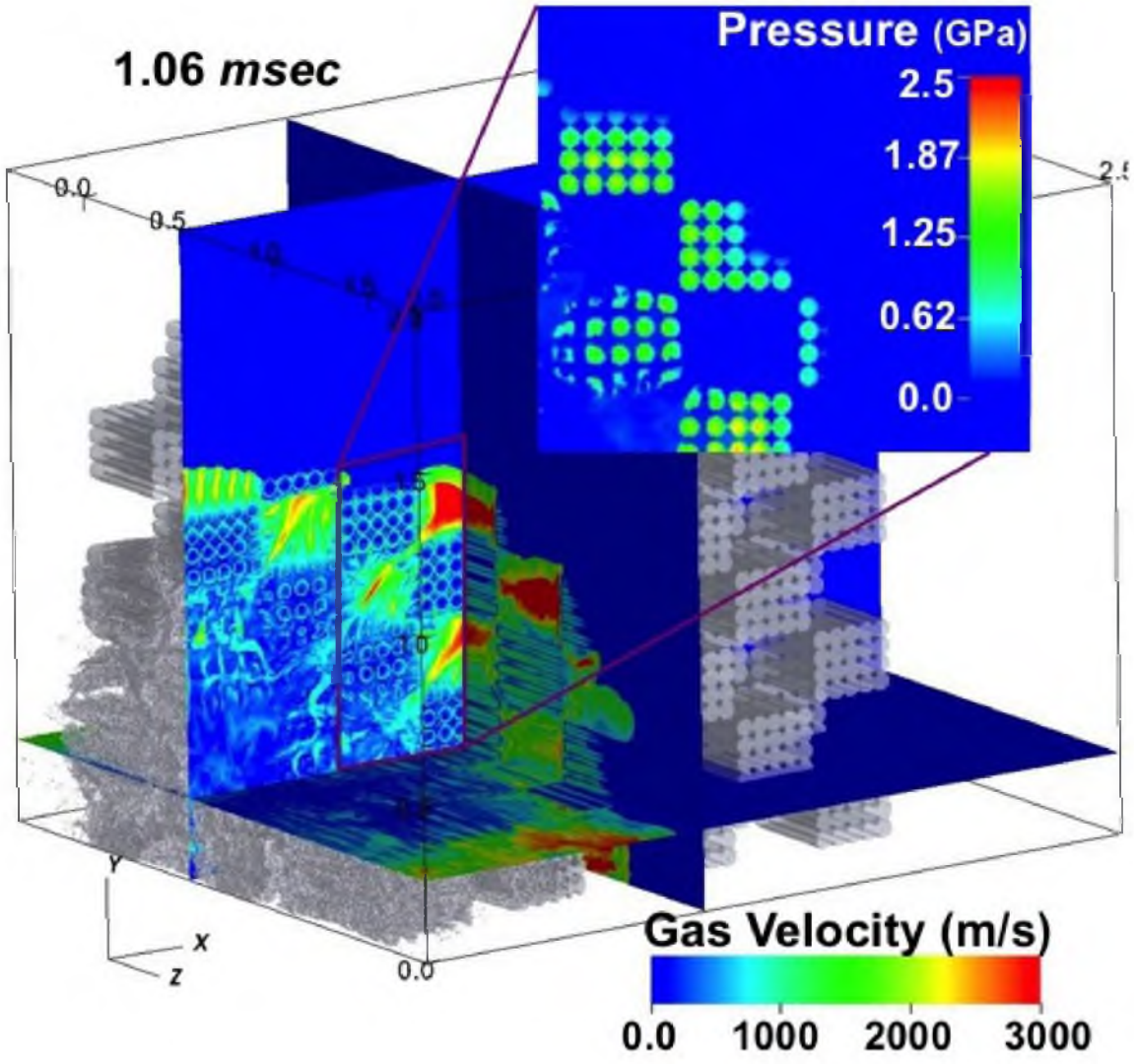

Figure 7.13: Contour plots of the magnitude of the gas velocity and the pressure in the 3D Offset configuration.

7.6 References

[1] *Robert Ford, President of Safety Management Services, personal communication, April 9, 2015.*

[2] **2015**. `http://www.uintah.utah.edu`.

[3] Q. Meng, M. Berzins, J. Schmidt, *Using Hybrid Parallelism to Improve Memeory use in Uintah* in *TeraGrid 2011 Conference, 2011*, Salt Lake City, UT, 2011, p. 24.

[4] J. E. Guilkey, T. B. Harman, B. Banerjee. An Eulerian-Lagrangian Approach for Simulating Explosions of Energetic Devices. *Comput. Struct.* **2007**, *85*, 660–674.

[5] D. Sulsky, Z. Chen, H. L. Schreyer. A Particle Method for History Dependent Materials:Dynamic Prioritation of Material Ineterfaces. *Comput. Methods Appl. Mech. Eng.* **1998**, *151*, 343–360.

[6] D. Sulsky, S. Zhou, H. L. Schreyer. Application of Particle-in-Cell Method to Solid Mechanics. *Comput. Phys. Commun.* **1995**, *87*.

[7] S. G. Bardenhagen, E. M. Kober. The Generalized Interpolation Material Point Method. *Comp. Mod. Eng. Sci.* **2004**, *5*.

[8] B. A. Kashiwa, E. S. Gaffney, *Design Basis for CFDLIB*, Tech. Report LA-UR-03-1295, Los Alamos Natl. Lab., **2003**.

[9] J. E. Guilkey, T. B. Harman, B. A. Kashiwa, J. Schmidt, P. A. McMurtry, *An Eulerian-Lagrangian Approach for Large Deformation Fluid-Structure Interaction Problems, part 1: Algorithm Development* in *Fluid Struct. Interact. II*, WIT Press, Cadiz, Spain, 2003.

[10] T. Harman, J. Guilkey, B. A. Kashiwa, J. Schmidt, P. A. McMurtry, *An Eulerian-Lagrangian Approach for Large Deformation Fluid-Structure Interaction Problems, Part 2: Multi-Physics Simulations within a Modern Computational Framework* in *Fluid Struct. Interact. II, 2003*, pp. 157–166.

[11] B. A. Kashiwa, *A Multifield Model and Method for Fluid-Stucture Interaction Dynamics*, Tech. Report LA-UR-01-1136, Los Alamos Natl. Lab., **2001**.

[12] B. A. Kashiwa, R. M. Rauenzahn, *A Multimaterial Formalism*, Tech. Report LA-UR-94-771, Los Alamos Natl. Lab., **1994**.

[13] J. R. Peterson, C. A. Wight. An Eulerian-Lagrangian Computational Model for Deflagration and Detonation of High Explosives. *Combust. Flame* **2012**, *159*, 2491–2499.

[14] J. Beckvermit, T. Harman, A. Bezdjian, C. Wight. Modeling Deflagration in Energetic Materials using the Uintah Computational Framework. *Procedia Comput. Sci.* **2015**, *51*, 552–561.

[15] J. R. Peterson, J. Beckvermit, T. Harman, M. Berzins, C. A. Wight, *Multiscale Modeling of High Explosives for Transportation Accidents* in *XSEDE '12: Proc. of 2012 XSEDE Conference*, ACM, New York, NY, 2012.

[16] C. A. Wight, E. Eddings. Science-Based Simulation Tools for Hazard Assessment and Mitigation. *Int. J. Energetic Mater. Chem. Propul.* **2009**, *8*, 373–389.

[17] M. Ward, S. F. Son, M. Brewster. Steady Deflagration of HMX with Simple Kinetics: A Gas Phase Chain Reaction Model. *Combust. Flame* **1998**, *114*, 556–568.

[18] J. G. Bennett, K. S. Haberman, J. N. Johnson, B. W. Asay, B. F. Henson. A Constitutive Model for the Non-Shock Ignition and Mechanical Response of High Explosives. *J. Mech. Phy. Solids* **1998**, *46*, 2303–2322.

[19] P. C. Souers, S. Anderson, J. Mercer, E. McGuire, P. Vitello. JWL++: A Simple Reactive Flow Code Package for Detonation. *Propellants Explos. Pyrotech.* **2000**, *25*, 54–58.

[20] P. Souers, R. Garza, P. Vitello. Ignition and Growth and JWL++ Detonation Models in Coarse Zones. *Propellants Explos. Pyrotech.* **2002**, *27*.

[21] J. Beckvermit, J. Peterson, T. Harman, S. Bardenhagen, C. Wight, Q. Meng, M. Berzins. Multiscale Modeling of Accidental Explosions and Detonations. *Comp. Sci. Eng.* **2013**, *15*, 76–86.

[22] M. Berzins, J. Beckvermit, T. Harman, A. Bezdjian, A. Humphrey, Q. Meng, J. Schmidt, C. Wight. Extending the Uintah Framework to Enable Petascale Modeling of Detonation in Arrays of High Explosive Devices. *Accepted SIAM J. Sci. Comput.* **2015**.

[23] Q. Meng, M. Berzins. Scalable Large-Scale Fluid-Structure Interaction Solvers in the Uintah Framework via Hybrid Task-Based Parallelism Algorithms. *Concurr. Comput.* **2014**, *26*, 1388–1407.

[24] Q. Meng, J. Luitjens, M. Berzins, *Dynamic Task Scheduling for the Uintah Framework* in *in Proc. of the 3rd IEEE Workshop on Many-Task Computing on Grids and Supercomputers (MTAS10), 2010*, pp. 1–10.

[25] J. Beckvermit, T. Harman, C. Wight, M. Berzins. Physical Mechanisms of DDT in an Array of PBX-9501 Cylinders. *Combust. Flame* **2016**, Submitted.

[26] J. Luitjens, M. Berzins. Scalable parallel regridding algorithms for block-stuctured adaptive mesh refinement. *Concurr. Comput.* **2011**, *23*, 1522–1537.

CHAPTER 8

CONCLUSIONS

Modeling the many aspects of a DDT on large scales is a very difficult task. This thesis focused on developing the tools necessary to computationally model multiple aspects of the combustion of PBX 9501 and how these tools were used to examine how a relatively unenergetic deflagration can transition into a fully developed detonation in an array of explosive cylinders. With a strong understanding of the initiation mechanism needed for a DDT to occur in an array of explosives, considerations can be made on the proper packing configuration needed to prevent large storage and transportation accidents. The ultimate goal was to reduce the probability of detonation in an ordered array of solid explosive cylinders. To do this, a computational framework must be capable of scaling to large core counts, run in parallel on massive computational infrastructures, and accurately represent the fluid-structure interactions. A collaboration with computer scientists and engineers has made the Uintah framework capable of scaling to 512 K cores on DOE's Mira, enabling large-scale simulations. The engineers have included fluid-structure interactions, described in Chapters 1 and 2, enabling the solid PBX 9501 to be converted to product gas. With this strong computational framework large-scale simulations of hard scientific problems are possible.

When running complex fluid-structure interaction simulations unforeseen problems arise. One of these problems was the reactant equation of state (JWL) producing negative pressures when the material was placed in tension, as seen in unconfined deflagration. Negative pressures are unphysical for gases and are not allowed within the Uintah infrastructure due to the MPMICE component. MPMICE requires that there be a very small amount of every material in every cell. To account for this, the JWL equation of state was modified for the reactant material, eliminating the possibility of negative pressure. The modified equation of state exhibited the same expansion behavior at pressures above the reference pressure (1 atm) and exponentially decays to zero below. This modification eliminated the pressure error occurring when the solid material was in tension.

Another challenge with large-scale simulations is understanding the resolution dependence within the models. The quantities examined when investigating a resolution dependence were the effect on the conductive and convective deflagration rates and the detonation velocity. It was observed that the conductive burn rate was not dependent on the resolution of the grid cells. Cell sizes from 1 mm to 10 mm were examined for on surface burning at three initial temperatures over a wide range of pressures and little to no change was observed. The detonation velocity and convective deflagration rate on the other hand did exhibit a resolution dependence. Cell resolutions of 1 to 12 mm were examined for the detonation velocity. It was observed as the cell resolution increased the reaction peak extended closer to the sonic plane, accelerating the detonation velocity. At a resolution of 12 mm an error of 8% was introduced. This suggested that grid resolutions of 10 mm or smaller should be used to reduce substantial error in the detonation velocity.

A resolution dependence in the convective deflagration rate was introduced from previously implementing the WSB model as a 3D model. In doing so the burn front area, needed to calculate the mass burn rate, was assumed to be a face of the deflagrating cell. As the resolution was doubled the burn rate then doubled due to the number of cell faces increasing by a factor of two. To account for this the burn front area for convective deflagration is now calculated as the volume of the cell divided by a reference burn front area (2 mm). This has eliminated all resolution dependence associated with convective deflagration. It is understood this was a simplified approach to model the convective deflagration rate. Until further experimental research is done to fully understand the mass burn rate with convective deflagration, this approach, to the best of our knowledge, accurately represents convective deflagration and decreases the nonlinearity in the simulations. Additionally, modifications to the burn model were made to more accurately represent the deflagration propagation velocity of conductive and convective deflagration. An induction time was introduced to slow down the flame velocity to that seen experimentally. With these changes Uintah accurately predicts a DDT in solid PBX 9501 with a resolution-independent DDT model. In order to run the large-scale simulations described in this thesis, it was essential that there was no resolution dependence, as larger cell sizes were needed for these very computationally expensive simulations.

The main focus of Chapter 7 was of analyzing a large 3D simulation run on 64,000 cores on DOE's Mira. This simulation consisted of 969 million particles in 206 million cells, representing 1/8th of the tractor-trailer involved in the 2005 transportation accident. The results from this simulation suggested that even without the additional compaction

and displacement of explosive cylinders moving in the accident, the original packing configuration would have still transitioned to detonation once ignited. It was observed in the large-scale simulation that the initiation mechanism for this transition occurred from inertial confinement. Inertial confinement occurred when the explosive cylinders were packed too closely together. This allowed for the cylinders to compact into one another, forming a high density barrier. Within the confines of this barrier the product gases were trapped and the compression of these gases transitioned to detonation. A second DDT initiation mechanism, Impact to Detonation, was observed when the cylinders were placed further apart. In these simulations the deflagrating cylinders were at an elevated pressures and the impact of a pressure wave or explosive fragment increased the localized pressure to that needed for detonation.

With a greater understanding on how deflagration can transition to detonation in an array of explosive cylinders, safer packing configurations were examined. The results showed that detonation can be inhibited by changing the packing configuration or number of devices packed in a box. It was observed that the fewer number of cylinders packaged per box, the closer the boxes could be packaged together without transitioning to detonation. This ultimately led to higher critical packing volume fractions, decreasing the amount of space needed to safely store explosive devices. The results also suggested that the packing configuration of the boxes greatly influenced the simulations' propensity to transition to detonation. Two simple packing configurations, the Offset and Checkered_Box configurations, were determined to be viable ways to safely package explosives. With this greater understanding of how arrays of explosive devices transition from deflagration to detonation and new suggestions on safer packing arrangements, we hope this research will decrease the probability of future transportation and storage accidents.

APPENDIX A

DDT1 MODEL

This appendix shows the logic of using the Uintah's DDT1 reaction model. The hot cell is defined as a surrounding cell which has a volume fraction of 0.7 or higher of the material that is above the temperature threshold for burning which ignites the cell of interest.

A.1 Compute Number of Particles per Cell

1. Count number of particles per cell (numPPC)

2. If used crack model, calculate crack width threshold[1]

$$CrackWidthThreshold = \sqrt{\frac{8e8}{P^{2.84}}} \tag{A.1}$$

   (a) If CrackRad >CrackWidthThreshold then crackedEnough[c]=1. CrackRad is calculated from ViscoSCRAM[2]

A.2 Compute Burn Logic

- **Determine intermediate values used for determining type of burning.**

1. Loop over all cells containing a reactant vol_frac >1e-10

   (a) Check to see if the output interval should be adjusted based on pressure defined in the input file.

   (b) Determine if cell is detonating

      i. Pressure threshold for detonation <press_CC

      ii. Detonating = 1

   (c) If pressure threshold for detonation >press_CC $\geq$ pressure threshold for burning

      i. Pressure in adjCell is determined based on the pressure in a surrounding cell with the largest product gas volume fraction

ii. Determine if cell is on surface of explosive

A. Vol_fac_CC[m][adjCell] >0.2

B. Temp_CC[m][adjCell] >ignition temp

C. numPPC >0

D. Mass fraction is <0.7 (make sure surface of explosive is exposed)

E. If A-D are true burning = on surface

F. If true break out of burn logic.

iii. Determine if surrounding cell is detonating

A. Pressure threshold for detonation <press_CC[adjCell]

B. Set detLocalTo[c] =1

iv. If use crack model = true; determine if temperature for burning is exceeded

A. Temp [adjCell] >ignition temperature

B. Set temperatureExceeded=1

2. If use induction time

(a) Determine if cell was burning in last timestep.

i. If true, continue warming up and add to countTime

(b) Determine if cell is on the surface

i. If minOverMax <0.7 and numPPC >0

ii. Loop over all cells

A. If burning = onsurface

- calculateInductionTime = true
- If the hot gas is in the cell
  - if vol_frac[m][c] >0.2 and temp_cc[m][c] >ignition temp
  - Θ_{hotgas}= 0
- If the hot gas is in a surrounding cell
  - if vol_frac[m][adjCell] >0.2 and temp_cc[m][adjCell] >ignition temp
  - Determine where the hot gas is in relation to the cell
  - Compute induction angle (Θ_{hotgas})

B. If on surface cell is ignited from burning cell

- Use crack model = true, cell is cracked enough and surrounding cell is burning
- calculateInducitonTime = true
- If the hot gas is in a surrounding cell
  - If vol_frac[m][adjCell] >0.2 and temp_cc[m][adjCell] >ignition temp
  - Determine where the hot gas is in relation to the cell
  - Compute Θ_{hotgas}

(c) If cell is not on the surface, is cracked enough and a surrounding cell is burning

i. Determine where the hot gas is in relation to the cell

ii. Compute Θ_{hotgas}

(d) Compute A_{id}

$$A_{id} = \frac{1+IC}{2} + \frac{1+IC}{2} sin(2\Theta_{hot_gas} - \gamma) \tag{A.2}$$

(e) Determine if ignited from conductive burning or conductive burning

(f) Calculate induction time

$$InductionTime = \frac{\Delta x A_{id}}{S_f} \tag{A.3}$$

$$S_f = 0.259 P_d^{0.538} \tag{A.4}$$

Flame spread on a surface from Son et al.[3]

(g) Add Δt to count time

(h) Determine if induction time is exceeded

3. Determine burning criteria

(a) If use induction time = true

i. Burning Criteria = conductive burning (on surface) if

A. detLocalTo[c] != 1 (surrounding cell is not detonating)

B. Burning = on surface

C. Press_CC $\geq$ threshold for burning

D. Induction time is exceeded

E. Ignited from conductive burning

ii. Burning Criteria = Convective burning if

A. detLocalTo[c] != 1 (surrounding cell is not detonating)

B. Use crack model = true

C. Cell is cracked enough

D. Temp_CC >burning temperature threshold

E. Induction time is exceeded

F. Ignited from convective burning

iii. Burning Criteria = Warming up if

A. Count time <induction time

B. Count time >0

(b) When use induction time = false

i. Burning Criteria = conductive if

A. detLocalTo[c] != 1 (surrounding cell is not detonating)

B. Burning = on surface

C. Press_CC $\geq$ Pressure threshold for burning

ii. Burning Criteria = Convective if

A. detLocalTo[c] != 1 (surrounding cell is not detonating)

B. Use crack model = true

C. CrackRad >CrackThreshold

D. temperatureExceeded=1

- **Compute Induction Angle**
  - Hot cell Vector = vector [(hotcellCord.x() - cellCord.x()),
    (hotcellCord.y() - cellCord.y()),
    (hotcellCord.z() - cellCord.z())]
  - $NormalizedDensityGradientVector = \frac{\frac{\delta\rho}{\delta x}, \frac{\delta\rho}{\delta y}, \frac{\delta\rho}{\delta z}}{\sqrt{(\frac{\delta\rho}{\delta x})^2+(\frac{\delta\rho}{\delta y})^2+(\frac{\delta\rho}{\delta z})^2}}$
  - $massHotCell = NormalizedDensityGradientVector*HotCellVector$
- **Update output intervals based on pressure exceeding threshold**
- **Compute Model Sources (mass, momentum and energy converted from solid $\rightarrow$ gas)**

1. Loop over all cells containing a reactant vol_frac >1e-10
2. If detLocalT[c] = 1 (cell is detonating)
   (a) Use JWL++ model for explosion to compute delF

$$F = \frac{\rho_{prod}}{\rho_{rct} + \rho_{prod}} \tag{A.5}$$

$$delF = G * P * (1 - F) \tag{A.6}$$

   (b) Determine rctMass, prdMass and MB
      i. MB = delF*(prdMass+rctMass)
      ii. A maximum of 20% of the cell can burn per timestep[4]
   (c) Clamp burned mass to total convertible mass in cell
   (d) Update totalBurnedMass, mass_src, momentum_src, energy_src, totalHeatReleased, sp_vol_src
3. If conductive burning (on surface burning) = true
   (a) Determine density gradient and BFA

$$NormalizedDensityGradientVector = \frac{\frac{\delta\rho}{\delta x}, \frac{\delta\rho}{\delta y}, \frac{\delta\rho}{\delta z}}{\sqrt{(\frac{\delta\rho}{\delta x})^2 + (\frac{\delta\rho}{\delta y})^2 + (\frac{\delta\rho}{\delta z})^2}} \tag{A.7}$$

$$BFA = \frac{\Delta x * \Delta y * \Delta z}{(\Delta x|g_x| + \Delta y|g_y| + \Delta z|g_z|)\frac{1}{(max(g))}^{(1/3)}} \tag{A.8}$$

   (b) Compute Burned Mass from WSB model a function of Tzero, Tsurf, prodPress, rctSpvol, surfArea, deltT, solidmass, min_mass_in_cell
      i. Update constants
      ii. T_s and m_b are iteratively solved

$$m_b(T_s) = \left[\frac{\kappa_c \rho_c A_c R T_s^2 exp\frac{-E_c}{RT_s}}{C_p E_c (T_s - T_0 - \frac{Q_c}{2C_p}}\right]^{1/2} \tag{A.9}$$

$$T_s(m_b, P) = T_0 + \frac{Q_C}{C_p} + \frac{Q_g}{C_p(1 + \frac{x_g(m_b,P}{x_{cd}(m_b)}} \tag{A.10}$$

$$x_g(m_b, P) = \frac{2x_{cd}(m_b)}{\sqrt{1 + D_a(m_b, P) - 1}} \tag{A.11}$$

$$x_{cd}(m_b) = \frac{\kappa_g}{m_b C_p} \tag{A.12}$$

$$D_a(m_b, P) = \frac{4B_g MW C_p P^2}{R^2 \kappa_g} x_{cd}(m_b)^2 \tag{A.13}$$

$$MB = \Delta T * BFA * m_b \tag{A.14}$$

(c) Clamp burned mass to total convertible mass in cell

(d) Update totalBurnedMass, mass_src, momentum_src, energy_src, totalHeatReleased, sp_vol_src

4. If convective burning

(a) Determine Burn Front Area

$$BFA = \frac{\Delta x \Delta y \Delta z}{BFA_{ref}} \tag{A.15}$$

This ensures the burned mass will not change with resolution.

(b) Compute burned Mass from WSB model a function of Tzero, Tsurf, productPress, rctSpvol, surfArea, deltT, solidmass, min_mass_in_cell

i. Update constants

ii. T_s and m_b are iteratively solved using Equations A.9-A.14

(c) Clamp burned mass to total convertible mass in cell.

(d) Update totalBurnedMass, mass_src, momentum_src, energy_src, totalHeatReleased, sp_vol_src.

5. If warming up = true

(a) Do nothing.

6. Save total quantities.

A.3 References

[1] H. L. Berghout, S. F. Son, B. W. Asay, *Convective Burning in Gaps of PBX 9501* in *Proc. Comb. Inst.*, pp. 911–917.

[2] J. G. Bennett, K. S. Haberman, J. N. Johnson, B. W. Asay, B. F. Henson. A Constitutive Model for the Non-Shock Ignition and Mechanical Response of High Explosives. *J. Mech. Phy. Solids* **1998**, *46*, 2303–2322.

[3] H. L. Berghout, S. F. Son, L. G. Hill, B. W. Asay. Flame Spread Through Cracks of PBX 9501 (a Composite Octrahydro-1,3,5,7-Tetranitro-1,3,5,7-Terazocine-Based Explosive). *J. App. Phys.* **2006**, *99*, 114901–7.

[4] P. C. Souers, S. Anderson, J. Mercer, E. McGuire, P. Vitello. JWL++: A Simple Reactive Flow Code Package for Detonation. *Propellants Explos. Pyrotech.* **2000**, *25*, 54–58.

APPENDIX B

MODIFIED JWL EQUATION OF STATE

Determining reference density to eliminate negative pressure in JWL EOS for the solid material when under tension.

B.1 Flow Chart

JWL EOS

$P = Ae^{(-R_1 V)} + Be^{(-R_2 V)} + \frac{C_v \omega T}{V}$

$V = \frac{\rho_o}{\rho + 1e^{-100}}$

Initialize Variables

$f = 0$

$\frac{df}{d\rho} = 0$

$ConvergenceCriteria = 1e - 15$

$\rho_{max} = 100000$

$\rho_{min} = 0$

$\rho_{ref} = \rho_{guess} = \rho_{orig}$

$\rho_{IR} = \rho_{max}$

$\rho_{IL} = \rho_{min}$

$iter = 0$

Initial Guess

while do

Bisection Methoud

$EOS_{JWL}(T, \rho_{ref})$ compute $\rightarrow$ $, P_{iter}$

$f = P_{iter} - P_{ref}$

$setInterval(\rho_{max}, \rho_{min}, f, \rho_{ref})$

if $|\frac{\rho_{IL} - \rho_{IR}}{\rho_{ref}}| <$ convergence criteria **then**

$\rho_{ref} = \frac{\rho_{IR}+\rho_{IL}}{2}$

Break Outer Loop

end if

$\delta_{new} = 1e100$

while do

Newton's Method

$EOS_{JWL}(T, \rho_{ref})$ compute $\rightarrow$ $, \frac{df}{d\rho}$

$\delta_{old} = \delta_{new}$

$\delta_{new} = \frac{-f}{\frac{df}{d\rho}}$

$\rho_{ref} += \delta_{new}$

if $|\frac{f}{\frac{df}{d\rho}\rho_{ref}}| <$ convergence criteria **then**

Break Outer Loop

end if

if $iter >= 100$ **then**

Throw Error

end if

if $\rho_{ref} < \rho_{IL}$, or $\rho_{ref} > \rho_{IR}$, or $|\delta_{new}| > |\delta_{old}0.7|$ **then**

Break Inner Loop

This catch is if the improvement from Newton Method is not shrinking try to use Bisection Methoud to make problem more local

end if

$EOS_{JWL}(\rho_{ref}, T)$ compute $\rightarrow$ $, P_{iter}$

$f = P_{iter} - P_{ref}$

iter++

end while

$setInterval(\rho_{IR}, \rho_{IL}, f, \rho_{ref})$

if Break Outer Loop **then**

$\rho_{ref} = \frac{\rho_{IL}+\rho_{IR}}{2}$

iter++

end if

end while